To the Graduate Council:

I am submitting herewith a thesis written by Kelley Parker Brown entitled "Design and Parameter Identification of a Discrete Variable Transmission System." I have examined the final electronic copy of this thesis for form and content and recommend that it be accepted in partial fulfillment of the requirements for the degree of Master of Science, with a major in Mechanical Engineering.

William R. Hamel
Major Professor

We have read this thesis
and recommend its acceptance:

Arnold Lumsdaine

Gary V. Smith

Accepted for the Council:

Anne Mayhew
Vice Chancellor and
Dean of Graduate Studies

(Original signatures are on file with official student records)

DESIGN AND PARAMETER IDENTIFICATION OF A DISCRETE VARIABLE TRANSMISSION SYSTEM

A Thesis

Presented for the

Master of Science

Degree

The University of Tennessee, Knoxville

Kelley Parker Brown

December 2004

To
My mom…

ACKNOWLEDGEMENTS

To all of those who supported me throughout my college career, thank you. To my girlfriend Kim who has given me great support, my mother who has made it possible for me to attend school both financially and emotionally, my stepfather who was a good friend and a great giver of advice and to my friends who at every turn tried to sabotage my efforts.

Great thanks are given to Dr. William R. Hamel for his technical guidance, suggestions, patience and financial assistance, which enabled me to complete this thesis and my master's degree. I am grateful as well to Dr. Arnold Lumsdaine for his ideas and understanding as a member of my thesis committee. Thank you Dr. Gary V. Smith for your making all the classes I have had under you very interesting and for being a member of my thesis committee.

To Dr. Spivey Douglas, Dr. Sewoong Kim, Kalyana Ghanti, Renbin Zhou and Ge Zhang who worked with me on the TBA project thank you for the support. To Sriram Sridharan for making all of the great Indian food and working with me day and night and the next day again on the DVT. To Danny Graham, Gary Hatmaker and Dennis Higdon, this would never have been done with you, thanks.

A special thanks is given to Mr. George Bowers, a retired design engineer from GM, who gave much of his time and knowledge to this project and to Donny Clemen a design engineer at Allison Transmissions who reviewed the prints.

ABSTRACT

Complex and expensive electro-hydraulic systems have shouldered the workload for remote cleanup operations in radiological and toxicological areas in the past; the payload, reach and speed requirements of most applications have demanded their use. Electromechanically actuated systems (EAS) however offer an alternative that in comparison is much more reliable and maintainable. The problems faced in implementing the EAS are in high payload operations where the hydraulic systems hold a clear power density advantage. For the EAS to compete in the area of torque, very large DC motors have been implemented which make them obsolete in restricted work space areas and prove to be lacking in high-speed applications. New research suggests that this may be overcome by the use of a variable speed transmission or discrete variable transmission (DVT) system to spread the EAS torque-speed characteristics over a wider output speed range. This concept is called Transmission Based Actuators (TBA). This concept will facilitate the use of much smaller high speed motors which, when coupled with a DVT, can offer low speeds at high torques and high speed at low torques thereby matching the performance and size of the hydraulic systems [1]. The work here provides the detailed design of such a DVT comprised of three planetary gear stages. The full design process is discussed along with kinematic, dynamic and parameter identification analyses. The design process consists of determining the configuration, mechanical design for each element and selection of components such as bearings. snap rings and materials. The parameter

identification portion attempts to quantify constants, such as damping and inertia, which affect the operation of the system. The Matlab System Identification Toolbox (SID) was utilized to accomplish this. This required the creation of a two-degree of freedom dynamic model and the capturing of operational data to estimate the parameters.

TABLE OF CONTENTS

1. Introduction……1

1.1 Overview……1

1.2 Baseline Requirements……1

2. Transmission Configurations……6

2.1 Survey of Gears and Gear Trains……6

2.2 Planetary or Epicyclic Arrangement……11

2.3 Design Layout of DVT……12

3. Transmission Design……15

3.1 Gear Design Overview……16

3.2 Non-Standard Gears……17

3.3 Heat Treating and Nitriding……21

3.4 Detailed Component Design……23

3.4.1 Sun Shaft and Gears……23

3.4.2 Ring Gears……25

3.4.3 Planet Gears……28

3.4.4 Planet Carriers……29

3.4.5 Housings……31

3.5 Selection of Accessory Components……34

3.5.1 Bearings……34

3.5.2 Involute Splines……37

3.5.3 Snap Rings……38

3.5.4 Shaft Coupling……..……...39

3.6 Summary……..……..…….42

4. Modeling and Identification……..43

4.1 Overview…….43

4.2 Identification Theory...…….……..44

4.3 Dynamic Model…....……..51

4.4 Experimental Setup and Data Collection……80

4.5 Data Analysis……..……89

5. Conclusions and Future Work……..……...106

5.1 Conclusions……...106

5.2 Future Work……..111

Bibliography……..112

Appendix…….115

Vita……124

LIST OF FIGURES

Figure 1 - Titan III……...2
Figure 2- Baseline model for TBA……..…4
Figure 3 - Torque versus acceleration for TBA…….…..4
Figure 4 - Power versus velocity for TBA……...…5
Figure 5 –Spur gears and an internal gear with pinion…….…...7
Figure 6 - Helical and worm gearing…….……..8
Figure 7 - Harmonic gear drive…….……...9
Figure 8 - Planetary gear set arrangement…….…....10
Figure 9 - Torque and speed for three speed DVT…….....13
Figure 10 - Carrier to carrier configuration……..……..…13
Figure 11 - Carrier to ring configuration…….……...…14
Figure 12 - DVT design configuration……...15
Figure 13 – Involute profile control chart…….…….....20
Figure 14 – Hardness versus case depth for 4340 steel..……....22
Figure 15 – Sun shaft and gears for the DVT…….....24
Figure 16 - Hobbing setups for external spur gears……24
Figure 17 – Finished ring gears stages 2 and 3……...27
Figure 18 - Ring gear used as housing for bearing……...…..27
Figure 19 - Planet gear for the DVT……...…28
Figure 20 - Carrier design for the DVT……...30
Figure 21 - Housing used to support AB motor……...32
Figure 22 - Side view of first section of housing…….32
Figure 23 - Housing 1 and carrier-planet-bearing assembly……33
Figure 24 - Fafnir 208K radial bearing…….34
Figure 25 - Fit regions for Fafnir radial bearings…….36
Figure 26 - Involute fillet root side fit spline geometry……37
Figure 27 - Snap ring technical data…….38
Figure 28 - Location of bellows coupling in the DVT……..40
Figure 29 - Bellows flex coupling and technical data…….……..41
Figure 30 - Single input single output system…….…..45
Figure 31 - System with disturbance…….…47
Figure 32 - Inputs and Outputs for the system model……...52
Figure 33 - Drive shaft free body diagram…….....55
Figure 34 - Planet configuration in the DVT…….....56
Figure 35- Planet gear free body diagram, motion about own center……..57
Figure 36 - Ring gear that is experiencing braking……..59
Figure 37 - Carrier 1 and ring 2 coupled together……59
Figure 38 – Free body diagram of carrier 3…….….61
Figure 39 - Braking mechanism layout…….....73
Figure 40 - Experimental results of static braking torque versus current……75
Figure 41 - Behavior at band-ring interface…….....75
Figure 42 - Brake band torque curves……..…77
Figure 43 - Curve to represent dynamic braking torque……..77

Figure 44 - Allen Bradley input motor……...79
Figure 45 - System setup for data collection……..81
Figure 46 - DC generator and pulley system……..81
Figure 47 - Calibration curve for DC generator……..…...83
Figure 48 - National Instruments A/D board……..83
Figure 49 - Data samples at an input shaft speed of 1500 rpm……...85
Figure 50 - Data samples at an input shaft speed at 1600 rpm……...86
Figure 51 - Data samples at an input shaft speed of 2000 rpm……...87
Figure 52 - Data samples at an input shaft speed of 2400 rpm……...88
Figure 53 - Simulated output for a constant shaft speed of 1500rpm……..…91
Figure 54 - Simulated output for a constant shaft speed of 1600
and 2000rpm……..92
Figure 55 - Simulated model for constant shaft speed at 2400 rpm……....93
Figure 56 - Modified data set for 2400rpm……..…95
Figure 57 - Close up of modified data…….....96
Figure 58 - Filtered data…….....97
Figure 59 - Results from OEM modeling with filtered data set……..…100
Figure 60 - Step response for data and model……100
Figure 61 - Comparison of OEM to 2000rpm data set…….…..102
Figure 62 - Results from DVT dynamometer test……..107
Figure 63 - Improper center distance for planets in carrier…….…...109
Figure 64 - Non-linear gear friction……...110

GLOSSARY

Symbol	Explanation
M_p	Mass of Baseline
M_a	Mass of Load
l	Length of Baseline
g	Acceleration due to gravity
T	Load Torque
N_s	Number of sun gear teeth
N_p	Number of planet gear teeth
N_r	Number of ring gear teeth
r_r	Radius of ring gear
B	Viscous Damping
J_c	Inertia of carrier and planet about center of DVT
J_p	Inertia of planet about own axis
J_s	Inertia of sun shaft and gears
J_r	Inertia of ring gear
D_{shaft}	Shaft diameter
T_{input}	Torque input to shaft
N_{fs}	Safety factor
S_{yp}	Yield strength

R_D	Ratio of inside and outside diameters
T_i	Kinetic energy of component i
T_m	Torque of Allen Bradley Motor
b_i	Damping due to bearings on component i
T_{Brake}	Braking torque
F_a	Actuation force
θ	Joint Position of Titan
$\ddot{\theta}$	Joint acceleration
$\dot{\theta}$	Joint Velocity
ω_c	Angular Velocity of the carrier
ω_s	Angular Velocity of the sun
ω_r	Angular Velocity of the ring
ω_p	Angular Velocity of the planet
δW_i	Virtual Work of component i
$\dot{\theta}_i$	Angular velocity of component i
$\delta\theta_i$	Virtual displacement of component i
$\dot{\theta}_i$	Angular velocity of component i
$\ddot{\theta}_i$	Angular acceleration of component i
τ	Torque exerted by brake band
α	Angle of wrap

C h a p t e r 1

Introduction

1.1 Overview

The objective of this project was to design and test a transmission based electrical servo actuator (TBA). The conceptual design was motivated by the need for electrical actuators over hydraulic actuators due to the leakage of hydraulic fluid during operation in hazardous working environments. This work has been hindered by the weight of the electric motors needed to produce sufficient torque to match the performance of the hydraulically actuated manipulators. The coupling of an electric motor with a multi-speed transmission offers a possible solution to the problem by replacing the large high torque motor with a lighter high speed motor-transmission combination and gaining the torque/speed profiles necessary to compete with hydraulics [1].

1.2 Baseline Requirements

To match the performance of a hydraulically actuated manipulator, specifically the Schilling Titan III in figure 1, a baseline reference of requirements to be used for the design of TBA was determined by Dr. Sewoong Kim and Renbin Zhou [2]. Table 1 shows the performance specifications for the Titan III at full extension. Based on the Titan III specifications, the TBA load is modeled as a rigid arm with a length of 71 in and a weight of 200 lbs, with one end connected to the TBA output shaft.



Figure 1 - Titan III.

Table 1 - Titan II specification.

	Metric	English
Maximum reach	1915 mm	75.4 in
Maximum payload at full extension	113 Kg	250 lb
Manipulator weight	103 Kg	225 lb
Approximate Center of Gravity	1000 mm	39.37 in
Maximum Angular Velocity- No load	42°/sec (0.73 rad/s or 7rpm)	(same)
Maximum Angular Velocity- Half load	30°/sec (0.52 rad/s or 5rpm)	(same)
Maximum Angular Velocity- Full load	20°/sec (0.35 rad/s or 3.3rpm)	(same)

A Load (up to 240lbs) is on the other end, as illustrated in figure 2. The required torque of the TBA output is calculated by:

$$T = (Mp + \tfrac{1}{3}Ma)l^2\ddot{\theta} + (Mp + \tfrac{1}{2}Ma)lg\cos\theta \quad (1.1)$$

when $\ddot{\theta}$ =constant, T reaches its maximum at θ =0:

$$T\max = (Mp + \tfrac{1}{3}Ma)l^2\ddot{\theta} + (Mp + \tfrac{1}{2}Ma)lg \quad (1.2)$$

The required power output of the TBA is calculated by

$$Power = T_{\max} * \dot{\theta}(Watts) \quad (1.3)$$

For the purpose of obtaining the TBA baseline requirement, a total TBA efficiency of 0.65 is used, which assumes each of the three planetary sets has an efficiency of ~0.87. The maximum TBA output torque is shown in figure 3. The input power of TBA is shown in figure 4. Based on the results, the TBA baseline requirements are as follows:

1) TBA torque output must be greater than 3200Nm;
2) Driving motor of TBA must provide power of at least 1.5 KW.

By meeting the requirements, TBA should have similar performance specifications as the Titan III.

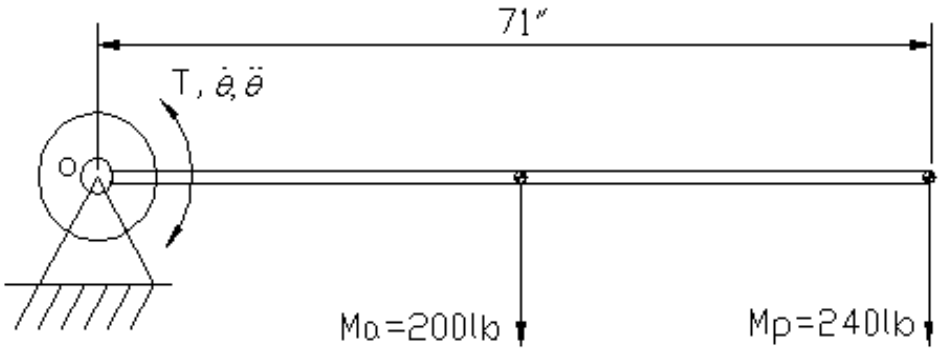


Figure 2 - Baseline model for TBA.

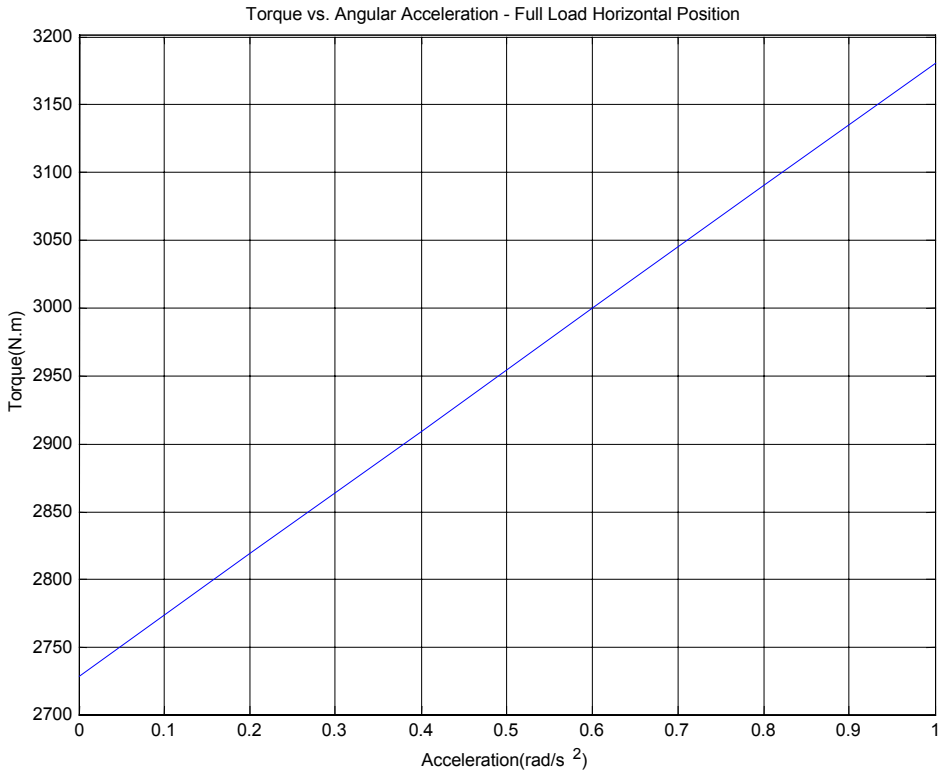


Figure 3 – Torque versus acceleration for the TBA.

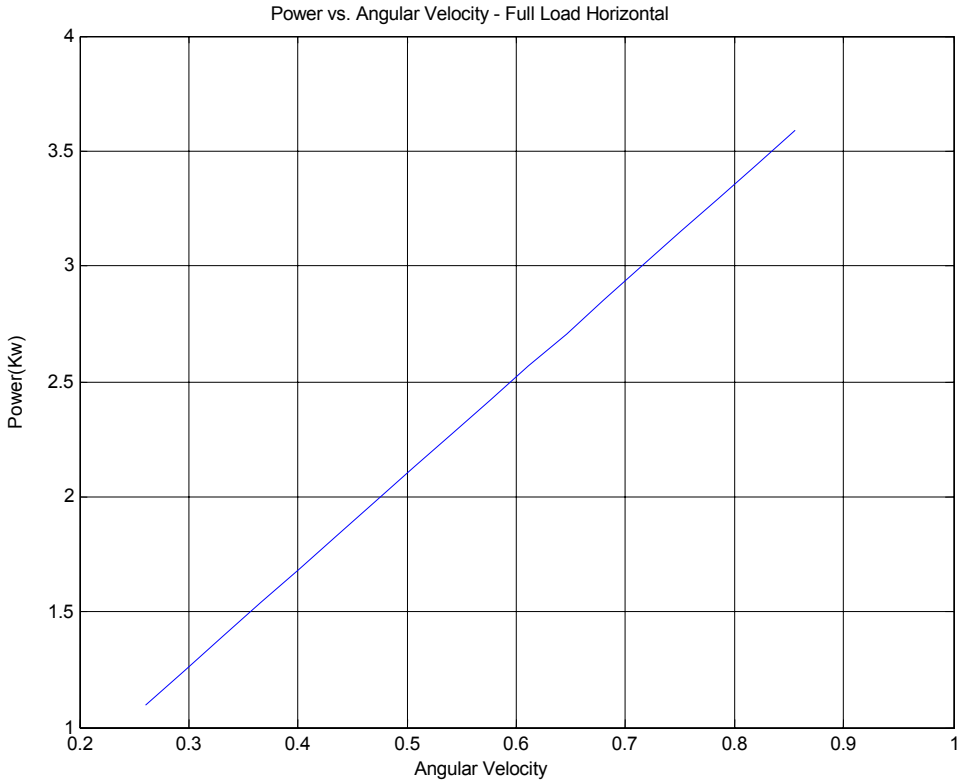


Figure 4 - Power versus velocity for the TBA.

Chapter 2

Transmission Configurations

2.1 Survey of Gears and Gear Trains

A gear train, simply stated, is a device, which transmits motion or power from one shaft to another using gears. There are many varieties of gear types and infinite arrangement possibilities. Space restrictions usually determine the possibilities of the arrangement before the design process has started. Some examples of gear teeth types include:

1. Spur
2. Internal
3. Helical
4. Straight Bevel
5. Hypoid
6. Worm
7. Face Gear

Each of these gear types has specific advantages over the others, for example helical gears provide an action that is smoother, quieter and tends to have somewhat of a larger transmitted load than an equivalent pair of spur gears but helical gears are less efficient. The lowered efficiency results from a higher normal tooth load on the helical than that on the spur for an equivalent tangential load [3]. Figures 5 and 6 show the basic geometry of some of these gear types and their relationships.

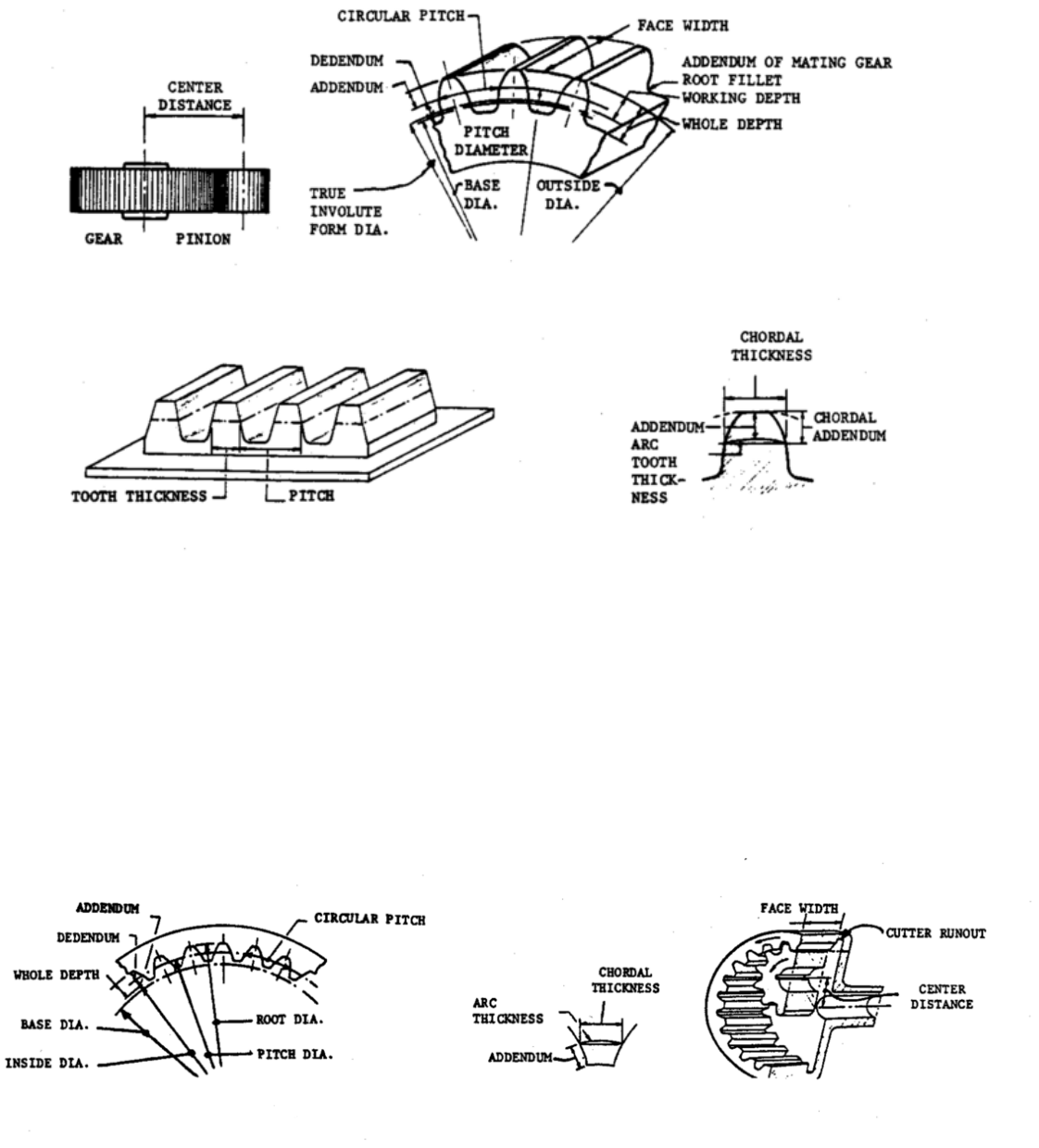


Figure 5 - Spur gears and an internal gear with pinion [21].

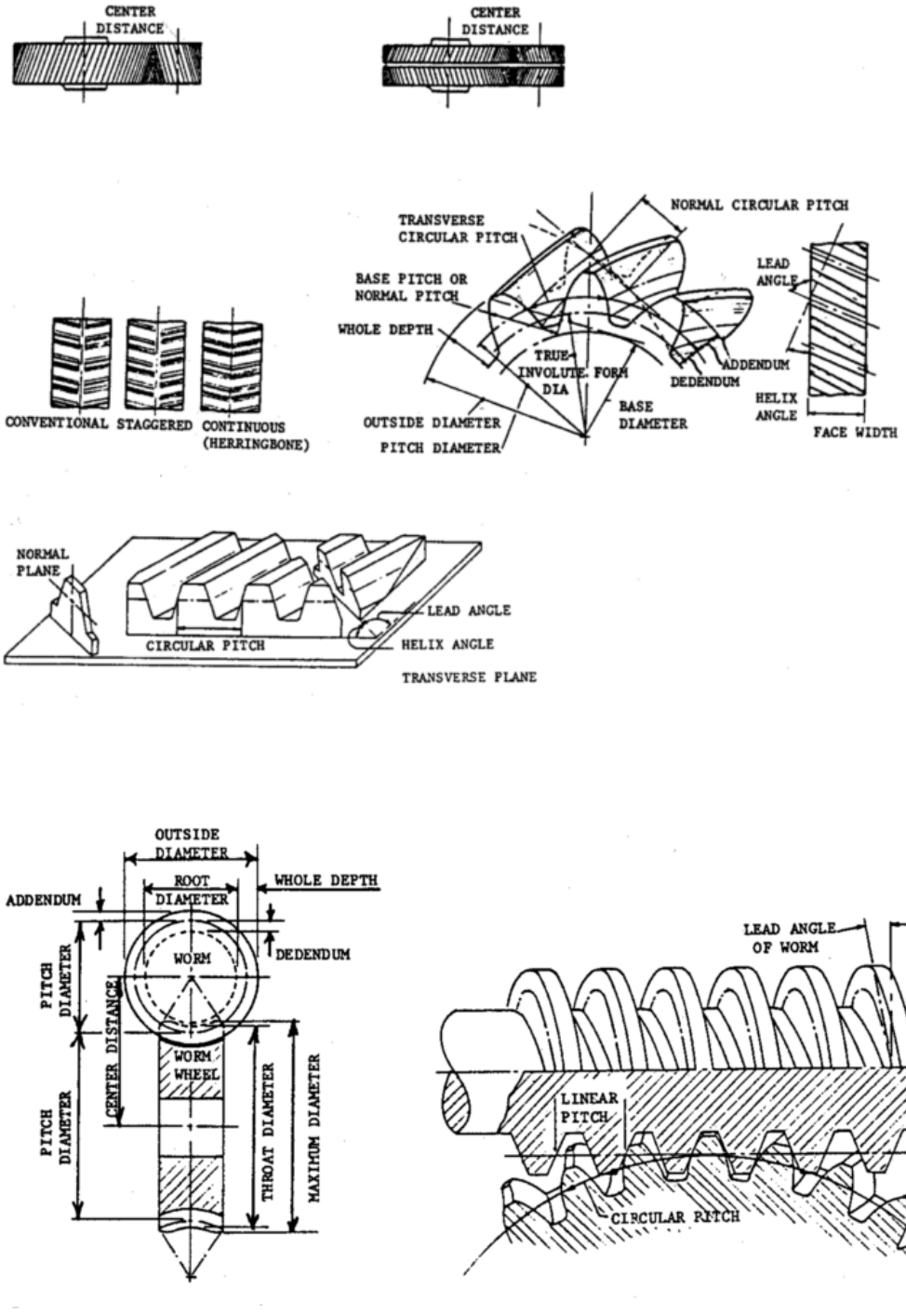


Figure 6 - Helical and worm gearing [21].

Some arrangement types for gear trains are the planetary or epicyclic and the harmonic gear drives. The harmonic drive shown in figure 7 is capable of producing massive ratios of up to 1,000,000:1 using a dual drive system or system within a system, has efficiencies approaching 96%, and has virtually no backlash [3]. Drawbacks include a huge amount of weight to support such reductions and many complexities involved in the manufacture of such systems. The type of arrangement chosen for the TBA was the Planetary or Epicyclic arrangement, shown in figure 8, due to its compact size and high load carrying capacity. The simplicity of this type of gear train was very attractive from a manufacturing standpoint. The ratios needed could be met and would enable the team to compete with the envelope constraint (size) dictated by that of the Titian.

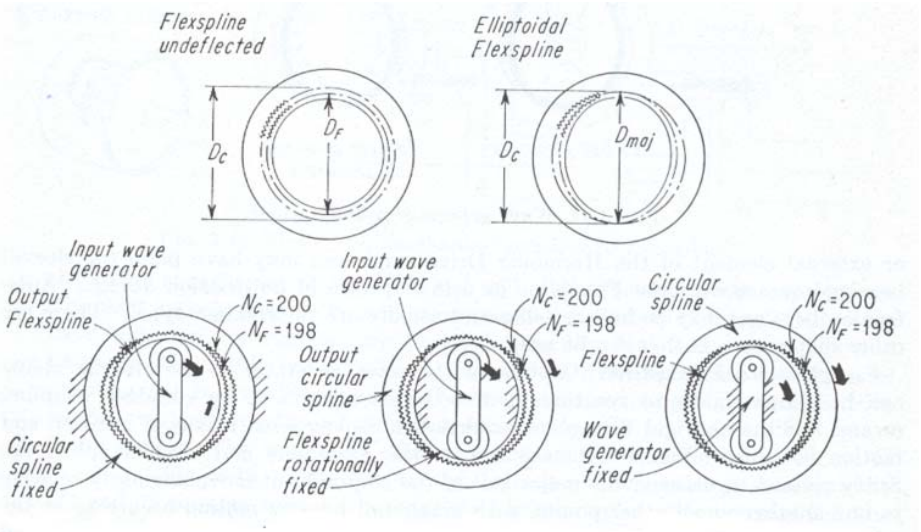


Figure 7 - Harmonic gear drive [3].

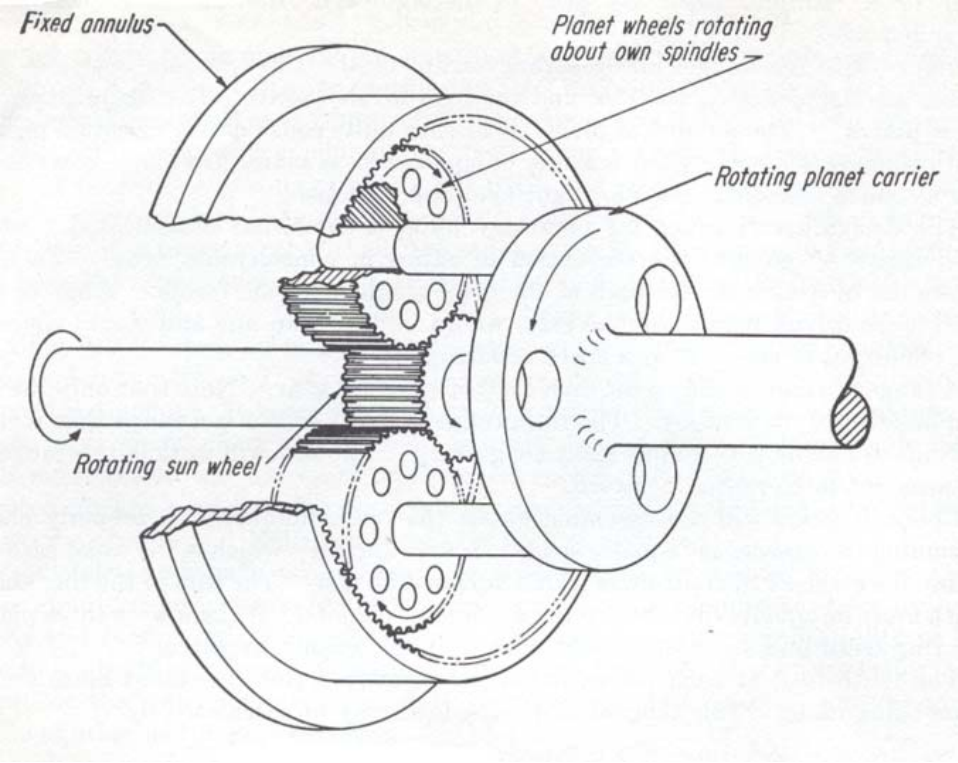


Figure 8 - Planetary gear set arrangement [3].

2.2 Planetary or Epicyclic Arrangement

A large family of gear arrangements goes under the name of "epicyclic" gearing. Generally speaking the epicyclic train has a central "sun" gear, several "planets" meshing with the sun and spaced uniformly around the sun and an "annulus" or ring gear meshing with the planets. The name epicyclic comes from the fact that points on the planets trace out epicycloidal curves in space. The name "planetary" gear is sometimes used interchangeably with epicyclic to denote the whole family of gears. In a more strict sense the planetary is one of the types of epicyclic gears. There are a large number of possible epicyclic arrangements and may be divided into three general groups [3].

1. Single Trains
2. Compound Trains
3. Coupled Trains

The epicyclic train has gained notoriety due to its high ratio possibilities while maintaining compact size, which is ideal for application in TBA. The power-torque relationship is the same as for other gear trains, but the tooth loading depends on the number of planets, ideally the torque is equally distributed over all. The drive is a two-degree of freedom system as it needs two independent inputs to achieve an output. For the applications here the driving input will be the sun gear while the ring gear will be grounded, maintaining zero speed for a particular stage.

2.3 Design Layout of DVT

In considering a design for the DVT the baseline requirements had to be revisited to ensure that the proper speed-torque relationships could be maintained. It was determined that three ratios would be enough to spread out the speed and torque [4]. This would mimic the continuous performance of the Titan III using 3 discrete gear ratios shown in figure 9. The next step was to configure the stages so that the proper ratios could be attained. The first design examined was a "carrier-to-carrier" configuration with 3 distinct ratios, figure 10. The carrier-to-carrier configuration was satisfactory from a kinematics viewpoint. However the detailed design had complications, the first of which was in deciding how to connect the carriers together. This would have required some type of spindle that would have increased the inertia of the system dramatically. Support for the ring gears and carriers was also a problem. Since the carriers would have run the entire length of the train, there would have been needed a bearing that had an inside diameter at least the diameter of spindle to properly seat the ring gears into the housing and to also support the carriers simultaneously. For these reasons, this model was discarded and a new approach was taken, the carrier to ring configuration. The carrier to ring configuration allowed for proper bearing support on all the members of the train and splines were utilized to connect the carriers to the rings eliminating the need for the spindles.

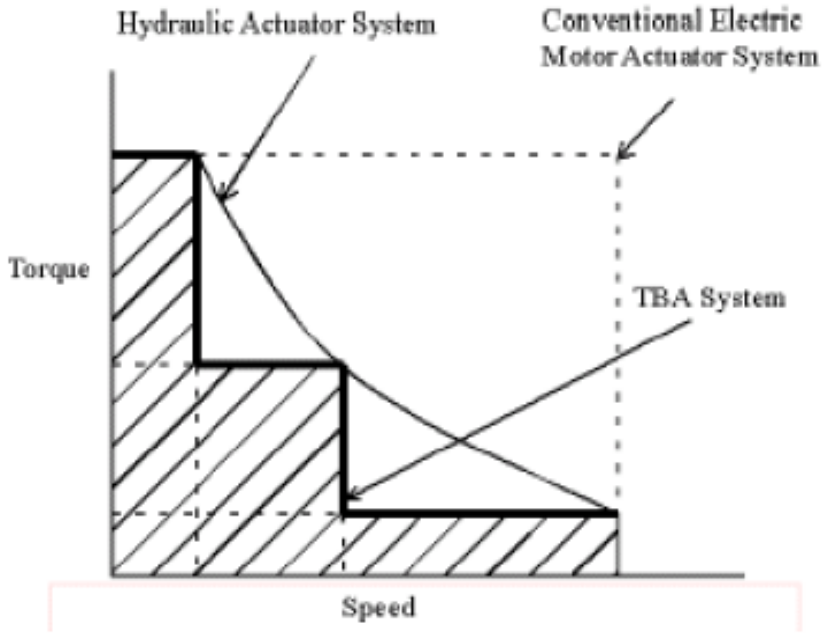


Figure 9 - Torque and speed for three speed DVT [4].

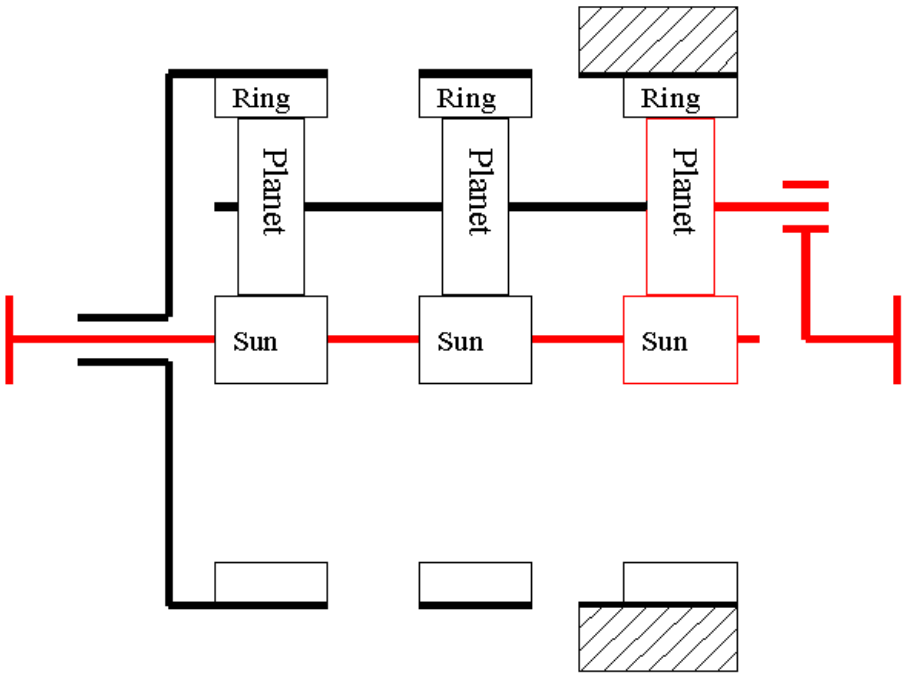


Figure 10 - Carrier to carrier configuration.

The housing support for each member could be attained with the use of a single bearing for both the carrier and the ring, figure 11, which supported the interface area and reduced the overall weight of the system Some design challenges for the carrier to ring configuration were supporting both the input shaft and ring gear in the first stage, actually connecting the carrier to the rings and properly supporting the members by way of the housing. These were each solved by creating a concentric bearing for the ring and shaft, by using involute splines to connect the carriers and rings, by press fitting bearings retained with snap rings in both the housings and on the members, respectively.

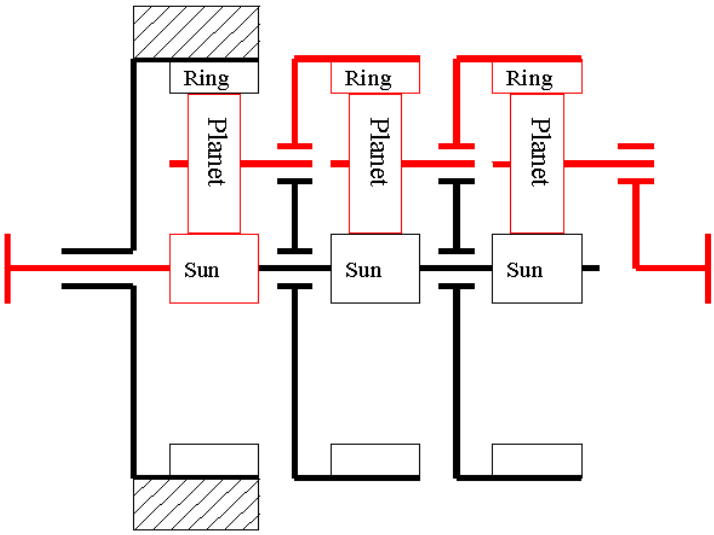


Figure 11 - Carrier to ring configuration.

Chapter 3

Transmission Design

A survey of available gearing was made to try and find existing commercial gears that could be modified to suit the design purposes. Some of the problems encountered in this search were that the ring gears had to be fashioned to accept a band brake and the sun gears were too small to make individually and then attach to a shaft by way of splines or keys. Both the carriers and rings had to be specially made to mate together using splines. This would have been a difficult challenge to create these pieces from existing gears. Therefore the decision was made to use custom gearing instead of buying gears because of the complexities of the system The design of all components of the DVT, figure 12, is discussed in this chapter as well as selection of bearings, snap rings, couplings and tolerancing methods.

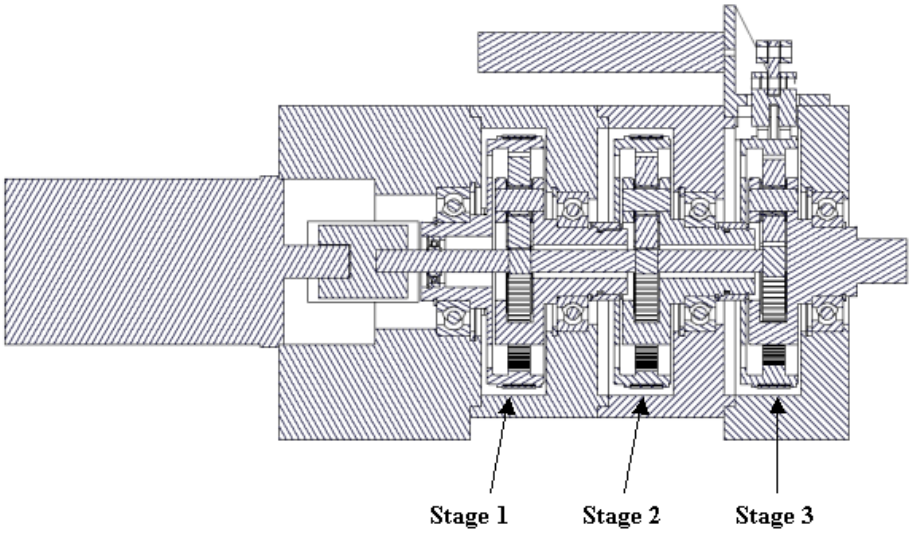


Figure 12 - DVT design configuration.

3.1 Gear Design Overview

To begin the process of gear design for a planetary gear train the gear ratios of the system must be decided upon. For the design here ratios of 3, 4 and 7 were chosen to properly maintain the baseline of the Titan III For the compound system of the carrier to ring it must be noted that these do not represent the ratios of the stages themselves but rather the combined ratio. Using the speed equation ratios the number of teeth were selected for an arbitrary gear then the other gears were designed around this one. Since a size envelope of 5 inches had to be met the number of teeth on the ring gear was chosen first because the outside diameter of the ring gear is the outer diameter of the system. The outside diameter was made as small as possible to compete with the baseline reference size of the Titan III. The ratios were determined to be:

1^{st} Stage=8.625

2^{nd} Stage=8.625

3^{rd} Stage=7.05

These were chosen so to give even teeth numbers for each stage and still maintain the 3, 4 and 7 reductions. At this point a system of standard gears could be designed to meet the requirements of speed and torque. If a standard system was used the center distances for the stages would be different for stages 1, 2 and 3, which would mean that the ring gears and carriers would also be different. This would dramatically increase the cost of fabrication due to labor costs. The labor

costs are incurred due to the setup time for each component. If the components are all the same, then there only needs to be one setup time and therefore less time spent on each component. To solve this problem the center distance was changed from standard to 1.375 inches on all three sets. Unfortunately, to cut standard gears on nonstandard center distances a special hob would need to be bought or made. This would have also increased the cost of machining greatly. Therefore, cutting nonstandard gears with standard tools was the problem to be solved. Nonstandard gear design is discussed in great detail in the next section.

3.2 Non-Standard Gears

Special thanks goes to George Bowers, an expert in the filed of gear design, for designing these gear teeth and giving a small portion of his knowledge to this project. The practice of designing nonstandard gears can be utilized for several reasons. In this case, as mentioned earlier, there was a fixed center distance and standard cutting tools that cut numbers of teeth that do not match the center distance prescribed. Cutting the gears on pitch diameters that are different from the operating pitch diameters can solve this problem. This results in two center distances, a nominal and operating where,

$$\text{Center Distance (nominal)} = \frac{pinion\ pitch\ diameter + gear\ pitch\ diameter}{2} \quad (3.1)$$

$$\text{Center Distance (operating)} = defined = 1.375\ inches \quad (3.2)$$

The center distance was chosen to allow for the ring gears to all be of the same size. From this and knowing that we have chosen a module of 1, the pitch diameters then become,

$$\text{Pitch Diameter (nominal)} = \frac{number\ teeth}{diametral\ pitch} \tag{3.3}$$

$$\text{Pitch Diameter (operating) of pinion} = \frac{2 * operating\ cent.dist.}{ratio + 1} \tag{3.4}$$

$$\text{Pitch Diameter (operating) of gear} = \frac{2 * operating\ cent.dist.}{ratio + 1} * ratio \tag{3.5}$$

$$ratio = \frac{no.\ gear\ teeth}{no.\ pinion\ teeth} \tag{3.6}$$

From this point hob data will need to be known. If a 1 module hob is being used as prescribed earlier then the theoretical pitch diameters of the gears becomes:

$$\text{Pinion P.D.} = no.\ pinion\ teeth * module \tag{3.7}$$

$$\text{Gear P.D.} = no.\ gear\ teeth * module \tag{3.8}$$

The spread ratio then becomes:

$$m' = \frac{\text{Pitch Diameter (operating) of pinion}}{\text{Pinion P.D.}} \tag{3.9}$$

The operating pressure angle becomes:

$$\alpha' = \arccos\left[\frac{\cos 20^o}{\text{Pitch Diameter (operating) of pinion}}\right] \quad (3.10)$$

Modifications to the addendums of both the pinion and gear must be chosen. There are standard tables to use in getting an idea of what ratios to use.

$$\text{operating pinion addendum} = \textit{addendum ratio} * \textit{mod ule} \quad (3.11)$$

$$\text{operating gear addendum} = \textit{addendum ratio} * \textit{mod ule} \quad (3.12)$$

Using the new or operating addendum the outside diameters of the gears become:

$$\text{P}\textit{inion O.D.} = 2 * \textit{operating pin.addendum} + \textit{operating pin. pitch diameter} \quad (3.13)$$

$$\textit{Gear O.D.} = 2 * \textit{operating gear addendum} + \textit{operating gear pitch diameter} \quad (3.14)$$

The finishing 1-module hob is designed slightly oversized so that when it is hobbing at full depth, the finished gear will have a good amount of backlash on standard center distance. The standard 1-module addendum is 1 mm. To cut the spread center gears the hob is held out these amounts:

$$\textit{Pinion}\,\Delta h. = \textit{theoretical pinion addendum} - 1\textit{mm} \quad (3.15)$$

$$\textit{Gear}\,\Delta h. = \textit{theoretical gear addendum} - 1\textit{mm} \quad (3.16)$$

This results in a thinner tooth at the operating pitch diameters and a larger than standard tooth thickness at the 20^o pitch line. The proportions are toleranced using an involute profile control chart, as in figure 13. In doing this backlash is increased and can be controlled by hobbing the gears shallow which will slightly increase the tooth thickness and keep the backlash approximately constant [5].

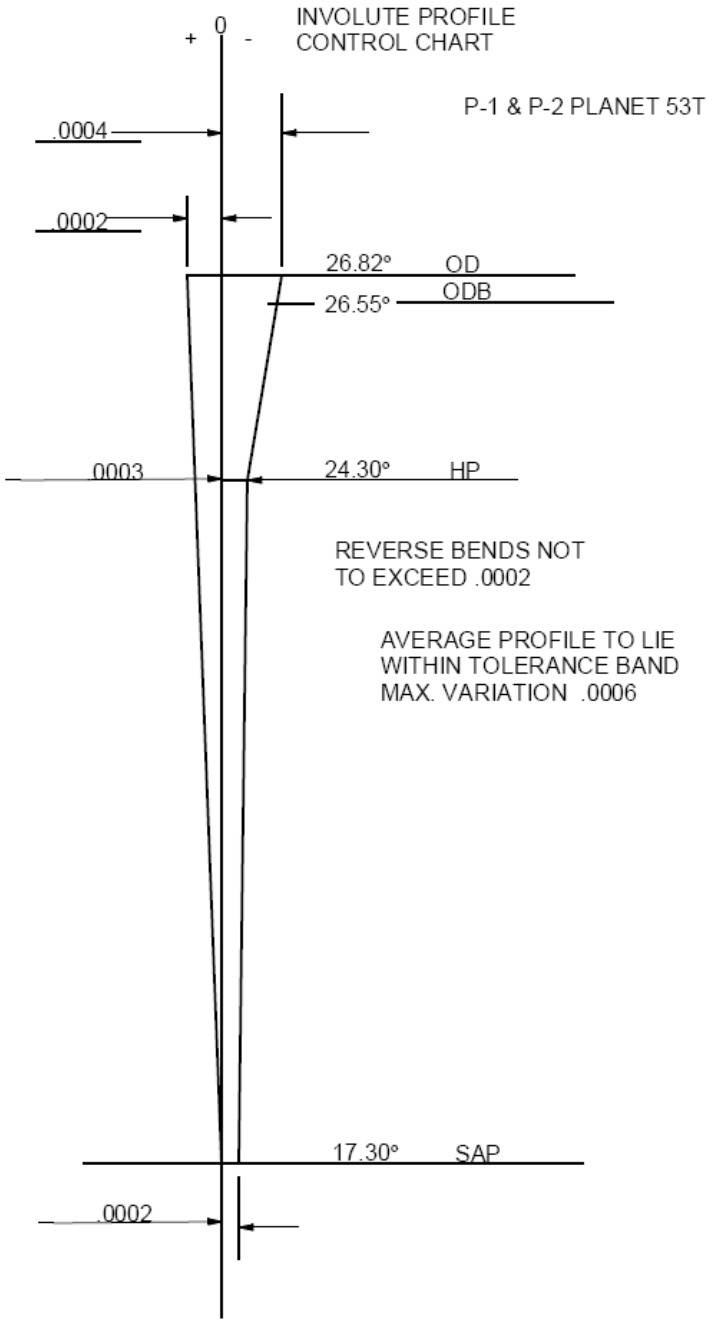


Figure 13 - Involute profile control chart.

3.3 Heat Treatment and Nitriding

Gear steels are heat treated for two general purposes. First, they must be put into condition for proper machinability, second, the necessary hardness, strength, and wear resistance for the intended use must be developed [5]. Since this was a prototype system the main concern was that it did not fail and accordingly each component was over designed by at least a factor of two with regard to the yield strength of the material. All gears were made from 4340 steel and were subjected to the same heat-treating and nitriding processes This was a core treat (quench and temper) to a 32-36 RC core hardness and nitride hardened to a case depth of .003 - .005 inches. The specifications were recommended by George Bowers as being good enough to handle whatever would be needed out of a system with 2 kilowatts of power. The heat treatment and resulting hardness made the gears hard to cut and is considered the limit of machining capability [5]. It is important to note as well that when gears are heat-treated they are distorted. This distortion has to be taken into account either before or after the heat treatment. If the gear blanks are treated before machining then the material is very hard and is difficult to machine this is very hard on tooling. If the gears are cut and then treated, as these were, the distortion must be estimated so that the machinist can compensate for it. It is impossible to exactly know the distortion resulting from heat treatment so when the gears are removed from the heat treat they are cooled, measured and then ground until they meet the tolerances. Also since the nitriding operation is done at about 1050 degrees Fahrenheit the tempering temperature must be above this to avoid tempering back the gear core and causing distortion after the

grinding process. Nitriding is a casehardening process in which the hardening agents are nitrides formed in the surface layers of steel through the absorption of nitrogen from a nitrogenous medium, usually dissociated ammonia gas [5]. The case depth results in a gear with an extremely hard surface. This resists pitting and scarring which may decrease the efficiency of the gear. This is done after the gears have been heat-treated and ground to specifications. Figure 14 shows the relationship between hardness and case depth for 4340 steel parts. The logic of nitride case depth is sill not understood too clearly. From the standpoint of tooth breakage, the nitride case does not generally give a high degree of strength. For spur gear teeth in the range of 4 module to 10 module, nitriding has some value in increasing the surface load-carrying capacity, but the beam strength has to be based almost entirely on the core hardness of the tooth.

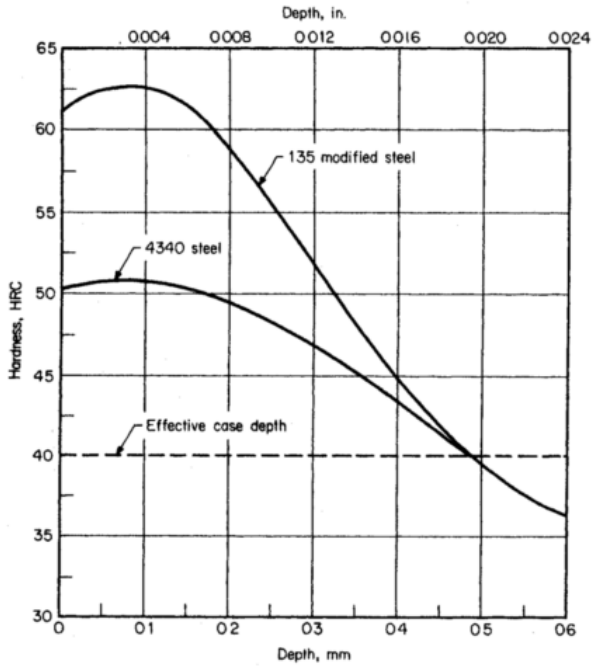


Figure 14 - Hardness versus case depth for 4340 steel [5].

3.4 Detailed Component Design

The next section gives a description of some of the steps taken in the design of the DVT components. Sriram Sridharan and the author designed all components, excluding the gear teeth proportions, which were designed by George Bowers.

3.4.1 Sun Shaft and Gears

Shaft design consists primarily on calculating the correct shaft diameter to ensure satisfactory strength and rigidity when the shaft is transmitting power under various operating and loading conditions [6]. The sun gears were made as small as possible to achieve the proper ratio; because of this an integral gear/shaft was chosen shown in figure 15. If the gears were to be connected to the shaft via snap rings or keyways it would increase the required minimum diameter of the shaft because of stress concentrations located around these shape changes. The shaft being designed here was subject to a diameter constraint due to the size of the sun gears. Each gear was hobbed, when hobbing a gear directly onto a shaft the maximum diameter allowable for the shaft is roughly the root diameter of the gear minus half a tooth height of the gear. Figure 16 shows three basic hob processes. This is to allow enough space for the hob to clear the outer diameter of the shaft. The determined maximum shaft size was then compared to the minimum allowable shaft diameter, where the diameter is determined by:

$$D_{shaft} = \left(\frac{16 T_{input} N_{fs}}{\pi S_{yp}} \right)^{\frac{1}{3}} \tag{3.17}$$

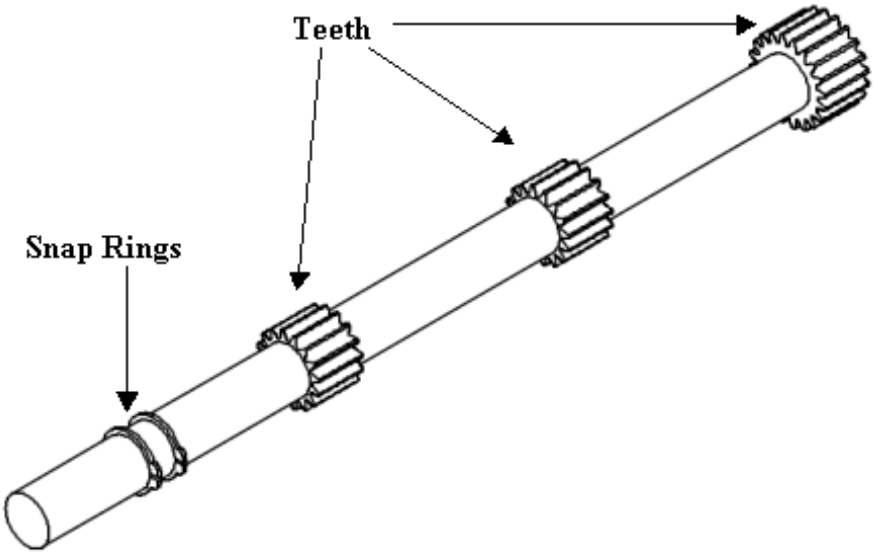


Figure 15 – Sun shaft and gears for the DVT.

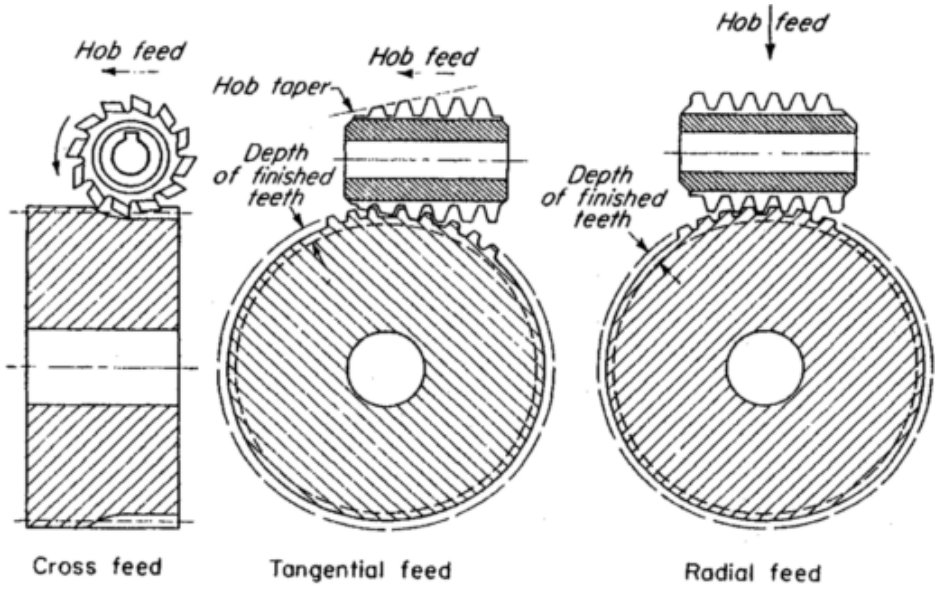


Figure 16 - Hobbing setups for external spur gears [5].

The diameter chosen was .5 inches to accommodate both bearing availability and the hobbing requirement. The torque input of the motor was taken to be the peak torque given by the manufacturer (12 Newton-meters) to ensure that the shaft would not fail during a direction change. A direction change could also produce a shock effect in the shaft and therefore a "high shock" safety factor of 2 was used. The high shock could result from the backlash in the gear meshes. If the shaft changes direction then the teeth will slam together as a result of this backlash. Because of the snap rings used to locate the shaft and bearing there was assumed to be no axial loading. This was done by using the clearance at the end of the shaft and the "loose fit" caused by the snap rings. This allows the shaft to float within the snap ring tolerances without interference at the end thereby preventing axial loading. The length of the shaft was dictated by the locations of the planet gears, which were influenced by spline lengths, and bearing widths that were determined first to ensure the shortest possible overall length. Because the gears were machined directly onto the shaft, the shaft had to undergo the same heat-treating procedure as the gears. The manufacturer had to be sure not to nitride the area between the snap ring grooves, as this would interfere with the bearing fit because it would have increased the shaft diameter by a possible .005 inches, the nitride case depth.

3.4.2 Ring Gears

The ring gears in this system have a dual purpose, they transmit power through the system, as does every other member, but they also interact with the brake band and provide the system with the necessary braking torque to achieve a desired

ratio. The braking torque was transmitted to the ring gear through the use of a brake band, which was actuated by an electric motor. The torque generated by the motor was carried through a braking mechanism composed of a slider crank and two links. Because the brake band was thin, two rails were designed on the shoulders of the ring gears to ensure that the band did not twist or slip off. The grooves turned out to be especially helpful during assembly by keeping the bands stable. The four holes in the back plate of the ring gear served a dual purpose; they enabled the transmission fluid to flow from stage to stage and were required to manufacturer the piece. Normally an internal gear such as this is broached but because of the back plate the rings had to be shaped as shown in figure 17. The shaper uses large amounts of cutting oil and since this oil has to have an escape route, the oil holes provided that. Splines were used to make the connection between the carrier and ring in the first and second stages and were held together using snap rings. The ring gear for stage one was much more complex. A concentric bearing was used to hold the sun shaft in place, which used the ring gear as it's housing, as shown in figure 18. This was done to shorten the overall length of the system. The bearing inside the ring gear was held into place with an internal snap ring and a shoulder. The locations of these retainers were crucial in maintaining the alignment of the gears through the length of the system. The advantage of the concentric bearing was that during the assembly procedure the sun shaft was not retained until the last stage was put into place. This allowed for the sun shaft to be moved if needed axially to accommodate the gear mesh until the snap rings could be used to attach the components.

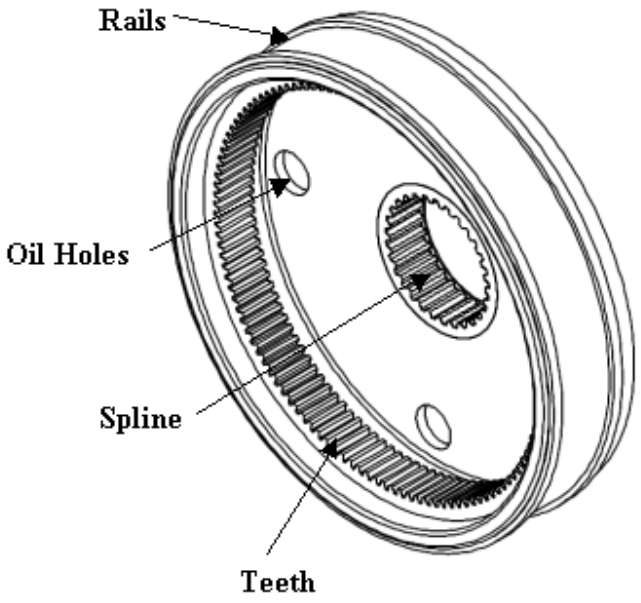


Figure 17 – Finished ring gears stages 2 and 3.

.

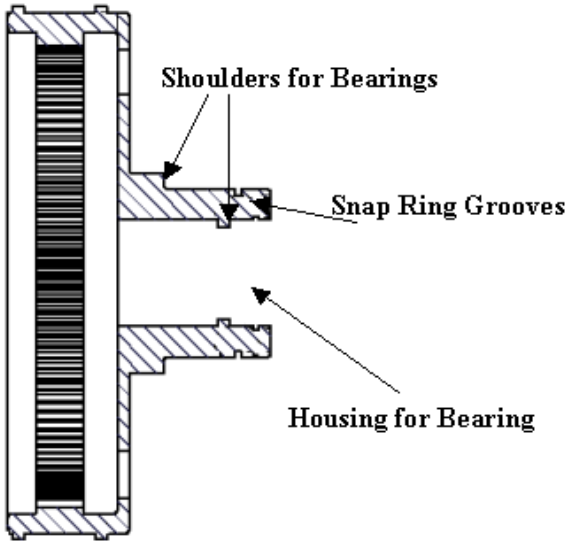


Figure 18 - Ring gear used as housing for bearing.

3.4.3 Planet Gears

The planet gears, shown in figure 19, were designed to accommodate a small set of cupped needle bearings that, along with a shaft made of hardened drill rod, created a spindle. The shaft served two purposes: to provide an inner race for the needle bearings and to transmit power to the carriers. The needle bearings were pressed into the holes, which required a high tolerance due to the delicateness of the bearings. As long as they were seated properly in the gear there would be no problems. If for instance the holes were loose and the bearing was allowed to shift, a bending moment could occur and shatter the high carbon steel bearings. The planets were arranged at a 1.375-inch center distance around the axis of the DVT. The load of the system was distributed equally among the three for each stage. To prevent the planets from contacting the carriers, which would have caused damage, steel washers were used which were placed onto the spindle.

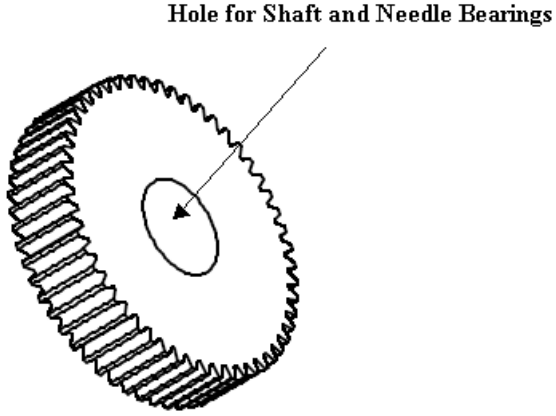


Figure 19 - Planet gear for the DVT.

3.4.4 Planet Carriers

The carriers, shown in figure 20, were the most exotic components of the transmission. They functioned as the coupling body between every other component in the system. A hole had to be cut through the center to allow the first two-stage sun gears to pass and was chosen to be .75 inches. In calculating the minimum carrier shaft outside diameter the following equation was used.

$$D_{shaft} = \left(\frac{32 T N_{FS}}{\pi (1 - R_D{}^4) S_{YP}} \right) \tag{3.18}$$

This diameter had to be matched up with available bearing bore sizes and external splines and was found to be 1.5748 inches. Bearings and snap ring grooves were used to hold and support the member to the housing. The material was changed from 4340 steel to 7075 aluminum to reduce the inertia of the system. The holes for the planet spindles had to be cut for a tight press fit. This was critical because of the yield strength differences in the hardened drill rod that was used for the spindle shaft and the aluminum. If the holes were too tight the steel would simply cut or shear the aluminum as it was pressed. This could lead to problems. The pins should have been made to fit loosely in the holes and then a woodruff pin or some type of stake been used to secure the spindles. This will make it difficult to ever remove the planets as the aluminum may eventually become loose around the spindle shafts, especially if there is to be a disassembling of the entire system.

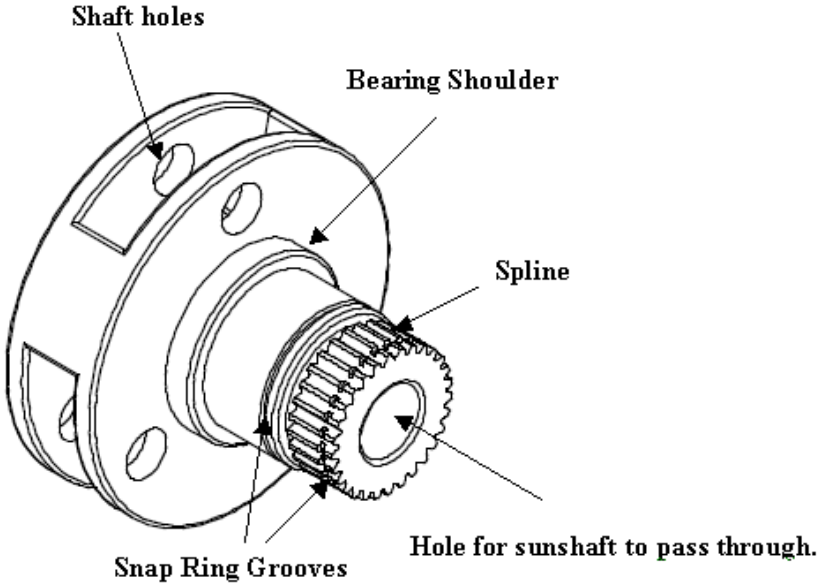


Figure 20 - Carrier design for the DVT.

The final, stage 3 carrier had to be altered at the last minute so that it would accept a smooth bore shaft coupling. The spline on the end was removed and replaced by a 1-inch smooth shaft. This was because the system to which it was to be connected was already set up. A key could have been used, but was deemed unwise with the 7075 aluminum. In retrospect the carriers should have been made out of steel since the system is a prototype. More exotic materials could have been examined later and possibly the use of steel sleeves to protect the material interfaces. The initial design also included some complex shapes inside that carrier. Rounded edges had been designed to connect the two faces of the carrier; unfortunately these areas were in accessible by the tools available. These were unable to be machined and were altered by the manufacturer.

3.4.5 Housings

The housings needed to be made properly or none of the members would have lined up, which is crucial to the meshing of the gear teeth. There were four pieces that made up the housing, all made of aluminum 7075; a brief description is given of 2 sections pointing out the design features. Four sections had to be used so that assembly could take place. After the internal components were designed the housings were then created around them to facilitate a somewhat manageable assembly procedure. The housing for the drive motor, shown in figure 21, had to be made so that the coupling, which attached the AB motor to the sun shaft, was accessible from the outside. There were Allan screws that had to be tightened on the coupling once the motor was secured to the housing. The other three sections of housings, shown in figure 22, are nearly identical with the exception of the interface hole location for the braking mechanism. Cutaways were used so that the housings could be bolted together without interference. The fits for the bearing to housing interface were loose for all components, the idea was to make the assembly process easier and it proved to be so. The stack up for a carrier-planet assembly is shown in figure 23. The large bearing outside diameter fits into the housing using a mean loose fit, the inside diameter was a tight fit press onto the carrier shaft. Both an external snap ring on the carrier and an internal snap ring inside the housing held the bearing in place, this created compartments, which linked one stage to the next and facilitated the assembly.

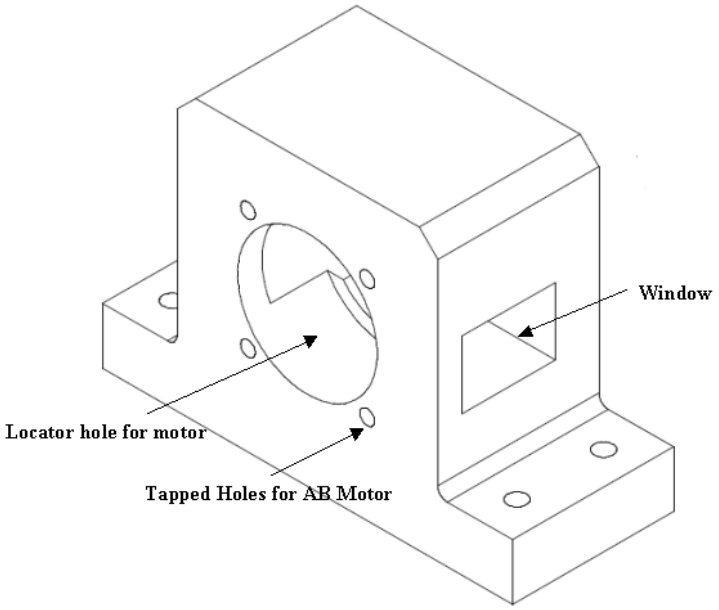


Figure 21 - Housing used to support AB motor.

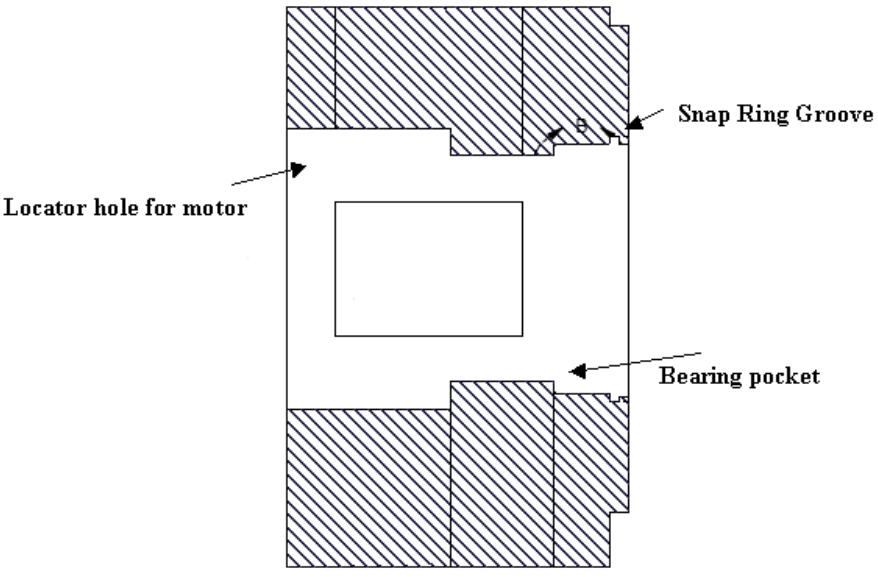


Figure 22 - Side view of first section of housing.

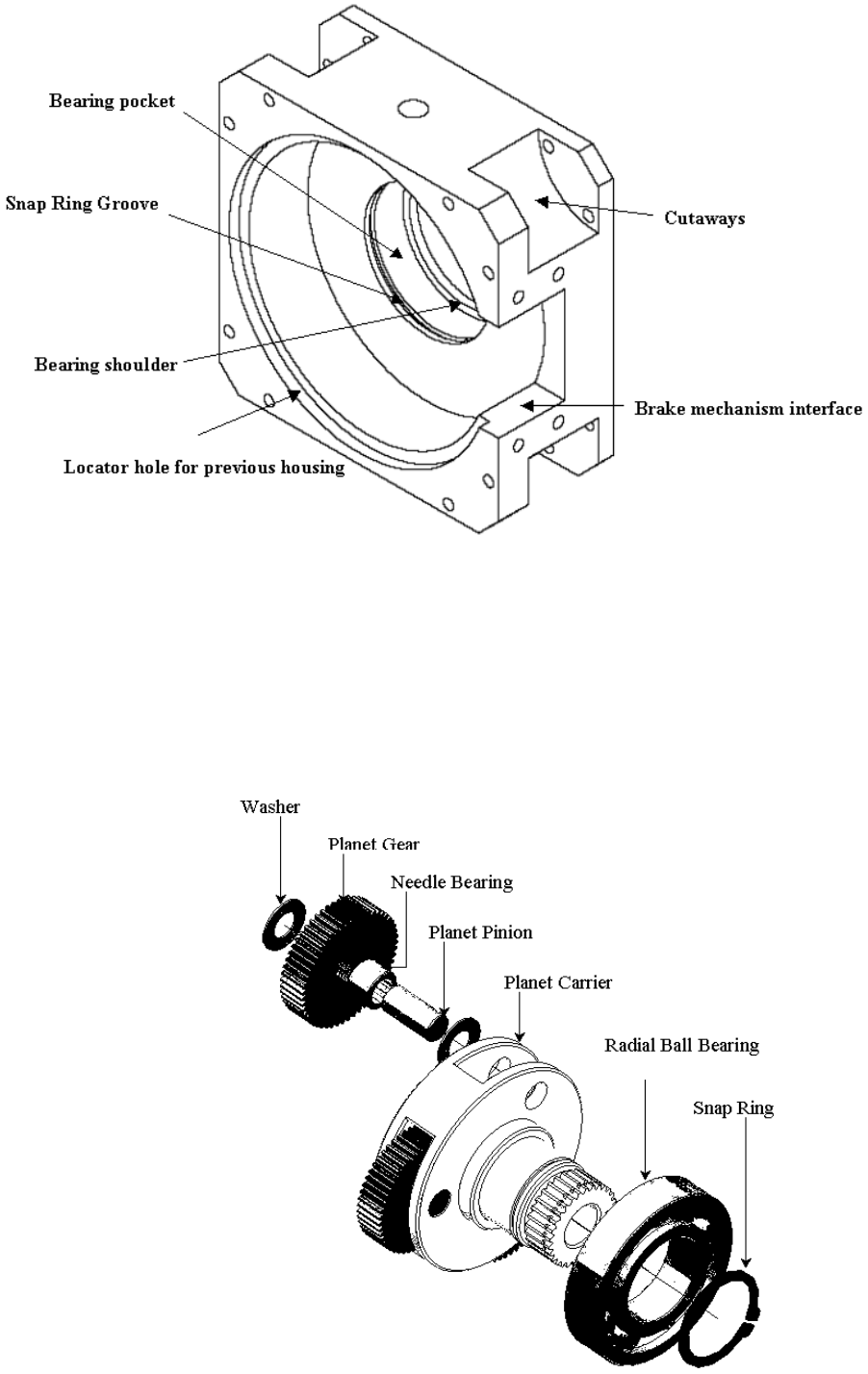


Figure 23 - Housing 1 and carrier-planet-bearing assembly.

3.5 Selection of Accessory Components

The accessory components were selected by Sriram Sridharan and the author and were purchased from various manufacturers. The availability of sizes and styles of each greatly influenced the design of the DVT. These included bearings snap rings and involute splines.

3.5.1 Bearings

Selection of bearings was a very time consuming endeavor. All bearings selected were from the Torrington Company bearing catalog. For the carriers a Fafnir 208K light series radial bearing, shown in figure 24, was chosen and for the single large bearing for ring 1, a 209K was chosen. The small sun shaft bearing was chosen to be a SK5 extra small series. This was the only bearing in the catalog that met our size requirements [7]. Half-inch full complement bearings with open ends were chosen for the spindles. Each bearing had a unique tolerance and dimension for housing and shaft size based on press fit, shoulder size and fillet radius, which are available on the drawings.

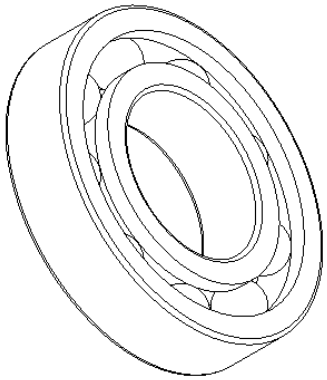


Figure 24 - Fafnir 208K radial bearing.

The assembly of the components was dependent upon the bearings and their fit. They were the members that held everything in place. The general rule used for press fits was that the rotating member was a tight press fit and the housing was a loose fit. This allowed the bearing to just drop in once they had been pressed onto the individual components in the system. The exception was the small bearing used on the input shaft, which was tight fit pressed into both the ring gear and onto the shaft itself. The needle bearings were cupped so they came equipped with an outer race, but the drill rod had to be polished so that it was a semi-loose fit into the bearing assembly. Figure 25 shows the relative press fits for both housing and shaft. For the rotating members (shafts) the selected fit was a k5. This was to ensure that there would be no movement of the shaft relative to the inner bearing race. If any movement occurred it could seriously damage the aluminum carriers. The fit used for the housings was an h6 and was used to ensure a clean fit but required no axial force to snug the components. The life of the bearings was not a major concern, since the DVT would not be expected to be in service for more than a few hours at a time. For a second-generation system serious consideration will have to be taken in selecting bearings that would handle the prescribed service. For here, only a simple life calculation was made based upon the following equation.

$$L_{10} = \frac{16667}{N}\left[\frac{C_E}{P}\right]^3 \text{ Hours} \tag{3.19}$$

Where N is the operating speed C_E, is the dynamic load rating and P is the radial load on the bearing [7].

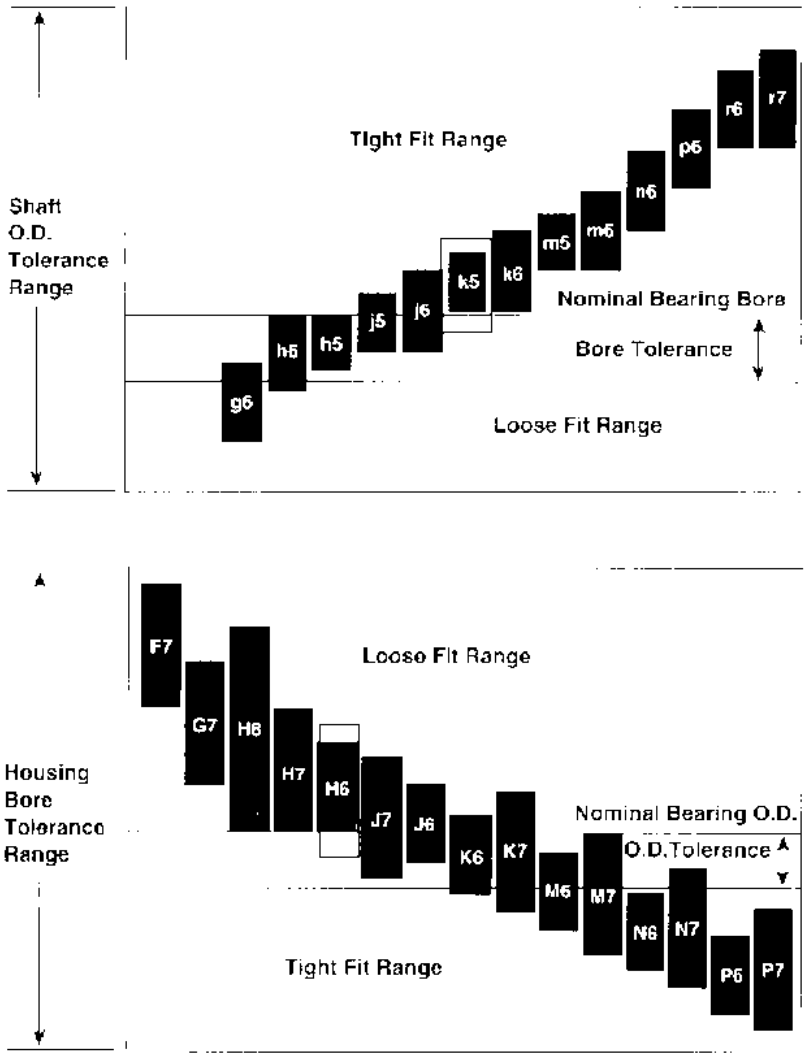


Figure 25 - Fit regions for Fafnir radial bearings [7].

3.5.2 Involute Splines

Involute spines have the same general form of internal and external involute gear teeth with a 30° pressure angle and one half the depth of a standard tooth [9]. In the design of a spline the length required to withstand the applied torque is:

$$L_{spline} = \frac{D_{re}^3}{D_p^2} \tag{3.20}$$

where D_{re} is the minor diameter of the external spline and D_p is the pitch diameter of the spline [8]. All splines were designed in accordance with ANSI standards and practices [9]. One major design concern was over the ability to join the carrier spline and the ring spline together since the rings were made of steel and the carriers were made of aluminum. As in figure 26, the splines come together in a tight fitting fashion. Obviously, if there were any errors in machining then the steel part could potentially ruin the aluminum part.

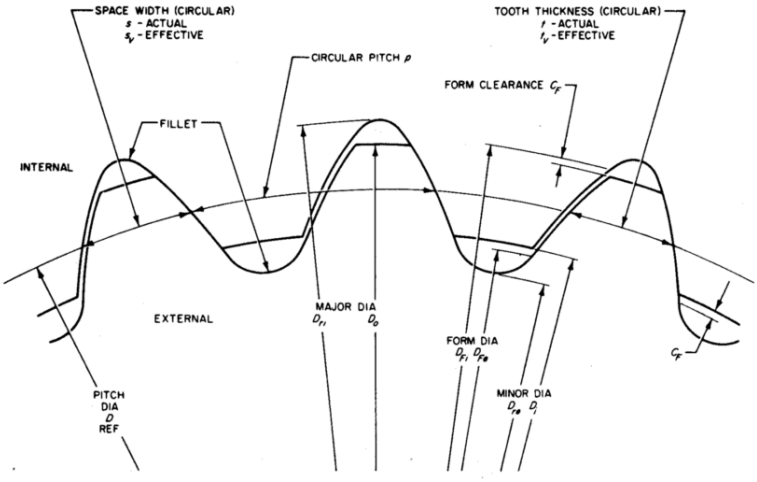
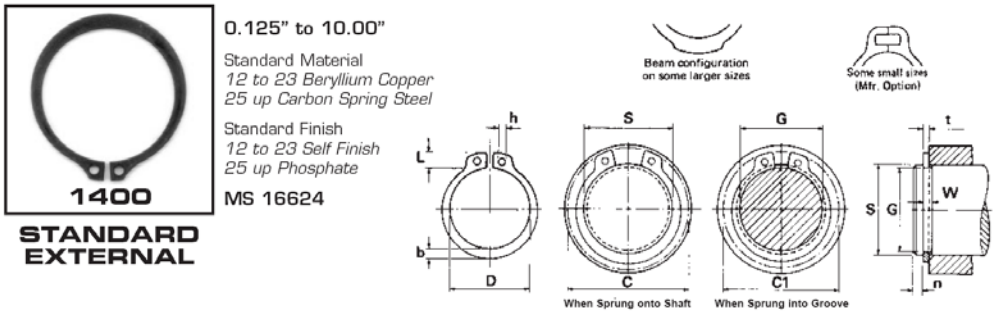


Figure 26 - Involute fillet root side fit spline geometry [9].

3.5.3 Snap Rings

The snap rings used in this design were made by ARCON. Both internal and externals were used [10]. Internal snap rings were used to retain bearings inside the housings and externals were used to secure the bearings to the shafts. Each roller bearing was retained with two. In the design of a snap ring groove width and depth, inner diameter and outer diameter are what need to be decided upon. The allowable tolerances for each of the dimensions are listed in figure 27. The most crucial part in designing for the fit of a snap ring is to ensure that the groove is wide enough and that there is plenty of room from the end of the grove to the object that the ring is retaining. This will guarantee that the assembly will take place without damaging the components. For example, if the groove has not been toleranced properly then scarring may occur during assembly or the part may need to be remade to accommodate the ring.



PART NUMBER	SHAFT DIAMETER S			RING									GROOVE					APPROX WT. LB / 1000 PCS.	THRUST LOAD (LBS)	PLIER No.
				THICKNESS		FREE DIAMETER							DIAMETER		WIDTH					
	Frac. inch	Dec. inch	mm	t inches	Tol. inches	D inches	Tol. inches	C	C1	L (max)	b ~	h (min)	G inches	Tol. inches	W inches	Tol. inches	n (min)			
1400-12	1/8	.125	–	.010	±.001	.112		.222	.214	.048	.018	.024	.117		.012		.014	.018	110	
1400-15	5/32	.156	–	.010		.142	+.002	.270	.260	.056	.026	.024	.146		.012		.017	.037	130	
1400-18	3/16	.188	–	.015		.168	-.004	.298	.286	.052	.025	.023	.175	±.0015	.018	+.002	.022	.059	240	Mini
1400-19	–	.197	5	.015		.179		.319	.307	.058	.026	.024	.185		.018	-.000	.020	.063	250	A
1400-21	7/32	.219	–	.015		.196		.338	.324	.058	.028	.024	.205		.018		.023	.074	280	
1400-23	15/64	.236	–	.015		.215		.355	.341	.058	.030	.024	.222		.018		.023	.086	310	
1400-25	1/4	.250	–	.025		.225		.45	.43	.083	.035	.039	.230		.029		.032	.21	700	
1400-27	–	.276	7	.025		.250		.48	.46	.094	.035	.039	.255		.029		.035	.23	770	

Figure 27 - Snap ring technical data [10].

3.5.4 Shaft Coupling

The input shaft of the system was designed using a flex coupling to connect the motor to the input shaft to allow for any misalignment, which could occur due to tolerancing or machining errors. This was done because the motor was bought from the factory without any modifications done to the motor output shaft, which limited the possible design configurations to either a keyway or smooth bore connection. The option taken was smooth bore to prevent weakening of the input shaft by a keyway. Considerations had to be made to keep rotational inertia and backlash to a minimum for the coupling. A survey of manufacturers was taken and Ruland Manufacturing Company, Inc. was chosen [11]. The coupling is made of Aluminum and the mechanism by which it corrects misalignment is a "bellows" or accordion type structure located between the two hubs. This will seat two shafts together without adding any backlash to the system, as shown in figure 28. The hub for the motor was machined to a 0.75-inch diameter and the input shaft hub to a 0.50-inch diameter. Tolerancing was of only a slight concern as each hub had a slice removed from it and had a tightening screw, which enabled the hub to be tightened down to the respective shaft. The specifications for the coupling are highlighted and found in figure 29.

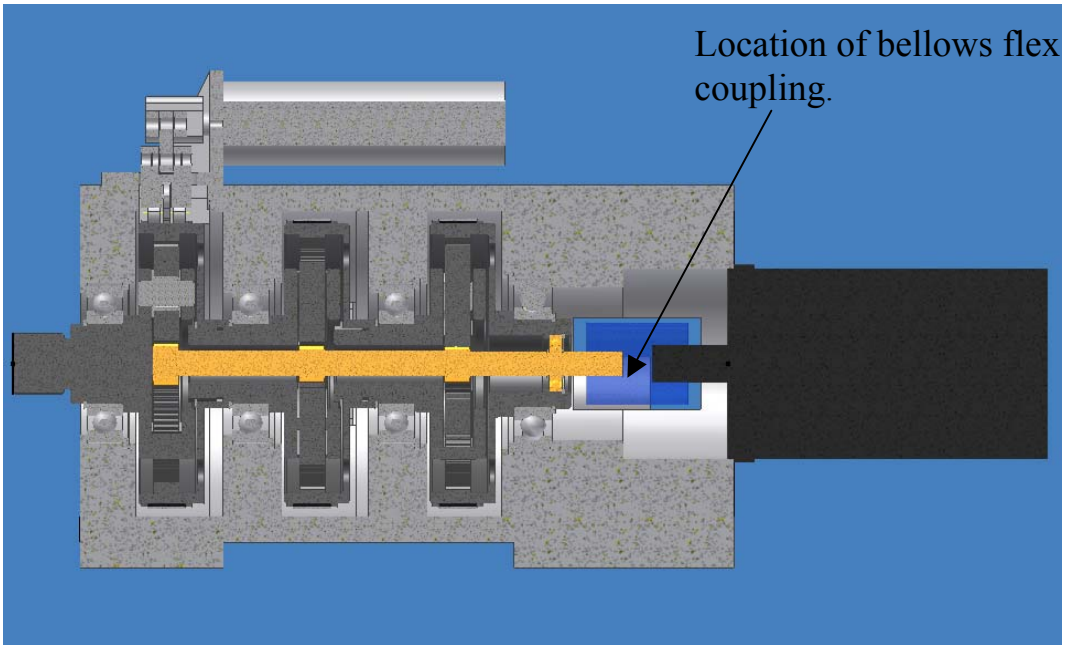
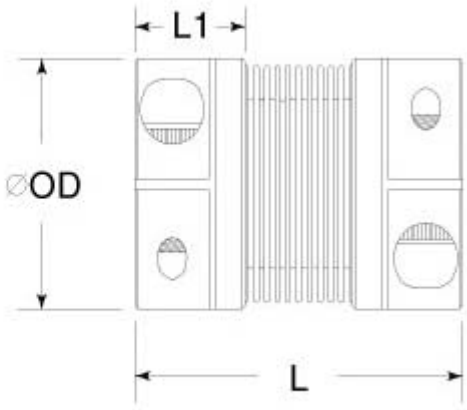


Figure 28 - Location of bellows coupling in the DVT.





PART NUMBER	BORE 1 (in)	BORE 2 (in)	OD (in)	LENGTH L (in)	CLAMP SCREW	HUB WIDTH L1 (in)	STATIC TORQUE (lb-in)	TORSIONAL STIFFNESS (lb-in/Deg)	MISALIGNMENT ANGULAR (Deg)	MISALIGNMENT PARALLEL (in)	AXIAL MOTION (in)
BC10	2 (.1250) 3 (.1875) 4 (.2500)	2 (.1250) 3 (.1875) 4 (.2500)	.590	29/32	#1-72	.340	22	88	1.50	.004	.008
BC12	3 (.1875) 4 (.2500) 5 (.3125)	3 (.1875) 4 (.2500) 5 (.3125)	.750	1 3/16	#2-56	.410	40	160	1.50	.004	.010
BC16	4 (.2500) 5 (.3125) 6 (.3750) 8 (.5000)	4 (.2500) 5 (.3125) 6 (.3750) 8 (.5000)	1.000	1 5/16	#4-40	.467	60	282	1.50	.004	.012
BC21	5 (.3125) 6 (.3750) 8 (.5000) 10 (.6250)	5 (.3125) 6 (.3750) 8 (.5000) 10 (.6250)	1.313	1 9/16	#6-32	.590	160	823	1.50	.006	.016
BC26	6 (.3750) 8 (.5000) 10 (.6250) 12 (.7500)	6 (.3750) 8 (.5000) 10 (.6250) 12 (.7500)	1.625	2	#8-32	.710	250	1640	2.00	.010	.020
BC32	8 (.5000) 10 (.6250) 12 (.7500) 14 (.8750) 16 (1.0000)	8 (.5000) 10 (.6250) 12 (.7500) 14 (.8750) 16(1.0000)	2.000	2 5/16	#10-32	.810	510	3320	2.00	.010	.020

Note 1 Static torque ratings are at maximum misalignment. To obtain dynamic rating, static ratings should be divided by 2 for non-reversing applications and by 4 for reversing applications.

Note 2 Performance ratings are for guidance only. The user must determine suitability for a particular application.

Figure 29- Bellows flex coupling and technical data [11].

3.6 Summary

The completed design went together and functioned almost flawlessly. More thought was needed on creating a better seal from housing to housing so that the transmission fluid wouldn't leak. Dissimilar material interfaces can also cause problems. It is not good to sacrifice quality for weight. If a phase two project is done then the DVT housing should be anodized to protect the housings. The design of the DVT was very challenging and much more was learned than was presented here.

Chapter 4

Modeling and Identification

It is impossible to sit at a desk and figure out how the world works: It also has to be studied. What this means is that at some point experimental data must be used to achieve an understanding of a physical system. This understanding can then lead to a physical or dynamic model that can be used to predict the behavior of the system. The technique used to build and complement models from such measurements is called identification [12]. If no information is known to develop a model then this process is referred to as "system identification", if the model form is known through the use of first principles and/or physical laws then it becomes "parameter identification". This chapter will discuss the theory and application of parameter identification and apply it to the aforementioned transmission.

4.1 Overview

There are, in principle, three different ways to use identification methods for modeling purposes.

1. Make simple experiments to facilitate the structuring of the problem.
2. Build models to describe how the outputs depend on the inputs that are not based on any physical insight of what is happening inside the system.
3. Use data to determine unknown parameters in a model obtained from physical modeling [12].

Because the simplified physical model form for the transmission could be estimated using first principles the third method was chosen. The System Identification Toolbox in Matlab was chosen to provide the platform for the analysis. The following lays out the steps taken to achieve a model based upon experimental data. Each of the following will be discussed at length in the proceeding sections.

1. Identification Theory
2. Model building
3. Experimental Setup
4. Data Collection
5. Data Analysis

4.2 Identification Theory

This section will give a brief description of some theory behind the SID and its application and is completely from Ljung [13]. The SID has many possible model types. For this application, the state space form was chosen due to the compatibility with the estimated equation of motion and the ease by which multi-input/output systems could be handled. For most physical systems it is easier to construct models with physical insight in continuous time rather than in discrete time, simply because most laws of physics (Newton's law of motion) are expressed in continuous time. Consider the system in figure 30 with a scalar input signal $u(t)$ and a scalar output signal $y(t)$.



Figure 30 - Single input single output system.

The system is said to be *time invariant* if its response to a certain input signal does not depend on absolute time. It is said to be *linear* if its output response to a linear combination of inputs is the same linear combination of the output responses of the individual inputs. It is also said to be *casual* if the output at a certain time depends on the input up to that time only. The general form of the state space model type for continuous time systems is the following.

$$\dot{x}(t) = F(\psi)\,x(t) + G(\psi)\,u(t) \tag{4.1}$$

$$y(t) = H\,x(t) \tag{4.2}$$

This is a linear time invariant system where F and G are matrices of appropriate dimensions ($n \times n$ and $n \times m$, respectively, for an n-dimensional state and an m-dimensional input). The over dot denotes differentiations with respect to time. ψ, is a vector of parameters that typically correspond to unknown values of physical coefficients such as moments of inertia or viscous damping. The modeling is carried out it terms of the state variables $x(t)$, which have physical significance, for this case velocity. The measured outputs $y(t)$ will be known combinations of the states. In this case the output vector $y(t)$ contains the measurements that

would be attained with ideal, noise free sensors. In reality, of course, some noise-corrupted version of $y(t)$ is obtained, as shown in figure 31, resulting from both measurement imperfections and disturbances. Within the linear framework it is assumed that these effects can be lumped into an additive term $v(t)$ at the output, which results in the adjusted output equation.

$$y(t) = H\,x(t) + v(t) \tag{4.3}$$

There are many sources and causes for such a disturbance term:

Measurement Noise: The sensors that measure the signals are subject to noise and drift.

Uncontrollable inputs: The system is subject to signals that have the character of inputs, but are not controllable by the user.

The character of the disturbances could also vary within wide ranges. Classical ways of describing disturbances in control have been to study steps, pulses, and sinusoids, while in stochastic control the disturbances are modeled as realizations of stochastic processes. The disturbances may in some cases be separately measurable, but in the typical situation they are noticeable only via their effect on the output. If the impulse response of the system is known, then of course the actual value of the disturbance $v(t)$ can be calculated at time t. Sometimes the measurements of the inputs to the system may also be noise corrupted. In such cases a pragmatic approach is taken and regard the measured input values as the actual inputs $u(t)$ to the process and their deviations from the true stimuli will be propagated through the system and lumped into the disturbance $v(t)$.

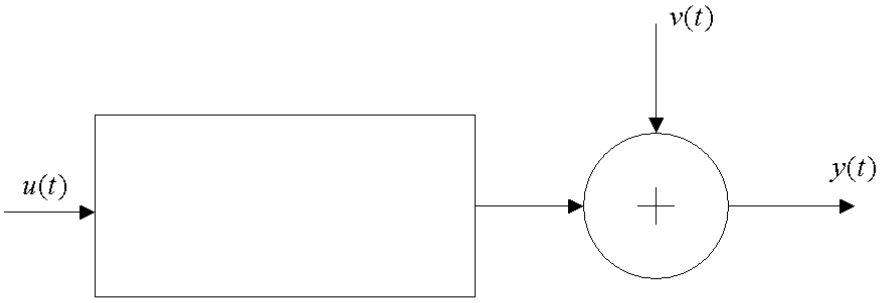


Figure 31 - System with disturbance.

For the case of a discrete system, from the perspective of time "t" statements regarding disturbances at times $t+k,\ k \geq 1$ are needed. A complete characterization would be to describe the conditional joint probability density function for $\{v(t+k),\ k \geq 1\}$, given $\{v(s),\ s \leq t\}$. This being too exhaustive a simpler approach is taken. Where the disturbances can be modeled as a function of white noise, $e(t)$.

$$v(t) = \sum_{k=0}^{\infty} h(k)\, e(t-k) \tag{4.4}$$

This could be suitable to describe "classical" disturbance patterns, steps, pulses, sinusoids, and ramps. At this point the continuous time state space equations must be converted to a discrete time model using the sampling interval T. The input then becomes the following:

$$u(t) = u_k = u(kT), \qquad kT \leq t < (k+1)T \tag{4.5}$$

with the disturbance effects at those time instants being:

$$v(t) = v_T(kT) \tag{4.6}$$

Then the differential equation can be solved from $t = kT$ to $t = kT + T$ yielding the equation:

$$x(kT+T) = A_T(\psi)\,x(kT) + B_T(\psi)\,u(kT) \tag{4.7}$$

where

$$A_T(\psi) = e^{F(\psi)T} \tag{4.8}$$

$$B_T(\psi) = \int_{\tau=0}^{T} e^{F(\psi)\tau} G(\psi)\,d\tau \tag{4.9}$$

Introducing q for the forward shift of T time units, the above can be rewritten as:

$$\left[qI - A_T(\psi)\right]x(kT) = B_T(\psi)\,u(kT) \tag{4.10}$$

or

$$y(kT) = G_T(q,\psi)\,u(kT) \tag{4.11}$$

$$G_T(q,\psi) = H\left[qI - A_T(\psi)\right]^{-1} B_T(\psi) \tag{4.12}$$

This results in an output equation in the sampled data form of:

$$y(t) = G_T(q,\psi)\,u(t) + v_T(t) \tag{4.13}$$

The term q is the forward shift operator and is defined by:

$$q\,u(t) = u(t+1) \tag{4.14}$$

The resulting state space expressed in discrete time is given by the following.

$$x(t+T) = A_T(\psi)\,x(t) + B_T(\psi)\,u(t) \tag{4.15}$$

$$y(t) = G_T(q,\psi)\,u(t) + v_T(t) \tag{4.16}$$

The SID toolbox however uses the innovations form of the above equation. This involves breaking the noise term $v(t)$ up into contributions from measurement

noise $v_m(t)$ and process noise $w(t)$ acting on the states and setting

$H = C(\psi)$ results in the equations:

$$x(t+T) = A_T(\psi)\,x(t) + B_T(\psi)\,u(t) + w(t) \tag{4.17}$$

$$y(t) = C(\psi)\,x(t) + v_m(t) \tag{4.18}$$

Here $w(t)$ and $v_m(t)$ are assumed to be sequences of independent random variables with zero mean values and covariances:

$$Ew(t)w^T(t) = R_1(\psi) \tag{4.19}$$

$$Ev_m(t)v^T(t) = R_2(\psi) \tag{4.20}$$

$$Ew(t)v_m^t(t) = R_{12}(\psi) \tag{4.21}$$

The disturbances $w(t)$ and $v_m(t)$ may often be signals whose physical origins are known. A load variation would be considered a "process noise", while inaccuracy in a potentiometer angular position sensor would be measurement noise. To predict the output $y(t)$ the Kalman filter is used. This is referred to as *prediction error modeling* (PEM). When the Kalman filter value is set to zero it then becomes *output error modeling* (OEM) which is the analysis procedure used on the DVT. The standard OEM is given by:

$$\hat{x}(t+T,\psi) = A(\psi)\,\hat{x}(t,\psi) + B(\psi)\,u(t) + K(\psi)\,e(t) \tag{4.22}$$

$$y(t) = C(\psi)\,\hat{x}(t,\psi) + e(t) \tag{4.23}$$

with

$$K(\psi) = 0 \tag{4.24}$$

and since $e(t)$ appears explicitly, this representation is known as *the innovations form* of the state-space description. The innovation is the part of the output $y(t)$ that cannot be predicted from past data. The Kalman filter or gain is a tool to help "fit' the model to the data, assuming that there are disturbances large enough to alter their agreement. This was excluded from the modeling process because the nature of the disturbances was unknown. Usually a good match between data and model will always be achieved using a PEM but understanding what the software has taken as disturbances is not straightforward and therefore results from such a model would not be reliable in determining parameters of the DVT. When, $K(\psi) = 0$, then the OEM is constructed from past inputs only and is considered a special case. The *natural predictor* for the OEM is then given by:

$$\hat{y}\langle t|\psi\rangle = C(\psi)\left[qI - A(\psi)\right]^{-1} B(\psi)u(t) \tag{4.25}$$

where the output is given by

$$y(t) = G_T(q,\psi)u(t) + H(q,\psi)e(t) \tag{4.26}$$

and

$$H(q) = 1 \tag{4.27}$$

This means that the noise source will be the difference between the actual output and the noise-free output. The aforementioned was given to familiarize and show the complexities involved in the identification process and why the SID toolbox was chosen to do the work. This is a fraction of what is fully contained in the SID toolbox and its capabilities.

4.3 Dynamic Model

To begin modeling, the inputs, outputs and all other quantities and variables that affect the system must be clarified. For this system the inputs are motor current from the Allan Bradley motor and brake motor current from the Maxon brake motor, for first gear. The outputs were chosen due to the ease of which they could be measured and were chosen to be drive shaft speed (sun speed) and carrier3 speed. This is a two-degree of freedom system, any two independent variables could have been chosen. Figure 32 shows the system. The transmission to be modeled has three distinct operating conditions; it is either in gear 1, 2 or 3. There are however transient conditions during the change from gear to gear. The transient results from the engagement of a particular band brake, which in turn brings the speed of the ring gear acted upon to zero after some time. The model was built to enable an analysis of the transient braking behavior experienced during ring gear engagement. In other words, it is a *general model* for any state the transmission may be in, granted that all components in the system are rigid. Since all of the brake systems are identical, gear 1 was chosen as the focus of the model. That is, band brake 1 will be the only brake engaged at any time. Due to the complexity of the system, Lagrange's Equations using virtual work were used to create the model. The model shown will be developed using Lagrange's Equations with virtual work. The following describes the theory involved in developing the model and was taken from Kelly [14].

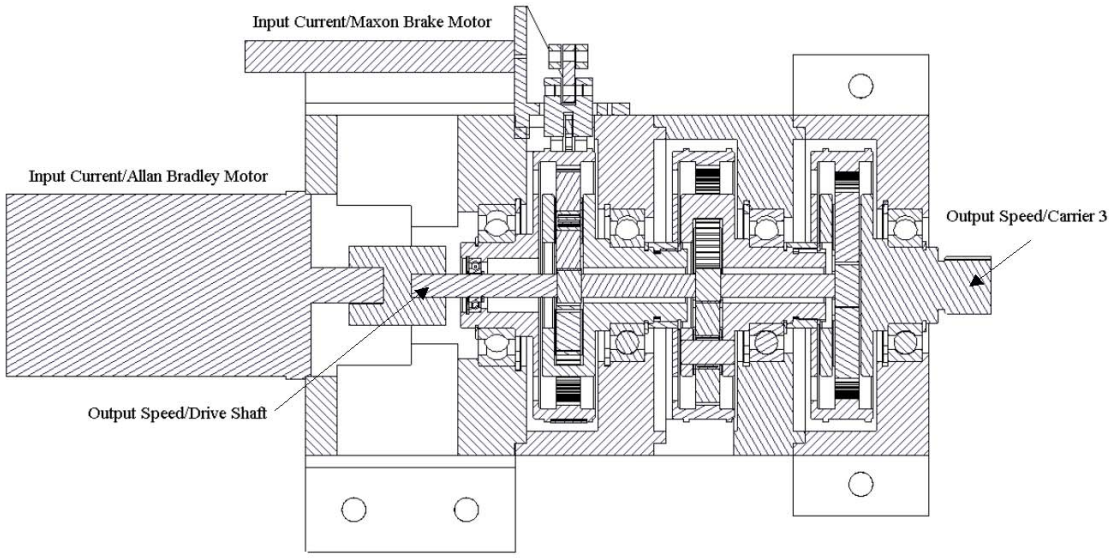


Figure 32 - Inputs and Outputs for the system model.

When viewing an N-degree of freedom system with generalized coordinates $\theta_1, \theta_2, \ldots, \theta_N$ acted on by external non-conservative forces, any kinematically admissible displacement may be specified by:

$$\theta_1 + \delta\theta_1, \theta_2 + \delta\theta_2, \ldots, \theta_N + \delta\theta_N \tag{4.28}$$

where a non-conservative force is one where the work of the force is not independent of the path taken from a to b. The variations in the displacements are called *virtual displacements.* The work done by the non-conservative forces as the system moves through the virtual displacements is called the *virtual work* and is calculated by using the usual definition of work done by a force. The virtual work can be written in the form,

$$\delta W = \sum_{i=1}^{N} Q_i \, \delta\theta_i \tag{4.29}$$

Where the Q_i terms are the generalized torques or applied torques excluding all constraint torques and internal torques and forces. The forces can be as a result from external driving forces, forces caused by viscous friction or any other force acting upon the system that are non-conservative. Lagrange's equations for a non-conservative system then take the form,

$$\frac{d}{dt}\left(\frac{\partial L}{\partial \dot{\theta}_i}\right) - \frac{\partial L}{\partial \theta_i} = Q_i \qquad i, \ldots, N \tag{4.30}$$

In the case of the DVT there are no changes in potential energy since the system is considered to be rigid therefore the Lagrangian "$L = K - V$", reduces to the

sum of the kinetic energies [15]. The first component to be modeled will be the drive shaft shown in figure 33.

Assuming the shaft is rigid:

$$\theta_m = \theta_{s1} = \theta_{s2} = \theta_{s3} = \theta_s \tag{4.31}$$

$$J_s = J_m + J_{s1} + J_{s2} + J_{s3} + J_{shaft} \tag{4.32}$$

$$K_s = \frac{1}{2} J_s \dot{\theta}_s^2 \tag{4.33}$$

$$\delta W_s = (T_m - b_{s1}(\dot{\theta}_s - \dot{\theta}_{r1}))\delta\theta_s \tag{4.34}$$

To determine energies about the planets own center, as shown in figures 34 and 35, the three sets of three planets will be simplified to three total planets one planet in each set (lumped).

For the first set:

$$K_{p1} = \frac{1}{2} J_{p1} \dot{\theta}_{p1}^{\,2} \tag{4.35}$$

$$\delta W_{p1} = -b_{p1} \dot{\theta}_{p1} \delta\theta_{p1} \tag{4.36}$$

Second set,

$$K_{p2} = \frac{1}{2} J_{p2} \dot{\theta}_{p2}^{\,2} \tag{4.37}$$

$$\delta W_{p2} = -b_{p2} \dot{\theta}_{p2} \delta\theta_{p2} \tag{4.38}$$

and the third set,

$$K_{p3} = \frac{1}{2} J_{p3} \dot{\theta}_{p3}^{\,2} \tag{4.39}$$

$$\delta W_{p3} = -b_{p3} \dot{\theta}_{p3} \delta\theta_{p3} \tag{4.40}$$

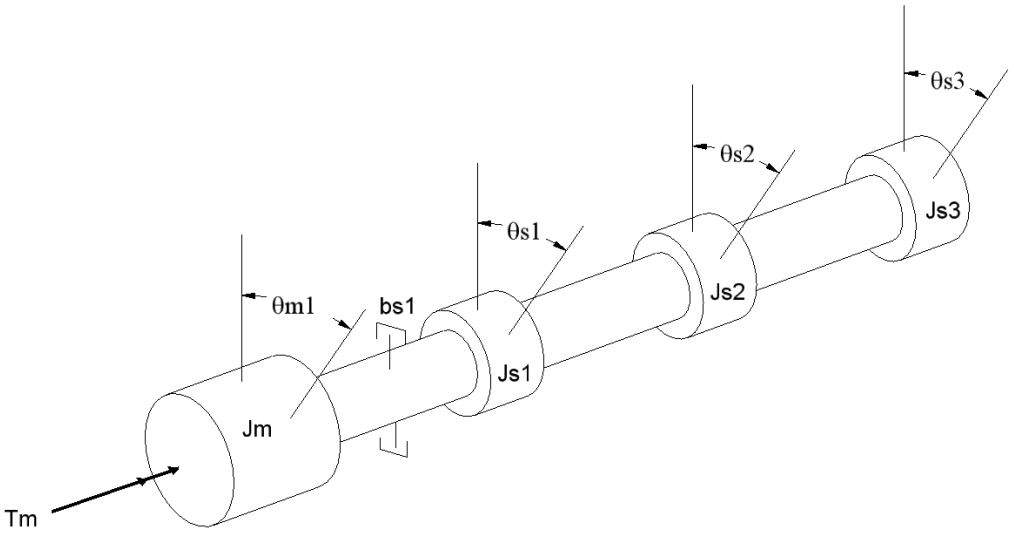
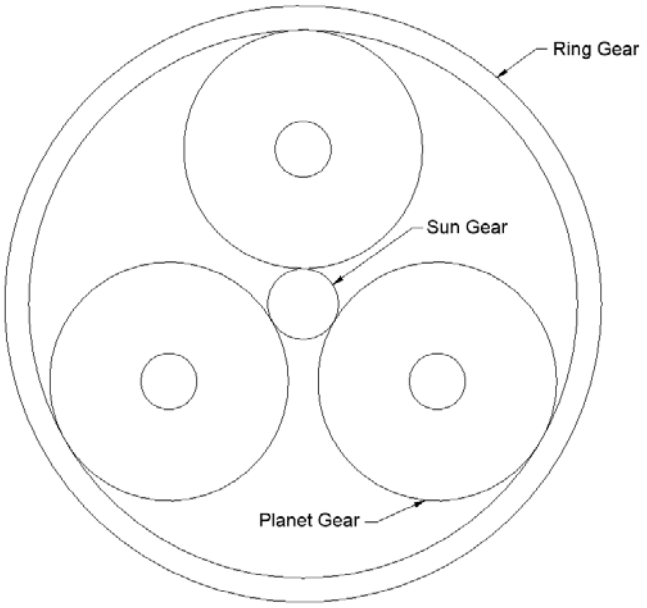


Figure 33 - Drive shaft free body diagram.



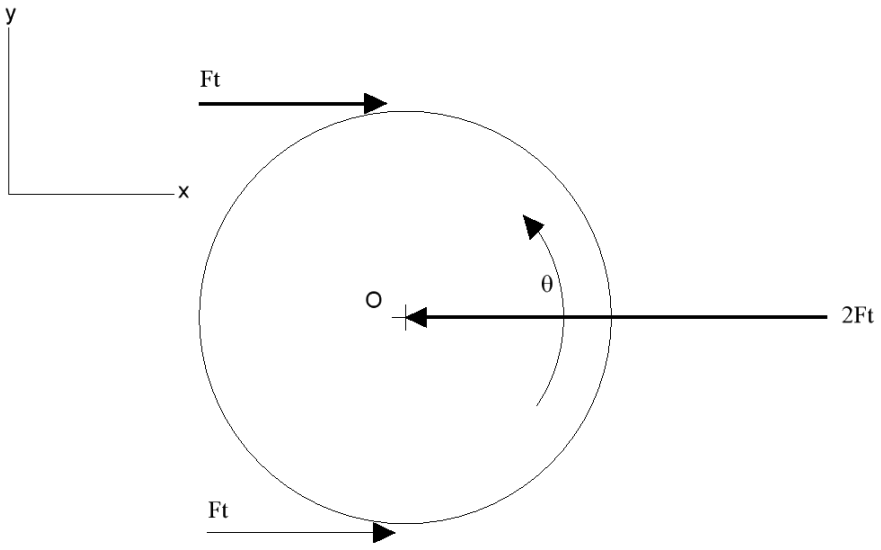


Figure 34 - Planet configuration in the DVT.

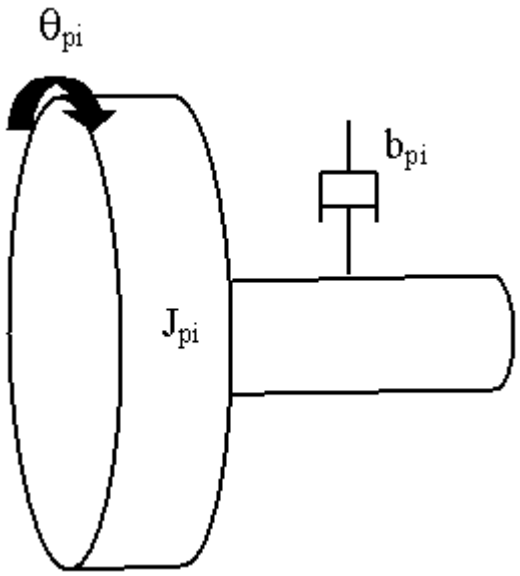


Figure 35- Planet gear free body diagram, motion about own center.

The free body diagram for the first stage ring is shown in figure 36 and the equations of motion for the first ring gear are:

$$K_{r1} = \frac{1}{2} J_{r1} \dot{\theta}_{r1}^{\ 2} \tag{4.41}$$

$$\delta W_{r1} = (T_{Brake} - b_{s1}(\dot{\theta}_{r1} - \dot{\theta}_s) - b_{r1}\dot{\theta}_{r1})\delta\theta_{r1} \tag{4.42}$$

The first carrier is rigidly connected with the ring of the second, as shown in figure 37, set therefore the mass of the carrier; ring and planets about the center of the carrier rotation are summed together:

$$\theta_{c1} = \theta_{r2} \tag{4.43}$$

$$K_{c1} = \frac{1}{2} J_{c1} \dot{\theta}_{c1}^{\ 2} \tag{4.44}$$

$$J_{c1} = J_c + J_{pc1} + J_{r2} \tag{4.45}$$

$$\delta W_{c1} = -b_{c1}\dot{\theta}_{c1}\delta\theta_{c1} \tag{4.19}$$

For second carrier and third ring the same holds:

$$\theta_{c2} = \theta_{r3} \tag{4.20}$$

$$K_{c2} = \frac{1}{2} J_{c2} \dot{\theta}_{c2}^{\ 2} \tag{4.21}$$

$$J_{c2} = J_c + J_{pc2} + J_{r3} \tag{4.22}$$

$$\delta W_{c2} = -b_{c2}\dot{\theta}_{c2}\delta\theta_{c2} \tag{4.23}$$

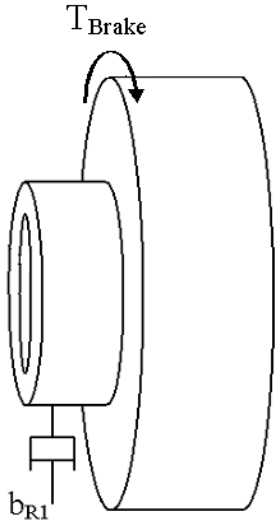


Figure 36 - Ring gear that is experiencing braking.

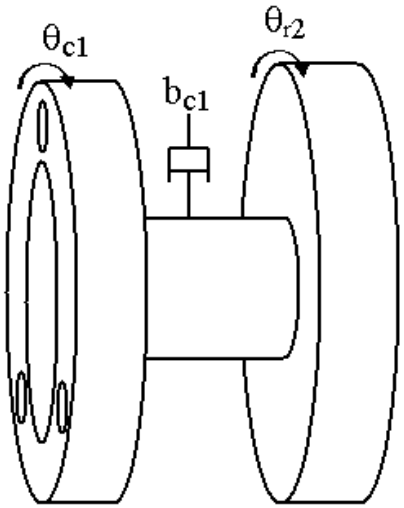


Figure 37 - Carrier 1 and ring 2 coupled together.

For the third carrier the free body diagram of figure 38 gives the equations of motion:

$$K_{c3} = \frac{1}{2} J_{c3} \dot{\theta}_{c3}^{\ 2} \tag{4.24}$$

$$\delta W_{c3} = (T_{Load} - b_{c3} \dot{\theta}_{c3}) \delta\theta_{c3} \tag{4.25}$$

Now that the equations for the individual component have been written they can be combined to represent the entire system.

$$K_{system} = \sum K_i \tag{4.26}$$

$$K_{system} = K_s + K_{p1} + K_{p2} + K_{p3} + K_{r1} + K_{c1} + K_{c2} + K_{c3} \tag{4.27}$$

$$\begin{aligned} K_{system} = {} & \frac{1}{2} J_s \dot{\theta}_s^2 + \frac{1}{2} J_{p1} \dot{\theta}_{p1}^{\ 2} + \frac{1}{2} J_{p2} \dot{\theta}_{p2}^{\ 2} + \frac{1}{2} J_{p3} \dot{\theta}_{p3}^{\ 2} + \frac{1}{2} J_{r1} \dot{\theta}_{r1}^{\ 2} \\ & + \frac{1}{2} J_{c1} \dot{\theta}_{c1}^{\ 2} + \frac{1}{2} J_{c2} \dot{\theta}_{c2}^{\ 2} + \frac{1}{2} J_{c3} \dot{\theta}_{c3}^{\ 2} \end{aligned} \tag{4.28}$$

The virtual work may be written as:

$$\delta W_{system} = \sum Q_i \delta\theta_i \tag{4.29}$$

$$\begin{aligned} \delta W_{system} = {} & Q_s \delta\theta_s + Q_{p1} \delta\theta_{p1} + Q_{p2} \delta\theta_{p2} + Q_{p3} \delta\theta_{p3} + Q_{r1} \delta\theta_{r1} \\ & + Q_{c1} \delta\theta_{c1} + Q_{c2} \delta\theta_{c2} + Q_{c3i} \delta\theta_{c3} \end{aligned} \tag{4.30}$$

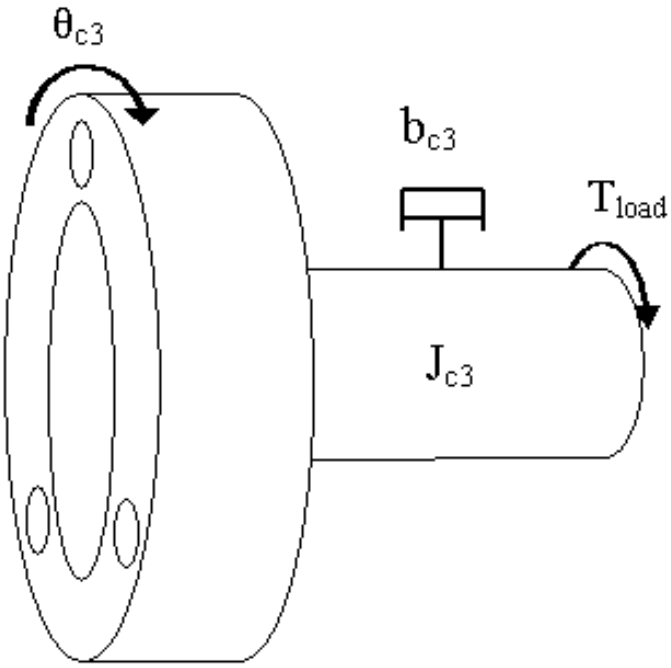


Figure 38 - Free body diagram of carrier 3.

$$\begin{aligned}\delta W_{system} = {} & (T_m - b_{s1}(\dot{\theta}_s - \dot{\theta}_{R1}))\delta\theta_s - b_{p1}\dot{\theta}_{p1}\delta\theta_{p1} - b_{p2}\dot{\theta}_{p2}\delta\theta_{p2} \\ & - b_{p3}\dot{\theta}_{p3}\delta\theta_{p3} + (T_{Brake} - b_{s1}(\dot{\theta}_{r1} - \dot{\theta}_s) - b_{r1}\dot{\theta}_{r1})\delta\theta_{r1} - b_{c1}\dot{\theta}_{c1}\delta\theta_{c1} \\ & - b_{c2}\dot{\theta}_{c2}\delta\theta_{c2} + (T_{Load} - b_{c3}\dot{\theta}_{c3})\delta\theta_{c3}\end{aligned} \tag{4.31}$$

At this point the speed equations are introduced, remembering that the outputs of the system are the shaft speed and the carrier 3 speed. Therefore the equations must be reduced to those coordinates. Note that this is a two degree of freedom system when there is no brake engaged and during the transient brake engagement. Only when the ring gear speed reaches a constant speed, as in zero, can this system be reduced to one degree of freedom. The excess coordinates are referred to as superfluous coordinates since only two coordinates are needed. Because the speed equations or constraints can be used to eliminate these then the constraints are referred to as holonomic [15].

Using the basic speed equations for the system kept in two degree of freedom form the following were derived [19].

$$\dot{\theta}_{c1} = \frac{\dot{\theta}_{r1}N_{r1} + \dot{\theta}_s N_{s1}}{N_{r1} + N_{s1}} \tag{4.32}$$

$$\dot{\theta}_{c2} = \frac{\dot{\theta}_{r2}N_{r2} + \dot{\theta}_s N_{s2}}{N_{r2} + N_{s2}} \tag{4.33}$$

$$\dot{\theta}_{c3} = \frac{\dot{\theta}_{r3}N_{r3} + \dot{\theta}_s N_{s3}}{N_{r3} + N_{s3}} \tag{4.34}$$

$$\dot{\theta}_{p1} = \frac{\dot{\theta}_s N_{s1} - \dot{\theta}_{c1}(N_{s1} + N_{p1})}{N_{p1}} \tag{4.35}$$

$$\dot{\theta}_{p2} = \frac{\dot{\theta}_s N_{s2} - \dot{\theta}_{c2}(N_{s2} + N_{p2})}{N_{p2}} \tag{4.36}$$

$$\dot{\theta}_{p3} = \frac{\dot{\theta}_s N_{s3} - \dot{\theta}_{c3}(N_{s3} + N_{p3})}{N_{p3}} \tag{4.37}$$

A general set of speed equations for each component was derived using only the coordinates needed, namely $\dot{\theta}_{c3}$ and $\dot{\theta}_s$. Doing this required some intensive algebra and MathCAD was utilized in maintaining accuracy in the derivations. Keep in mind that the carrier of one set is connected to the ring of the next, as mentioned earlier.

For planet 1 about it's own axis:

$$\begin{aligned}\dot{\theta}_{p1} = & \left(\frac{N_{s1}}{N_{p1}} - \frac{(-N_{s3}N_{r2} - N_{s3}N_{s2} - N_{r3}N_{s2})(N_{s1} + N_{p1})}{N_{r3}N_{r2}N_{p1}}\right)\dot{\theta}_s \\ & + \left(\frac{(-N_{s3}N_{s2} - N_{r3}N_{r2} - N_{r3}N_{s2} + N_{s3}N_{r2})(N_{s1} + N_{p1})}{N_{r3}N_{s2}N_{p1}}\right)\dot{\theta}_{c3}\end{aligned} \tag{4.38}$$

For planet 2 about it's own axis:

$$\dot{\theta}_{p2} = \left(\frac{N_{s2}}{N_{p2}} + \frac{(N_{s3})(N_{s2} + N_{p2})}{N_{r3}N_{p2}}\right)\dot{\theta}_s + \left(\frac{(-N_{r3} - N_{s3})(N_{s2} + N_{p2})}{N_{r3}N_{p2}}\right)\dot{\theta}_{c3} \tag{4.39}$$

For planet 3 about it's own axis:

$$\dot{\theta}_{p3} = \frac{\dot{\theta}_s N_{s3} - \dot{\theta}_{c3}(N_{s3} + N_{p3})}{N_{p3}} \tag{4.40}$$

For ring gear 1 in terms of output coordinates:

$$\dot{\theta}_{r1} = \frac{(-N_{r3}N_{s2}N_{s1} - N_{r3}N_{r2}N_{s1} - N_{s3}N_{s2}N_{r1} - N_{s3}N_{s2}N_{s1} - N_{s3}N_{r2}N_{r1} - N_{s3}N_{r2}N_{s1} - N_{r3}N_{s2}N_{r1})}{N_{r3}N_{r2}N_{r1}}\dot{\theta}_s$$
$$+ \frac{(N_{r3}N_{s2}N_{r1} + N_{r3}N_{s2}N_{s1} + N_{s3}N_{r2}N_{s1} + N_{s3}N_{s2}N_{r1} + N_{s3}N_{s2}N_{s1} + N_{s3}N_{r2}N_{r1} + N_{r3}N_{r2}N_{r1} + N_{r3}N_{r2}N_{s1})}{N_{r3}N_{r2}N_{r1}}\dot{\theta}_{c3} \tag{4.41}$$

For carrier1/ring 2/planet1, the planet has two velocities, one about it's own center and one about the center of the carrier:

$$\dot{\theta}_{c1} = \frac{(-N_{s3}N_{r2} - N_{s3}N_{s2} - N_{r3}N_{s2})}{N_{r3}N_{r2}}\dot{\theta}_s + \frac{(N_{s3}N_{s2} + N_{r3}N_{r2} + N_{r3}N_{s2} + N_{s3}N_{r2})}{N_{r3}N_{s2}}\dot{\theta}_{c3} \tag{4.42}$$

For carrier2/ring 3/planet3:

$$\dot{\theta}_{c2} = \frac{-N_{s3}}{N_{r3}}\dot{\theta}_s + \frac{(N_{r3} + N_{s3})}{N_{r3}}\dot{\theta}_{c3} \tag{4.43}$$

The number of teeth on each gear, determined by George Bowers to meet the ratio requirements, is constant and therefore using:

$$N_{s1} = 16$$
$$N_{s2} = 16$$
$$N_{s3} = 20$$
$$N_{p1} = 53$$
$$N_{p2} = 53$$
$$N_{p3} = 50$$
$$N_{r1} = 121$$
$$N_{r2} = 121$$
$$N_{r3} = 123$$

The speed equations were reduced to for the planets:

$$\dot{\theta}_{p1} = \frac{279970}{391193}\dot{\theta}_s - \frac{671163}{391193}\dot{\theta}_{c3} \tag{4.44}$$

$$\dot{\theta}_{p2} = \frac{1666}{3233}\dot{\theta}_s - \frac{4899}{3233}\dot{\theta}_{c3} \tag{4.45}$$

$$\dot{\theta}_{p3} = \frac{2}{5}\dot{\theta}_s - \frac{7}{5}\dot{\theta}_{c3} \tag{4.46}$$

For ring 1:

$$\dot{\theta}_{r1} = \frac{-439498}{893101}\dot{\theta}_s + \frac{1332599}{893101}\dot{\theta}_{c3} \tag{4.47}$$

For carrier 1:

$$\dot{\theta}_{c1} = \frac{-2346}{7381}\dot{\theta}_s + \frac{9727}{7381}\dot{\theta}_{c3} \tag{4.48}$$

For carrier 2:

$$\dot{\theta}_{c2} = \frac{-10}{61}\dot{\theta}_s + \frac{71}{61}\dot{\theta}_{c3} \tag{4.49}$$

Making the appropriate substitutions into the kinetic energy equation,

$$\begin{aligned} K_{system} = {} & \frac{1}{2}J_s\,\dot{\theta}_s^2 + \frac{1}{2}J_{p1}\,\dot{\theta}_{p1}{}^2 + \frac{1}{2}J_{p2}\,\dot{\theta}_{p2}{}^2 + \frac{1}{2}J_{p3}\,\dot{\theta}_{p3}{}^2 \\ & + \frac{1}{2}J_{r1}\,\dot{\theta}_{r1}{}^2 + \frac{1}{2}J_{c1}\,\dot{\theta}_{c1}{}^2 + \frac{1}{2}J_{c2}\,\dot{\theta}_{c2}{}^2 + \frac{1}{2}J_{c3}\,\dot{\theta}_{c3}{}^2 \end{aligned} \tag{4.50}$$

$$\begin{aligned} K_{system} = {} & \frac{1}{2}J_s\,\dot{\theta}_s^2 + \frac{1}{2}J_{p1}\left(\frac{279970}{391193}\dot{\theta}_s - \frac{671163}{391193}\dot{\theta}_{c3}\right)^2 + \frac{1}{2}J_{p2}\left(\frac{1666}{3233}\dot{\theta}_s - \frac{4899}{3233}\dot{\theta}_{c3}\right)^2 \\ & + \frac{1}{2}J_{p3}\left(\frac{2}{5}\dot{\theta}_s - \frac{7}{5}\dot{\theta}_{c3}\right)^2 + \frac{1}{2}J_{r1}\left(\frac{-439498}{893101}\dot{\theta}_s + \frac{1332599}{893101}\dot{\theta}_{c3}\right)^2 \\ & + \frac{1}{2}J_{c1}\left(\frac{-2346}{7381}\dot{\theta}_s + \frac{9727}{7381}\dot{\theta}_{c3}\right)^2 + \frac{1}{2}J_{c2}\left(\frac{-10}{61}\dot{\theta}_s + \frac{71}{61}\dot{\theta}_{c3}\right)^2 + \frac{1}{2}J_{c3}\,\dot{\theta}_{c3}{}^2 \end{aligned} \tag{4.51}$$

The next step in finding the Lagrangian is to take the partial derivatives of the kinetic energy term with respect to both coordinates.

$$\begin{aligned} \frac{\partial K_{system}}{\partial \dot{\theta}_s} = {} & \left(J_s + .512201J_{p1} + .265545J_{p2} + .16J_{p3} + .026874J_{c2} + .101024J_{c1} + .242166J_{r1}\right)\dot{\theta}_s \\ & + \left(-1.22788J_{p1} - .780856J_{p2} - .56J_{p3} - .190809J_{c2} - .418867J_{c1} - .734269J_{r1}\right)\dot{\theta}_{c3} \end{aligned} \tag{4.52}$$

$$\frac{\partial K_{system}}{\partial \dot{\theta}_{c3}} = \left(-1.228J_{p1} - .781J_{p2} - .56J_{p3} - .191J_{c2} - .419J_{c1} - .734J_{r1}\right)\dot{\theta}_s + \left(2.944J_{p1} + 2.296J_{p2} + 1.96J_{p3} + 1.355J_{c2} + 1.737J_{c1} + J_{c3} + 2.226J_{r1}\right)\dot{\theta}_{c3} \tag{4.53}$$

Once the partials are found then the derivative of each must be taken with respect to time, which results in,

$$\frac{d}{dt}\left(\frac{\partial K_{system}}{\partial \dot{\theta}_s}\right) = \left(J_s + .512201J_{p1} + .265545J_{p2} + .16J_{p3} + .026874J_{c2} + .101024J_{c1} + .242166J_{r1}\right)\ddot{\theta}_s + \left(-1.22788J_{p1} - .780856J_{p2} - .56J_{p3} - .190809J_{c2} - .418867J_{c1} - .734269J_{r1}\right)\ddot{\theta}_{c3} \tag{4.54}$$

$$\frac{d}{dt}\left(\frac{\partial K_{system}}{\partial \dot{\theta}_{c3}}\right) = \left(-1.228J_{p1} - .781J_{p2} - .56J_{p3} - .191J_{c2} - .419J_{c1} - .734J_{r1}\right)\ddot{\theta}_s + \left(2.944J_{p1} + 2.296J_{p2} + 1.96J_{p3} + 1.355J_{c2} + 1.737J_{c1} + J_{c3} + 2.226J_{r1}\right)\ddot{\theta}_{c3} \tag{4.55}$$

From the principal of virtual work we recall that if there is no change in the potential energy,

$$\frac{d}{dt}\left(\frac{\partial K_{system}}{\partial \dot{\theta}_s}\right) = Q_s \tag{4.56}$$

$$\frac{d}{dt}\left(\frac{\partial K_{system}}{\partial \dot{\theta}_{c3}}\right) = Q_{c3} \tag{4.57}$$

To determine the Q's,

$$\begin{aligned}\delta W_{system} &= (T_m - b_{s1}(\dot{\theta}_s - \dot{\theta}_{R1}))\delta\theta_s - b_{p1}\dot{\theta}_{p1}\delta\theta_{p1} - b_{p2}\dot{\theta}_{p2}\delta\theta_{p2} - b_{p3}\dot{\theta}_{p3}\delta\theta_{p3} \\ &+ (T_{Brake} - b_{s1}(\dot{\theta}_{r1} - \dot{\theta}_s) - b_{r1}\dot{\theta}_{r1})\delta\theta_{r1} - b_{c1}\dot{\theta}_{c1}\delta\theta_{c1} \\ &- b_{c2}\dot{\theta}_{c2}\delta\theta_{c2} + (T_{Load} - b_{c3}\dot{\theta}_{c3})\delta\theta_{c3}\end{aligned} \tag{4.58}$$

At this point the speed equations are known and can be substituted but the virtual displacements must also be found in order to properly distribute the effects of damping and of the input torques, this is done by determining the constraint between the virtual displacements. Since the system is rigid and there is no relative movement between the gears the speed equations can be applied as position constraints as well. Therefore the general constraints for the system are,

$$\partial\theta_{p1} = \frac{279970}{391193}\partial\theta_s - \frac{671163}{391193}\partial\theta_{c3} \tag{4.59}$$

$$\partial\theta_{p2} = \frac{1666}{3233}\partial\theta_s - \frac{4899}{3233}\partial\theta_{c3} \tag{4.60}$$

$$\partial\theta_{p3} = \frac{2}{5}\partial\theta_s - \frac{7}{5}\partial\theta_{c3} \tag{4.61}$$

$$\partial\theta_{r1} = \frac{-439498}{893101}\partial\theta_s + \frac{1332599}{893101}\partial\theta_{c3} \tag{4.62}$$

$$\partial\theta_{c1} = \frac{-2346}{7381}\partial\theta_s + \frac{9727}{7381}\partial\theta_{c3} \tag{4.63}$$

$$\partial\theta_{c2} = \frac{-10}{61}\partial\theta_s + \frac{71}{61}\partial\theta_{c3} \tag{4.64}$$

Making all of the substitutions into the virtual work term,

$$\begin{aligned}
\delta W_{system} &= (T_m - b_{s1}(\dot{\theta}_s - \dot{\theta}_{R1}))\delta\theta_s \\
&\quad - b_{p1}\left(\frac{279970}{391193}\dot{\theta}_s - \frac{671163}{391193}\dot{\theta}_{c3}\right)\left(\frac{279970}{391193}\partial\theta_s - \frac{671163}{391193}\partial\theta_{c3}\right) \\
&\quad - b_{p2}\left(\frac{1666}{3233}\dot{\theta}_s - \frac{4899}{3233}\dot{\theta}_{c3}\right)\left(\frac{1666}{3233}\partial\theta_s - \frac{4899}{3233}\partial\theta_{c3}\right) - b_{p3}\left(\frac{2}{5}\dot{\theta}_s - \frac{7}{5}\dot{\theta}_{c3}\right)\left(\frac{2}{5}\partial\theta_s - \frac{7}{5}\partial\theta_{c3}\right) \\
&\quad + (T_{Brake} - b_{s1}\begin{pmatrix}\left(\frac{-439498}{893101}\dot{\theta}_s + \frac{1332599}{893101}\dot{\theta}_{c3}\right) - \dot{\theta}_s) \\ -b_{r1}\left(\frac{-439498}{893101}\dot{\theta}_s + \frac{1332599}{893101}\dot{\theta}_{c3}\right)\end{pmatrix}\left(\frac{-439498}{893101}\partial\theta_s + \frac{1332599}{893101}\partial\theta_{c3}\right) \\
&\quad - b_{c1}\left(\frac{-2346}{7381}\dot{\theta}_s + \frac{9727}{7381}\dot{\theta}_{c3}\right)\left(\frac{-2346}{7381}\partial\theta_s + \frac{9727}{7381}\partial\theta_{c3}\right) \\
&\quad - b_{c2}\left(\frac{-10}{61}\dot{\theta}_s + \frac{71}{61}\dot{\theta}_{c3}\right)\left(\frac{-10}{61}\partial\theta_s + \frac{71}{61}\partial\theta_{c3}\right) + (T_{Load} - b_{c3}\,\dot{\theta}_{c3})\delta\theta_{c3}
\end{aligned} \tag{4.65}$$

The next step is to group all like virtual displacements together in the form and combine them with the proper partial derivative,

$$\delta W_{system} = Q_s\,\partial\theta_s + Q_{c3}\,\partial\theta_{c3} \tag{4.66}$$

The resulting equations are with the load torque being zero,

$$Q_s = (-.265545b_{p2} - .512201b_{p1} - 2.22637b_{s1} - .101024b_{c1} - .242166b_{r1} - .0266874b_{c2} - .16b_{p3})\dot{\theta}_s + (2.226b_s + .781b_{p2} + .734b_{r1} + .191b_{c2} + .56b_{p3} + .419b_{c1} + 1.228b_{p1})\dot{\theta}_{c3} + T_m - .492T_{Brake} \quad (4.67)$$

$$Q_{c3} = (.781b_{p2} + 1.228b_{p1} + 2.2263b_{s1} + .56b_{p3} + .419b_{c1} + .734b_{r1} + .191b_{c2})\dot{\theta}_s + (-2.226b_s - 2.296b_{p2} - 2.944b_{p1} - 2.226b_{r1} - 1.355b_{c2} - 1.96b_{p3} - 1.737b_{c1} - b_{c3})\dot{\theta}_{c3} + 1.492T_{Brake} \quad (4.68)$$

The estimated values for moment of inertia and estimated value of damping are as follows. The values for inertia were calculated from AutoDesk Inventor, a 3-D modeling software package.

$$J_s = .000029\,Kg \cdot m^2$$
$$J_{ci} = .004734\,Kg \cdot m^2$$
$$J_{p1,2} = .000088\,Kg \cdot m^2$$
$$J_{p3} = .000066\,Kg \cdot m^2$$
$$J_{r1} = .00393\,Kg \cdot m^2$$
$$J_{r2,3} = .003795\,Kg \cdot m^2$$

The damping term is one taken as a very rough estimate for that of a ball bearing [16]. Upon substitution,

$$b_i = .0075N \cdot m \cdot s$$

$$\frac{d}{dt}\left(\frac{\partial T_{system}}{\partial \dot{\theta}_s}\right) = .001665\,\ddot{\theta}_s - .0059856\,\ddot{\theta}_{c3} \quad (4.69)$$

$$\frac{d}{dt}\left(\frac{\partial T_{system}}{\partial \dot{\theta}_{c3}}\right) = -.0059856\,\ddot{\theta}_s + .0028709\,\ddot{\theta}_{c3} \tag{4.70}$$

$$Q_s = -.0265\dot{\theta}_s + .04604\dot{\theta}_{c3} + T_m - .492T_{Brake} \tag{4.71}$$

$$Q_{c3} = .04604\dot{\theta}_s - .1180\dot{\theta}_{c3} + 1.492T_{Brake} \tag{4.72}$$

$$\frac{d}{dt}\left(\frac{\partial T_{system}}{\partial \dot{\theta}_s}\right) = Q_s \tag{4.73}$$

$$\frac{d}{dt}\left(\frac{\partial T_{system}}{\partial \dot{\theta}_{c3}}\right) = Q_{c3} \tag{4.74}$$

$$.001665\,\ddot{\theta}_s - .0059856\,\ddot{\theta}_{c3} = -.0265\dot{\theta}_s + .04604\dot{\theta}_{c3} + T_m + .492T_{Brake} \tag{4.75}$$

$$-.0059856\,\ddot{\theta}_s + .0028709\,\ddot{\theta}_{c3} = .04604\dot{\theta}_s - .1180\dot{\theta}_{c3} - 1.492T_{Brake} \tag{4.76}$$

In matrix form,

$$\begin{bmatrix} .001665 & -.0059856 \\ -.0059856 & .0028709 \end{bmatrix}\begin{bmatrix} \ddot{\theta}_s \\ \ddot{\theta}_{c3} \end{bmatrix} = \begin{bmatrix} -.0265 & .04604 \\ .04604 & -.1180 \end{bmatrix}\begin{bmatrix} \dot{\theta}_s \\ \dot{\theta}_{c3} \end{bmatrix} + \begin{bmatrix} 1 & -.492 \\ 0 & 1.492 \end{bmatrix}\begin{bmatrix} T_m \\ T_{Brake} \end{bmatrix} \tag{4.77}$$

Solving for the highest order derivatives,

$$\begin{bmatrix} \ddot{\theta}_s \\ \ddot{\theta}_{c3} \end{bmatrix} = \begin{bmatrix} 6.425608 & -27.006 \\ -2.6398 & -15.204 \end{bmatrix}\begin{bmatrix} \dot{\theta}_s \\ \dot{\theta}_{c3} \end{bmatrix} + \begin{bmatrix} -92.468 & -242.147 \\ -192.789 & 14.839 \end{bmatrix}\begin{bmatrix} T_m \\ T_{Brake} \end{bmatrix} \tag{4.78}$$

A simple reduction of order can be accomplished by realizing that,

$$\begin{bmatrix} \ddot{\theta}_s \\ \ddot{\theta}_{c3} \end{bmatrix} = \begin{bmatrix} \dot{\omega}_s \\ \dot{\omega}_{c3} \end{bmatrix} \tag{4.79}$$

$$\begin{bmatrix} \dot{\theta}_s \\ \dot{\theta}_{c3} \end{bmatrix} = \begin{bmatrix} \omega_s \\ \omega_{c3} \end{bmatrix} \tag{4.80}$$

Which gives the final dynamically coupled equations of motion for the two degrees of freedom system.

$$\begin{bmatrix} \dot{\omega}_s \\ \dot{\omega}_{c3} \end{bmatrix} = \begin{bmatrix} 6.4256 & -27.006 \\ -2.639 & -15.204 \end{bmatrix} \begin{bmatrix} \omega_s \\ \omega_{c3} \end{bmatrix} + \begin{bmatrix} -92.468 & -242.147 \\ -192.789 & 14.839 \end{bmatrix} \begin{bmatrix} T_m \\ T_{Brake} \end{bmatrix} \tag{4.81}$$

The above equations are in terms of input and output. However the input torques cannot be measured directly, only the current to the devices generating the torques. The first motor investigated was the Maxon brake motor. The mechanical configuration of the device is depicted in figure 39. Analytically the static braking torque should be given by the equation,

$$F_a = \frac{\tau\left(e^{f\alpha}+1\right)}{r_r\left(e^{f\alpha}-1\right)} \sin\left(\frac{\alpha}{2}\right) - \mu \frac{\tau}{r_r} \cos\left(\frac{\alpha}{2}\right) \tag{4.82}$$

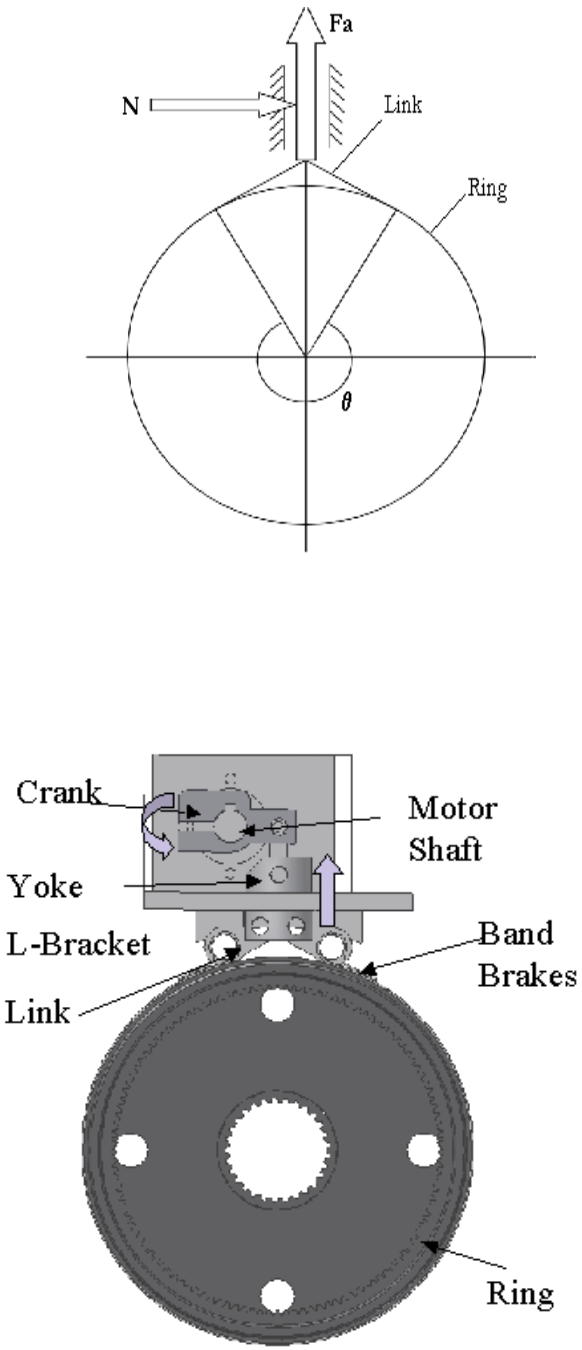


Figure 39 - Braking mechanism layout [4].

Ghanti validated this equation through experimentation, shown in figure 40, which is for a strictly static situation [4]. If there were no movement of the ring then this data could be used to approximate the braking torque for the model using measured current. Further investigation into the dynamic behavior of "wet band brakes" led to research conducted by Fujii [17], which describes the behavior as the following.

At the beginning of the engagement, the oil film transfers torque from the band to the drum through viscous shear, as shown in figure 41. This initial phase of the engagement is called hydrodynamic lubrication since the entire surface of the friction material is wetted with oil. As the band tightens around the drum, a normal loading force is exerted against the drum and rapidly squeezes the oil film. This phenomenon is called squeeze film. Once the film thickness becomes comparable with the friction material asperity height, the asperity friction starts contributing to the torque transfer. Since only part of the friction material surface is lubricated with the oil, this phase is called partial lubrication. The viscous torque and asperity torque are sometimes referred to as wet and dry torques, respectively. The wet and dry torques convert the ring gear's rotational energy into heat and increase the interface temperature between the ring and band. The elevated surface temperature and decreasing ring speed lead to a smaller viscous shear.

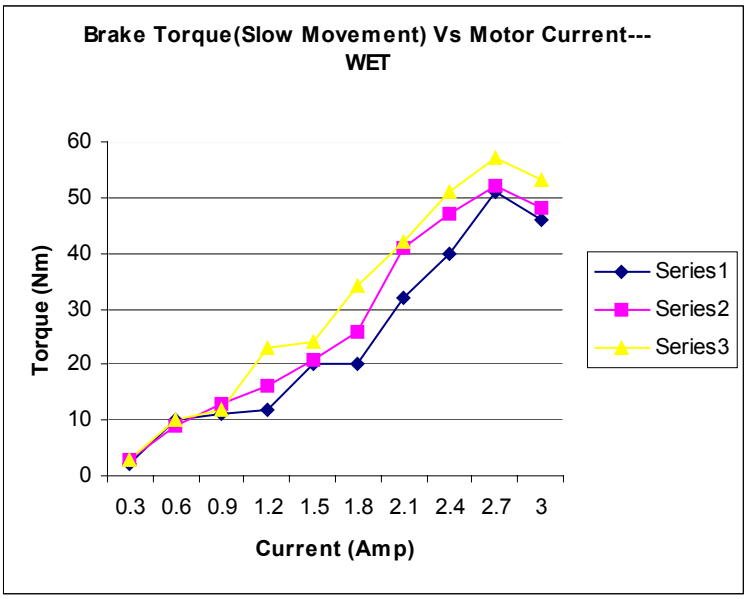


Figure 40 - Experimental results of static braking torque versus current [4].

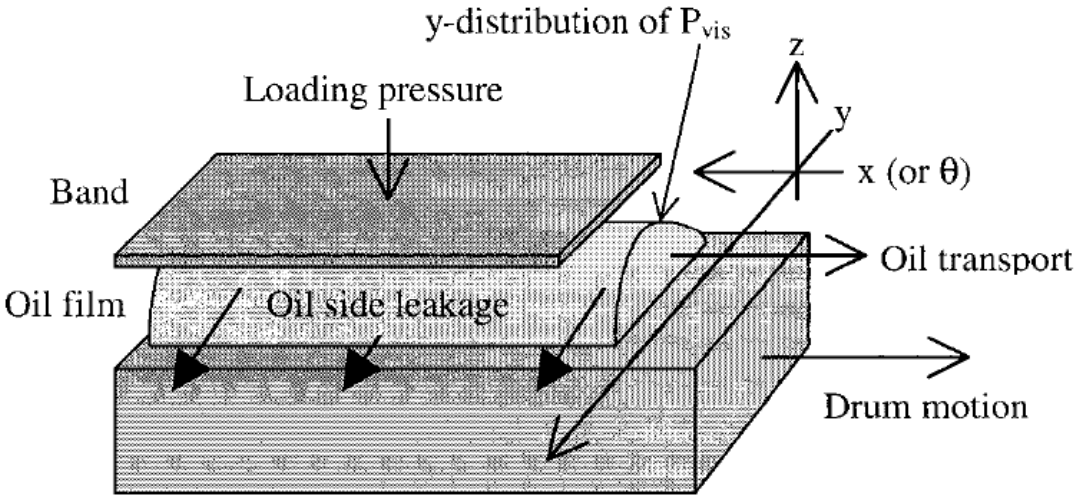


Figure 41 - Behavior at band-ring interface [17].

Thus, as the engagement proceeds, the wet torque diminishes and the dry torque eventually constitutes the entire dynamic torque. The engagement completes when the ring motion stops [17]. From this we can glean that there are quite a few complications in describing what occurs during the engagement of a wet band brake including fluid mechanics, heat transfer and dynamics. There are alternatives to creating such a complex model. Dynamic data for band engagement could be used to "get the shape of the torque curve" and then estimate what the model is based on that data. Figure 42 shows data from [17], where curve of interest is for the low oil temperature (upper right). If it is assumed that the behavior follows an exponential such as:

$$T_{Brake} = T_{static}(1 - e^{\frac{-t}{\tau}}) \tag{4.83}$$

T_{static} being a function of braking motor current and τ, the time constant. The time constant here was one estimated from data taken from the DVT. This value was dependent upon the braking time for a particular set of operating conditions. The resulting curve for the braking torque is shown in figure 43. Since the static braking torque is known from experimentation and the characteristic curve for the dynamic engagement is known then a reasonable approximation can be made of the dynamic braking torque that occurs.

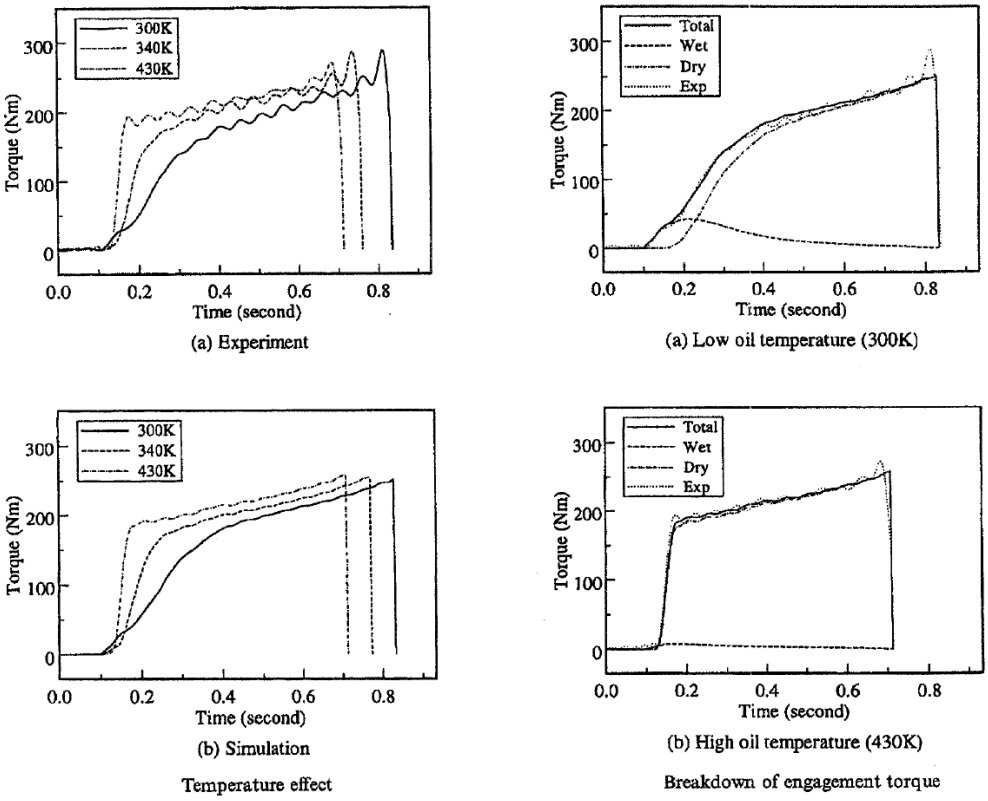


Figure 42 - Brake band torque curves [17].

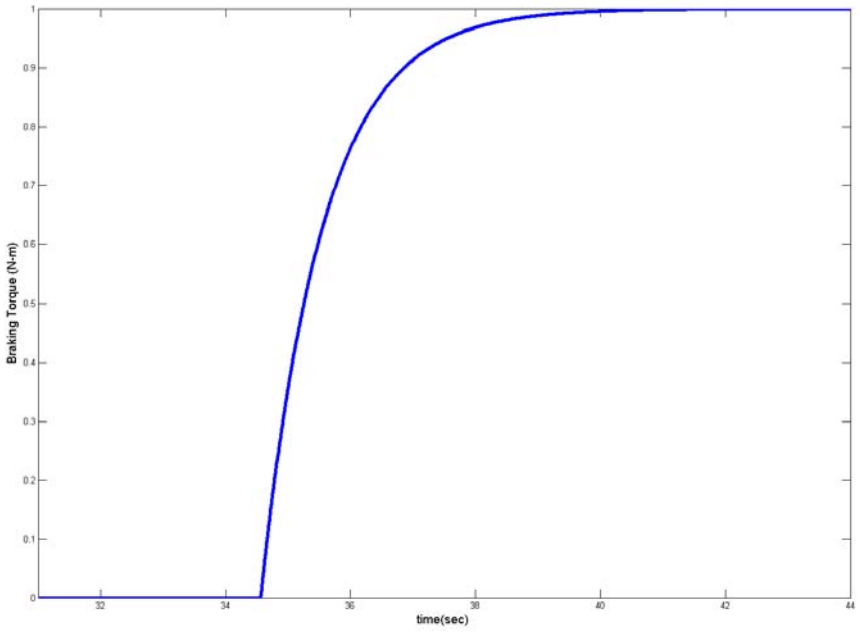


Figure 43 - Curve to represent dynamic braking torque.

The Allen Bradley input motor, shown in figure 44, will be modeled as though the torque output is proportional to the current, $i_M(t)$, by way of the motor constant, K_M.

$$T_m = K_M\, i_M(t) \tag{4.84}$$

This is a simplification, however the damping and inertia of the motor were included in the overall dynamic model. Therefore, the resulting model for the system becomes,

$$\begin{bmatrix} \dot{\omega}_s \\ \dot{\omega}_{c3} \end{bmatrix} = \begin{bmatrix} -6.425608 & 18.49189 \\ 2.6398 & -2.5479 \end{bmatrix} \begin{bmatrix} \omega_s \\ \omega_{c3} \end{bmatrix} + \begin{bmatrix} -92.468 & 242.147 \\ -192.789 & -14.839 \end{bmatrix} \begin{bmatrix} K_M\, i_M(t) \\ T_{static}(1 - e^{\frac{-t}{\tau}}) \end{bmatrix} \tag{4.85}$$

This equation will be used as the basis for the parameter identification model. The numbers here are not meant to be exact but to give a rough estimate of the order or size of the coefficient matrices. Non-linearities such as non-constant gear friction and backlash are not being considered here. However the use of a bias on the input motor will be used so that it can only run in one direction, thereby eliminating some backlash from the system. Backlash will occur, however upon the engagement of the brake due to directional changes of some of the components.



Figure 44 - Allen Bradley input motor.

4.4 Experimental Setup and Data Collection

Presented here will be a brief description of the hardware used to collect the data and the data collected. In all there were four data streams collected during each run of the transmission, with a total of four runs,

1. Allan Bradley Motor Current
2. Maxon Brake Motor Current (on or off)
3. Drive Shaft Speed
4. Final Carrier Speed

The system setup is shown in figure 45. The control software created by Dr. Sewoong Kim and Renbin Zhou, took measurements 1,2 and 3 internally using the LabView software platform. For measurement 4 a small D.C. generator was attached to the output shaft/carrier 3 of the DVT using notched timing belts and a notched pulley, the resulting voltage generated was calibrated with the output speed as shown in figure 46. Timing belts were selected because there is no slip due to notches cut into them and they have no elasticity so a stable connection could be achieved. Attaching the timing belt to the output shaft proved to be daunting. A .125-inch groove (width and depth) was turned into the shaft coupling and the timing belt was super glued into it backwards. This acted as a notched pulley when another band was placed on top of it in mesh. The generator was mounted to an aluminum bracket, which was machined using a drill press.

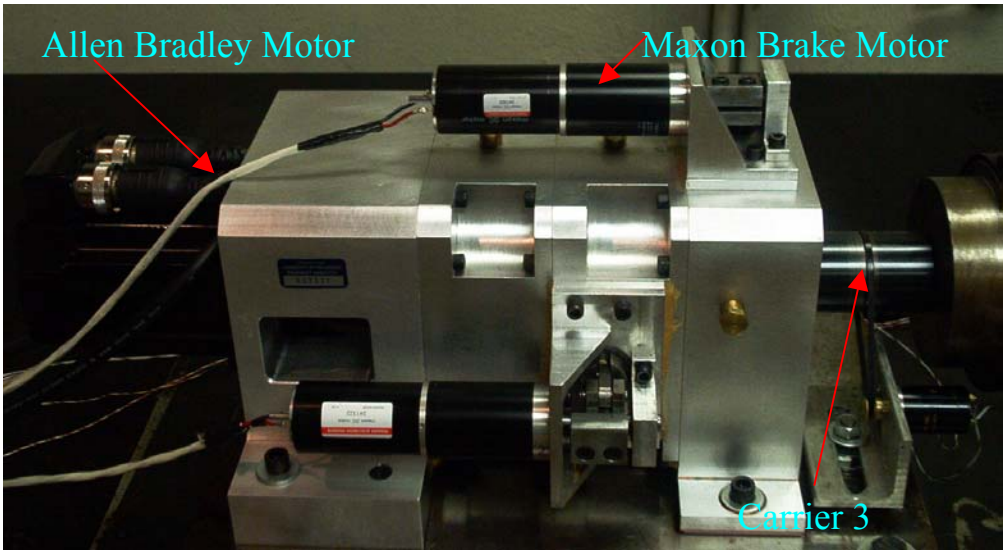


Figure 45 - System setup for data collection.

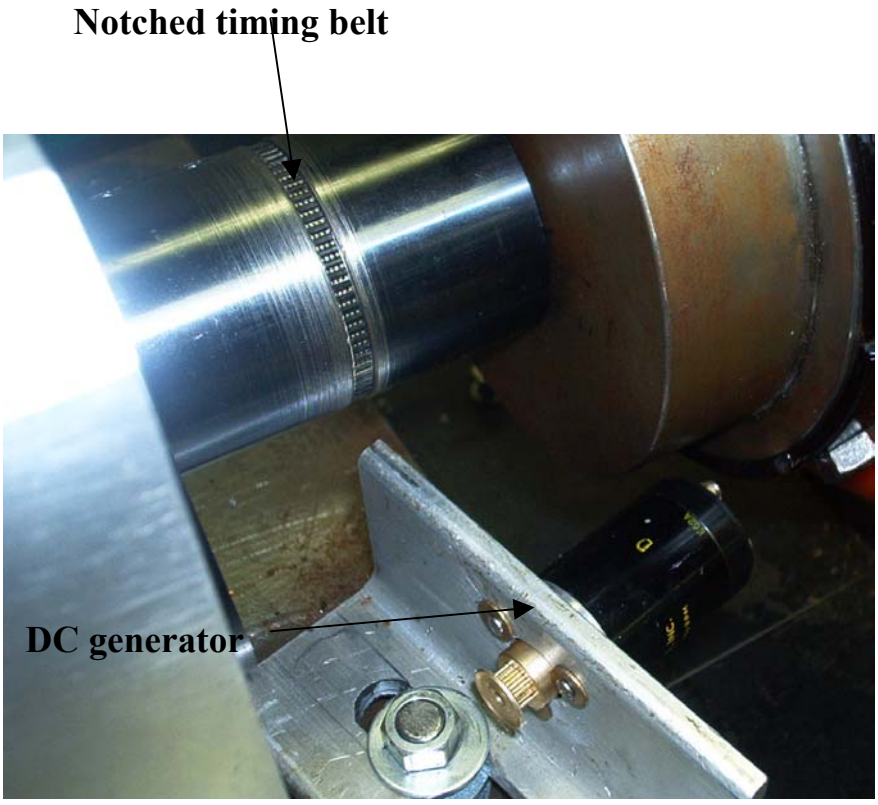


Figure 46 - DC generator and pulley system.

To calibrate the speed sensor, data points were taken using a voltmeter for the generator and LabView for the output speed. A curve fit was then performed to find an algorithm to match the behavior; the curve is shown in figure 47. The algorithm was found to be:

$$OutputSpeed = 90.793\, DC\ generator\ volts \tag{4.86}$$

which was then implemented in the LabView software. This was used to transform the voltage data being received from the A/D board into speed data to be used later in the analysis. A National Instruments CB-68LP A/D board, shown in figure 48, sampled the voltage from the DC generator once the algorithm was found. The data collection sampling time was limited to .016 seconds because a serial line was used to connect the controller to the PC. A serial line only sends one data stream at a time, which causes a lag within the system because the data is sent in series, whereas a parallel line could have sent the data simultaneously at the given sampling time. This was of great concern because the shift occurred, in normal operation, within 40 milliseconds. To overcome the slow sampling rate the brake engagement process was slowed down. This was done by maximizing the kinetic energy of the system before engagement and then using as small a brake motor current as possible, thereby extending the time of engagement. The first measurements were taken at a constant input shaft speed of 1500rpm. The input shaft speed was kept constant using feedback so that the effect of the braking action could be seen more clearly. Due to safety concerns the maximum input shaft speed used in the data collection procedure was 2400 rpm.

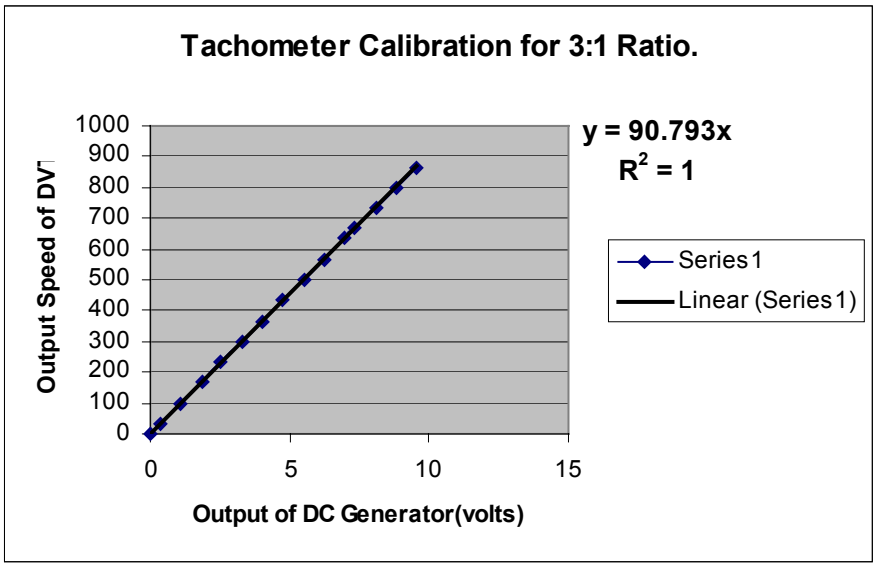


Figure 47 - Calibration curve for DC generator.

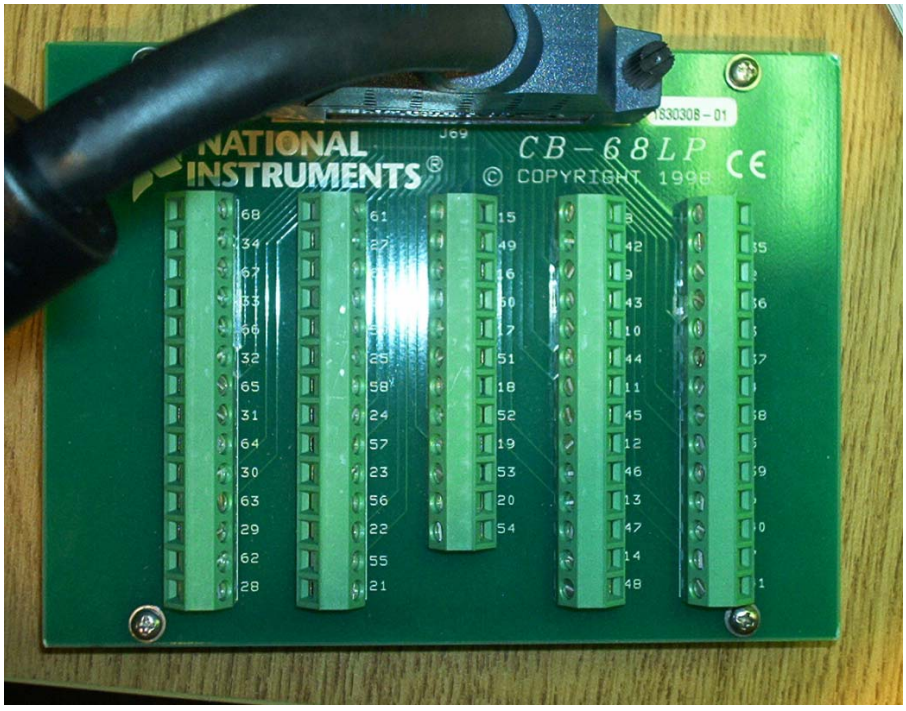


Figure 48 - National Instruments A/D board.

The smallest attainable brake motor current was .125 amperes due to instabilities in the brake motor; at currents below this the motor would oscillate and not engage. The oscillation would cause the braking mechanism to engage and then disengage until the mechanism "locked" in a binding position above the ring gear. Data from the first three runs shows a linear increase in speed for the output shaft during the engagement where as the fourth set resembles the exponential curve mentioned earlier. This is evidence that the system was slowed enough so that the slow sampling speed could capture some of the braking characteristics. The effect of the slowed braking time may cause the viscous shear torque region to become more dominant in the overall torque profile. This would be caused by a lower braking torque, which would cause the squeeze film to exit the ring-band interface at a slower rate. The effect could also be magnified due to the lower energy dissipation rate that would occur using a lower braking torque. Since the kinetic energy is dissipated as heat to the transmission fluid, the viscosity would remain higher throughout the entire process. The data taken at each operating condition is shown in figures 49 through 52. The time for the engagement is roughly 5 seconds for the fourth run while the other three take a mere second or so. Many more data sets were taken but the above-mentioned had the lowest noise and best appearance from an expected value point of view. The data sets taken with braking motor currents above .125 amperes had nearly vertical brake engagement regions and occurred in 40 milliseconds, which was deemed unusable for this analysis. This is the normal operational condition for the DVT.

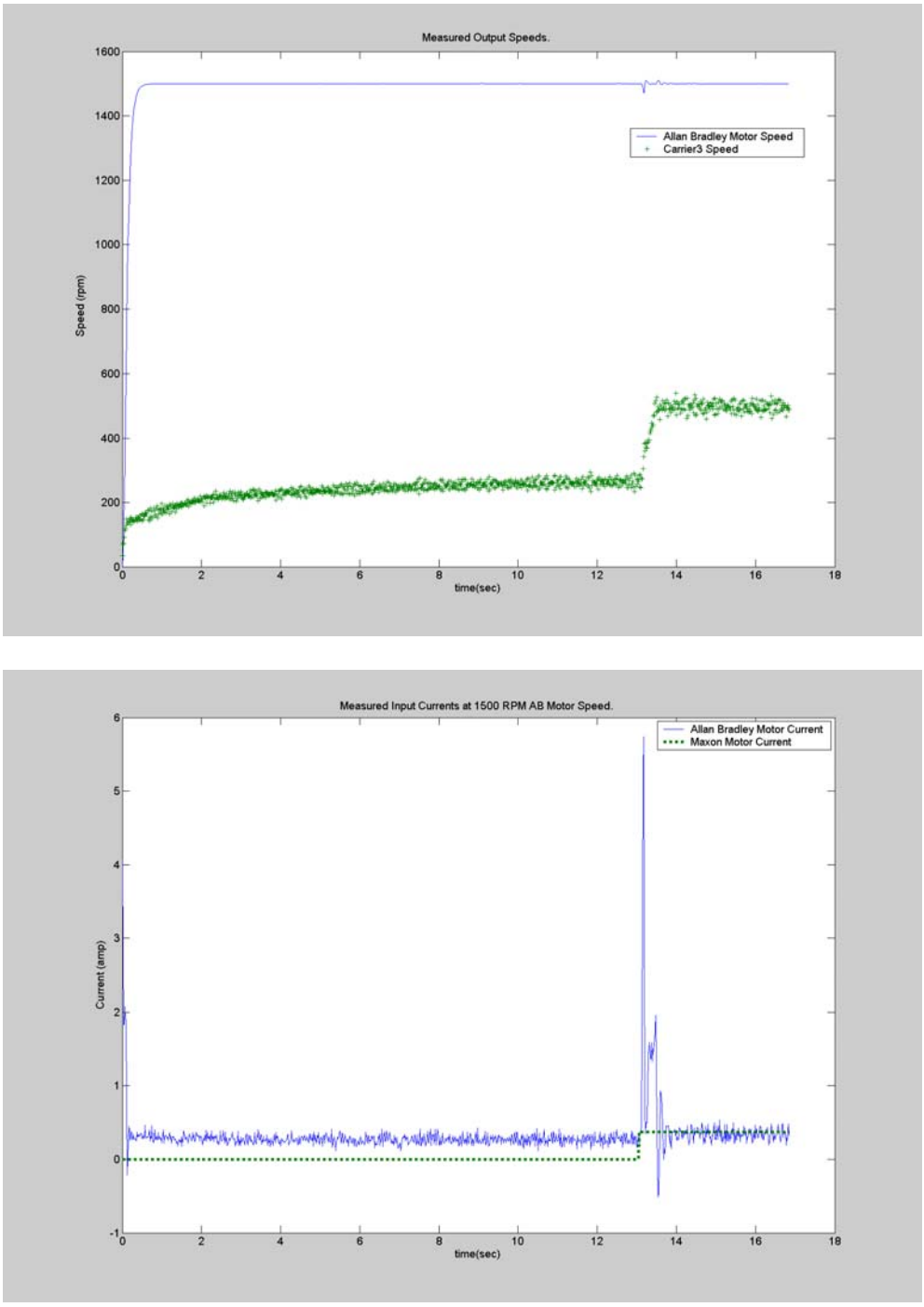


Figure 49 - Data samples at an input shaft speed of 1500 rpm.

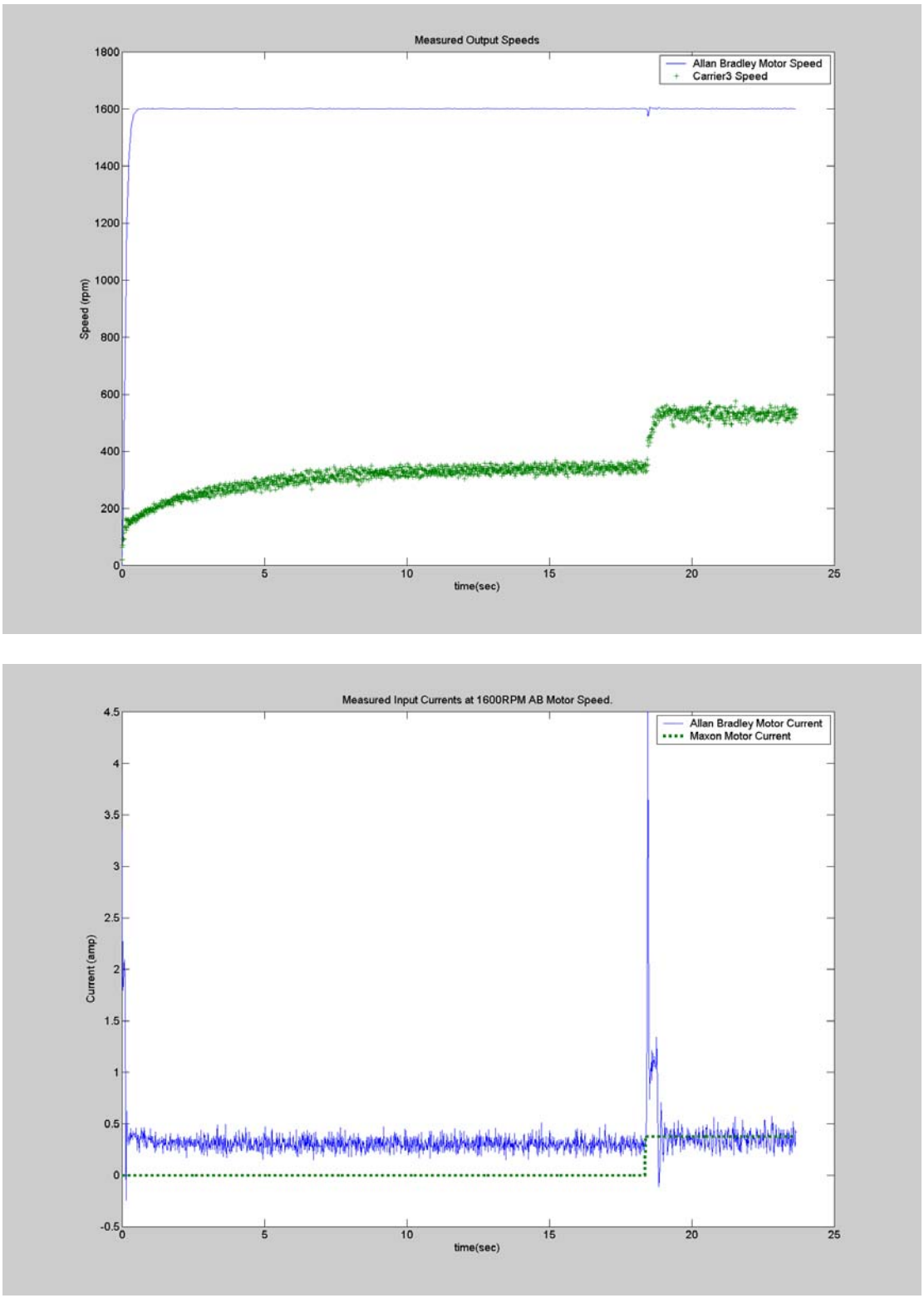


Figure 50 - Data samples at an input shaft speed at 1600 rpm

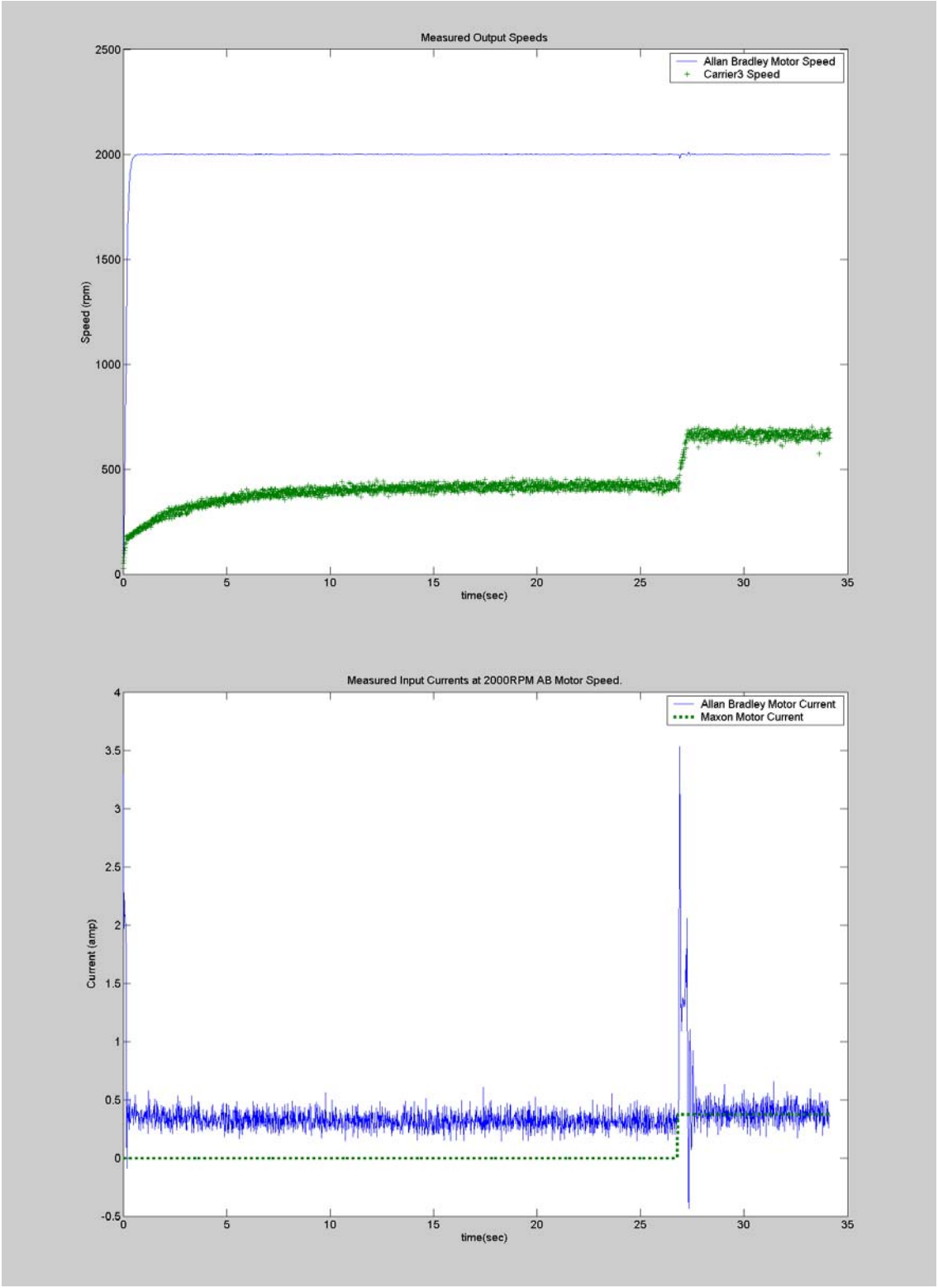


Figure 51- Data samples at an input shaft speed of 2000 rpm

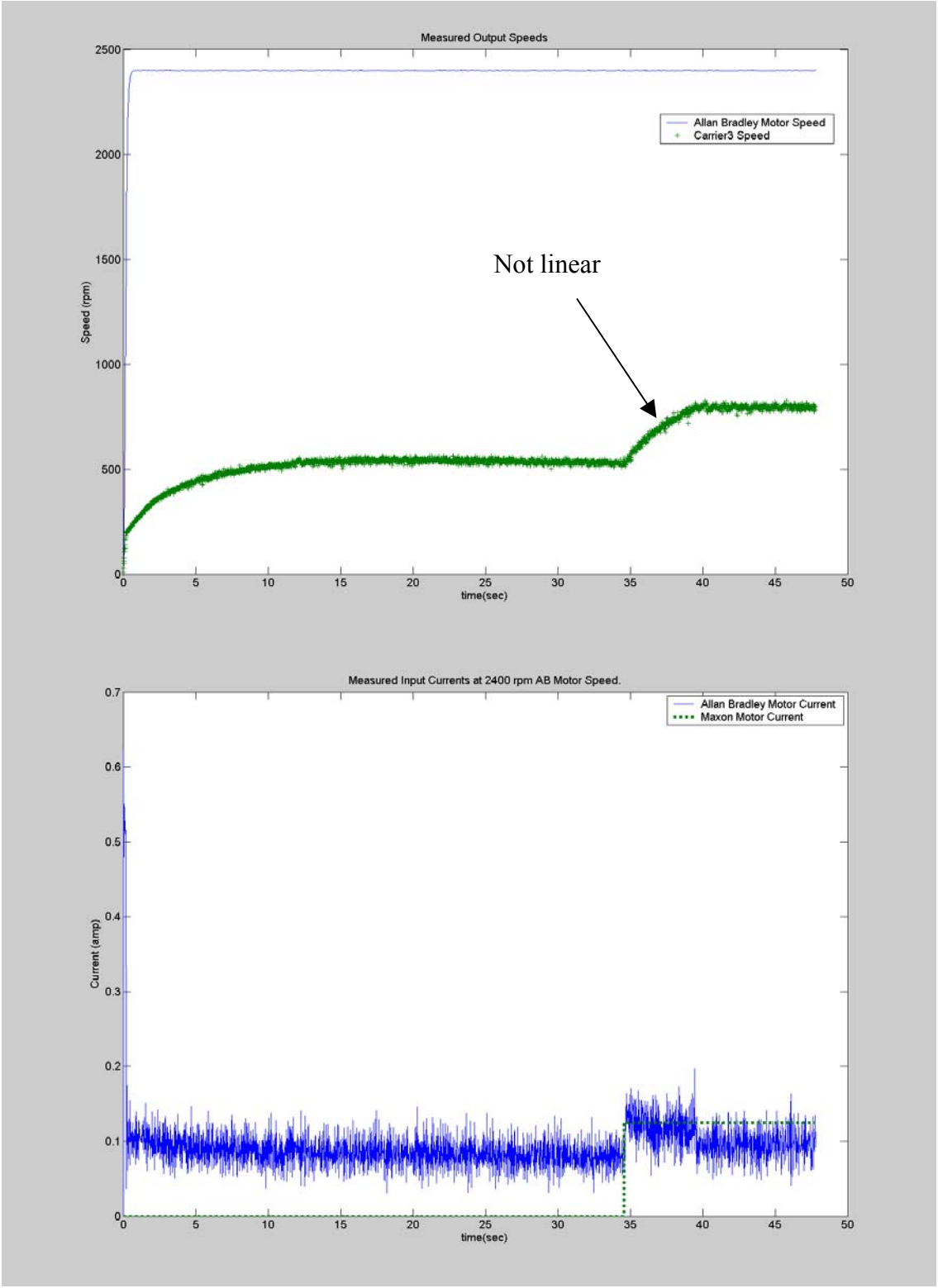


Figure 52 - Data samples at an input shaft speed of 2400 rpm

4.5 Data Analysis

As mentioned earlier in the theory section, a continuous time model must be converted to a discrete time model in order to use the equations in the software. The SID is capable of performing the needed operations to do so internally, specifying that a continuous time model will be used and a time step, which the SID then uses to modify the equation. The equation of motion for the DVT derived earlier was used as the base model to begin the parameter identification process.

$$\begin{bmatrix} \dot{\omega}_s \\ \dot{\omega}_{c3} \end{bmatrix} = \begin{bmatrix} 6.4256 & -27.006 \\ -2.639 & -15.204 \end{bmatrix} \begin{bmatrix} \omega_s \\ \omega_{c3} \end{bmatrix} + \begin{bmatrix} -92.468K_M & -242.147T_{static} \\ -192.789K_M & 14.839T_{static} \end{bmatrix} \begin{bmatrix} i_M(t) \\ (1-e^{\frac{-t}{\tau}}) \end{bmatrix} \tag{4.87}$$

There were four vectors, two inputs and two outputs. The two outputs were,

$$\begin{bmatrix} \omega_s \\ \omega_{c3} \end{bmatrix} \tag{4.88}$$

and the two inputs were,

$$\begin{bmatrix} i_M(t) \\ (1-e^{\frac{-t}{\tau}}) \end{bmatrix} \tag{4.89}$$

These were the collected data vectors that were entered into the SID. The parameters to be found were be designated in the code, located in the appendix, as NaN,

$$\begin{bmatrix} \dot{\omega}_s \\ \dot{\omega}_{c3} \end{bmatrix} = \begin{bmatrix} NaN & NaN \\ NaN & NaN \end{bmatrix} \begin{bmatrix} \omega_s \\ \omega_{c3} \end{bmatrix} + \begin{bmatrix} NaN & NaN \\ NaN & NaN \end{bmatrix} \begin{bmatrix} i_M(t) \\ (1-e^{\frac{-t}{\tau}}) \end{bmatrix} \tag{4.90}$$

which denotes that the matrix element is a free parameter and is manipulated by the software to produce the best possible model. To begin the analysis all the data was run as is and a default state-space prediction error model (PEM) was found, this was done to see if the software could handle the basic relationships between the variables. The results for each case seem good, the loss function is low and the model fit reproduces a good deal of the data, of course the system is compensating for any disagreements in output with the noise matrix. The loss function here is the determinant of the estimated covariance matrix of the noise source $e(t)$ [13]. For the model obtained for the 1500-rpm case, shown in figure 53, the corresponding coefficient matrices were,

$$A(\psi) = \begin{bmatrix} 1.0003 & -8.3078e-005 \\ -0.14379 & 0.99778 \end{bmatrix}$$

$$B(\psi) = \begin{bmatrix} -2.2893e-005 & 0.0001708 \\ 0.027367 & -0.00054737 \end{bmatrix}$$

$$C(\psi) = \begin{bmatrix} 3106.6 & 1.8793 \\ 525.35 & 29.51 \end{bmatrix}$$

$$K(\psi) = \begin{bmatrix} 0.00058436 & 3.7597e-006 \\ -0.0099573 & 0.00024665 \end{bmatrix}$$

The loss function for this model was 0.694335. All of the follow models, shown in figures 54 and 55, had roughly the same coefficients and loss functions.

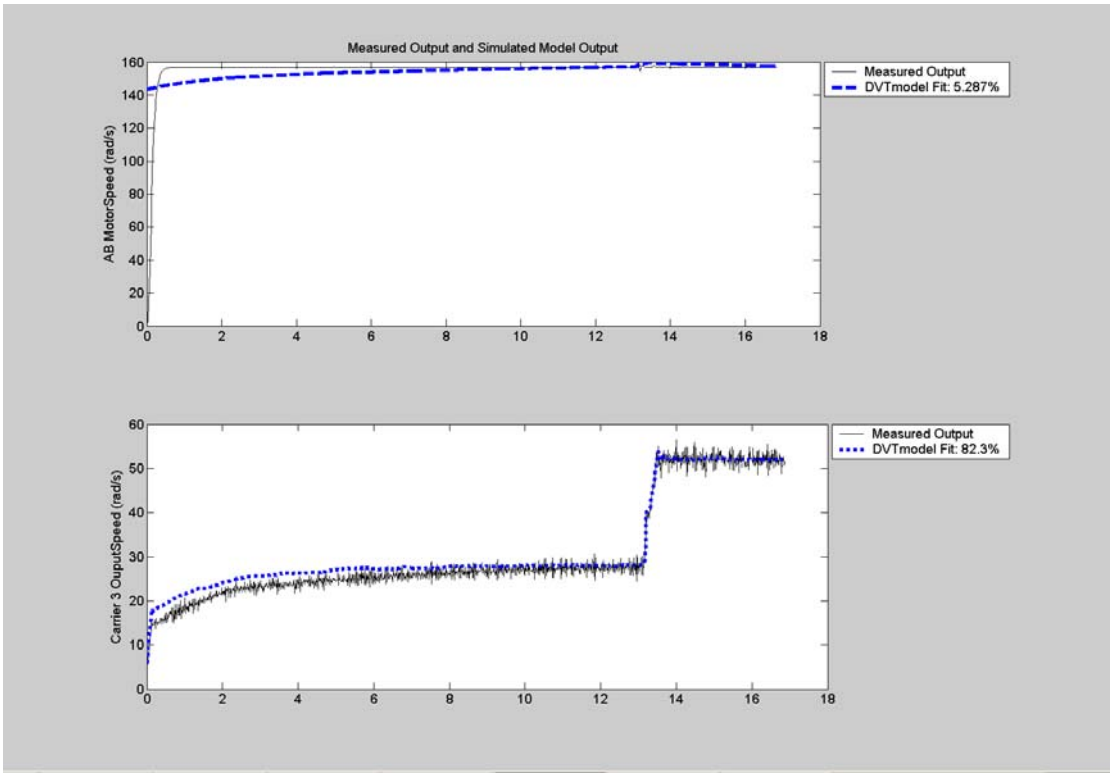


Figure 53 - Simulated output for a constant shaft speed of 1500rpm.

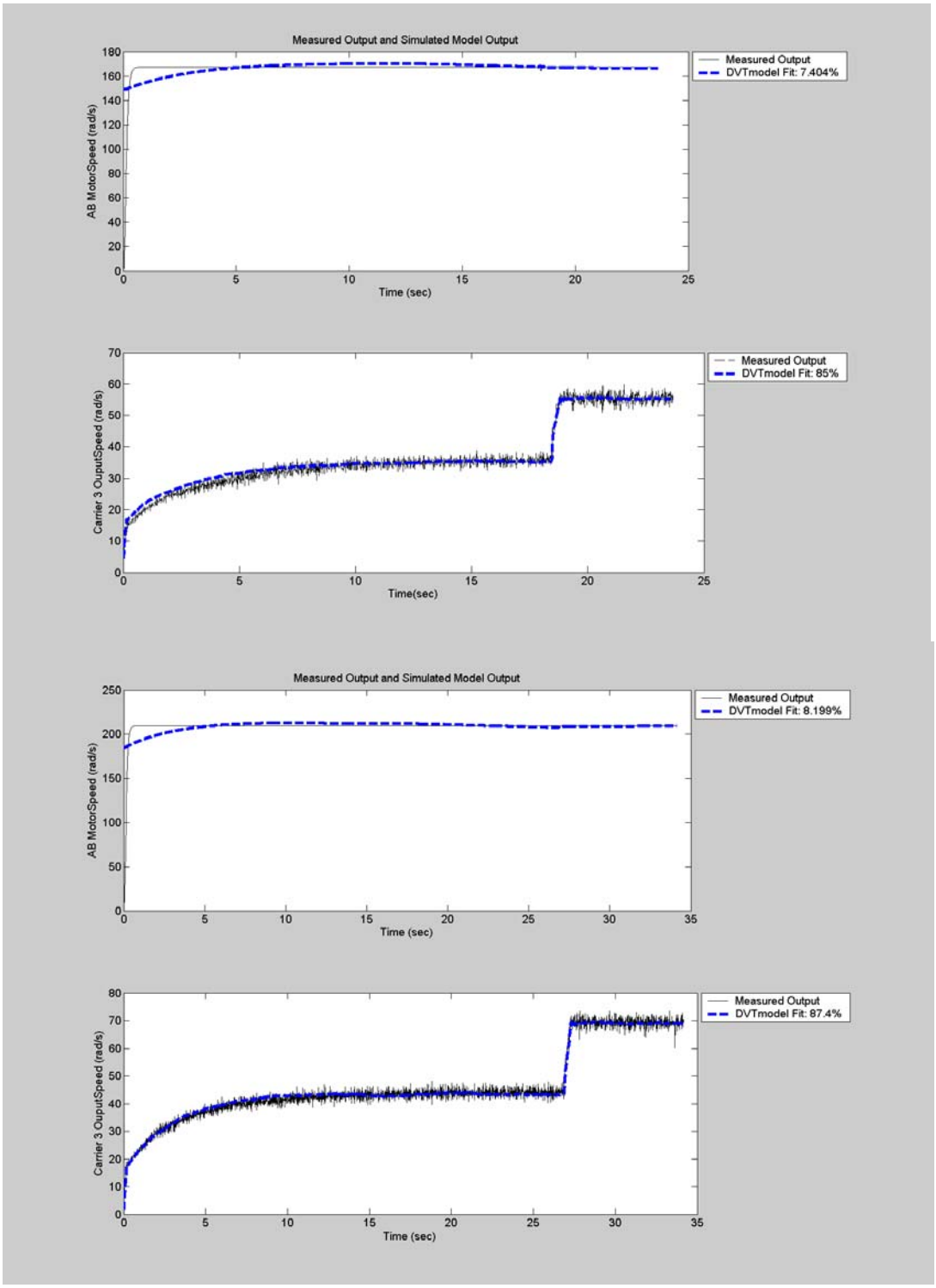


Figure 54 - Simulated output for a constant shaft speed of 1600 and 2000rpm.

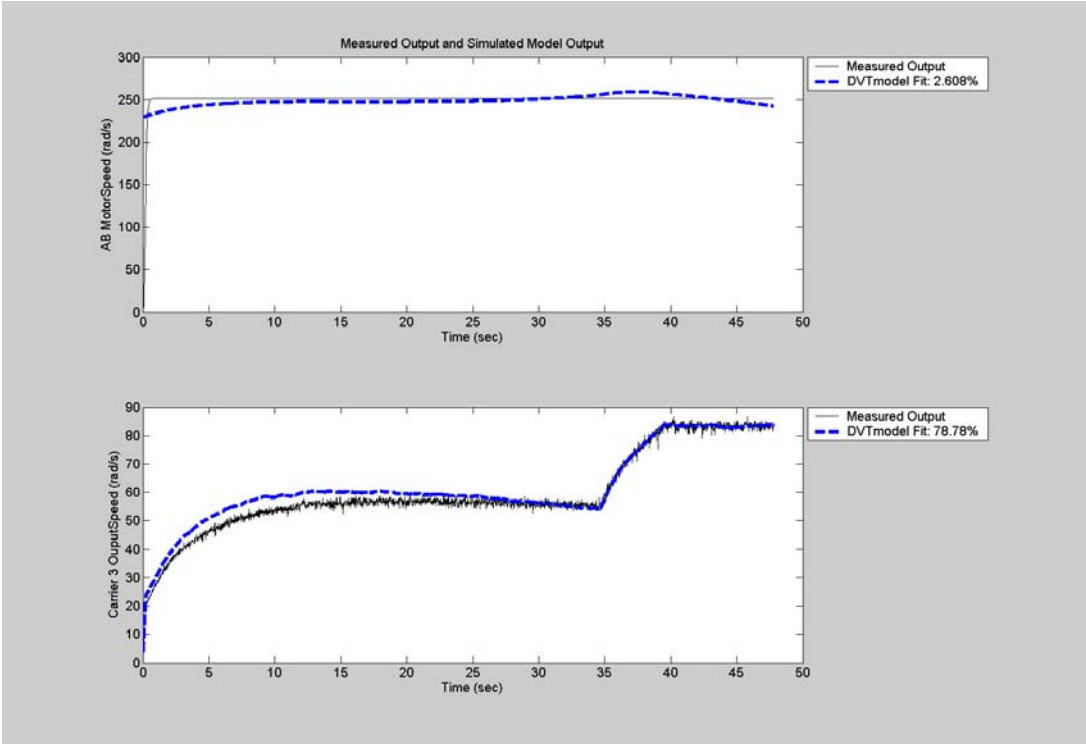


Figure 55 - Simulated model for constant shaft speed at 2400 rpm.

The fourth data set, 2400rpm, was chosen to do a deeper analysis on because it seemed to fit the expected shape of the engagement process better than the other data sets. The raw data for brake motor current was then altered to fit the estimated torque profile for the band engagement. The experimental values discussed earlier indicated that an exerted braking torque of roughly 1N-m should be expected at static conditions at the .125-ampere current level. Figure 56 and 57 show the altered braking torque curve using the equation,

$$T_{Brake} = T_{static}(1 - e^{\frac{-t}{\tau}}) \tag{4.92}$$

where τ was set at 1. This was merely a guess at what the actual braking torque profile would be as discussed earlier. The high frequency noise content of the data was very high, especially for the carrier 3-output speed and the AB motor current. A low pass filter was used to reduce the noise in the data; the Matlab function IDFILT was utilized with a cutoff frequency of .1, in Matlab the cut off frequency is measured as a fraction of the nyquist frequency [13]. The filtered data is shown in figure 58. It should be noted that the filtering was done after the data was taken and merely results in a smoothing of the existing curve. Since the sampling frequency was 62.5 Hz the nyquist frequency was 31.25 Hz. The result of this is that if any high frequency noise was in the region above 31.25 Hz, then it was folded over into the lower frequency band and was returned as an alias signal. This very well could alter the outcome of the analysis especially if a small window of the data was used, such as a one second time gap.

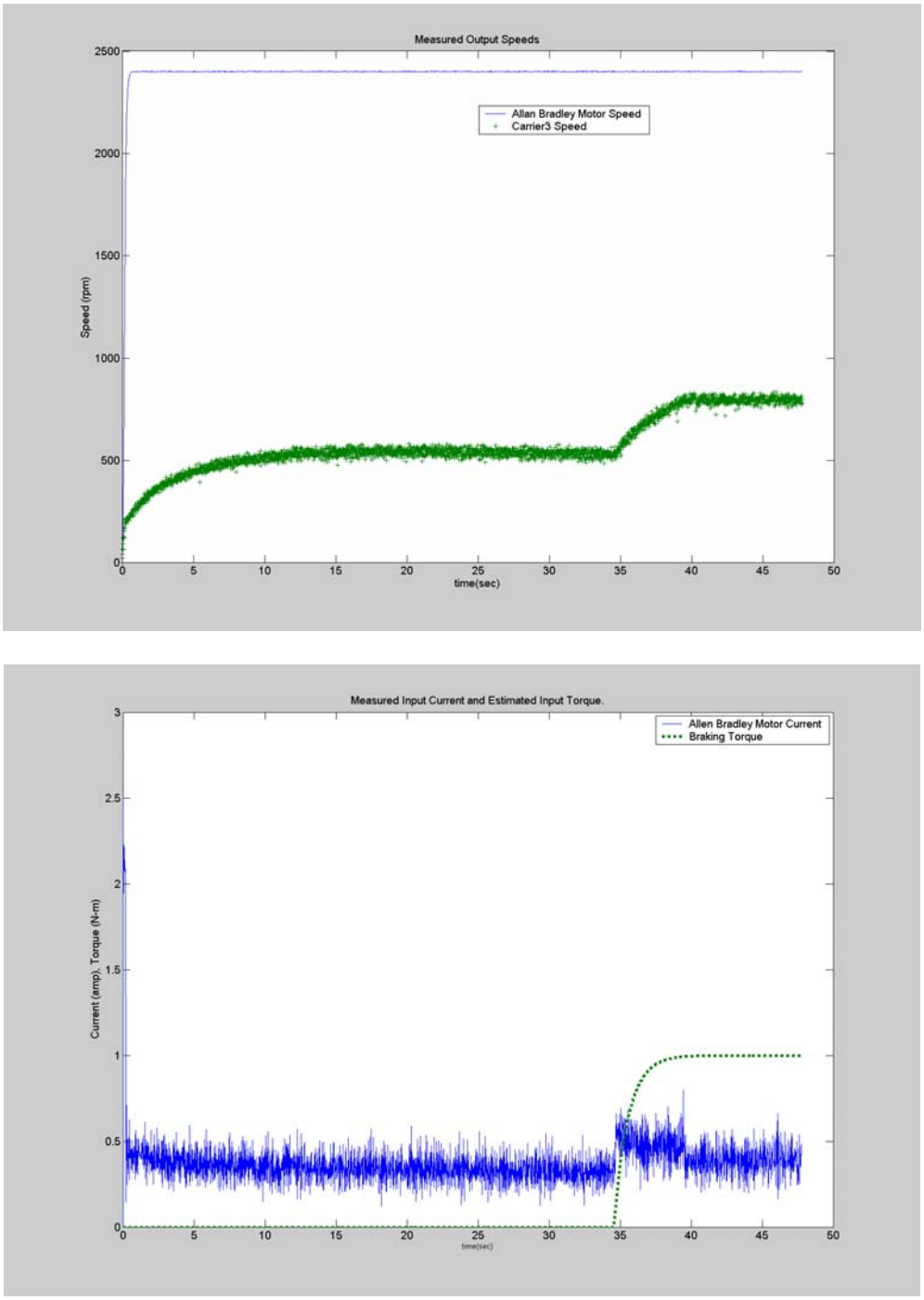


Figure 56 - Modified data set for 2400rpm.

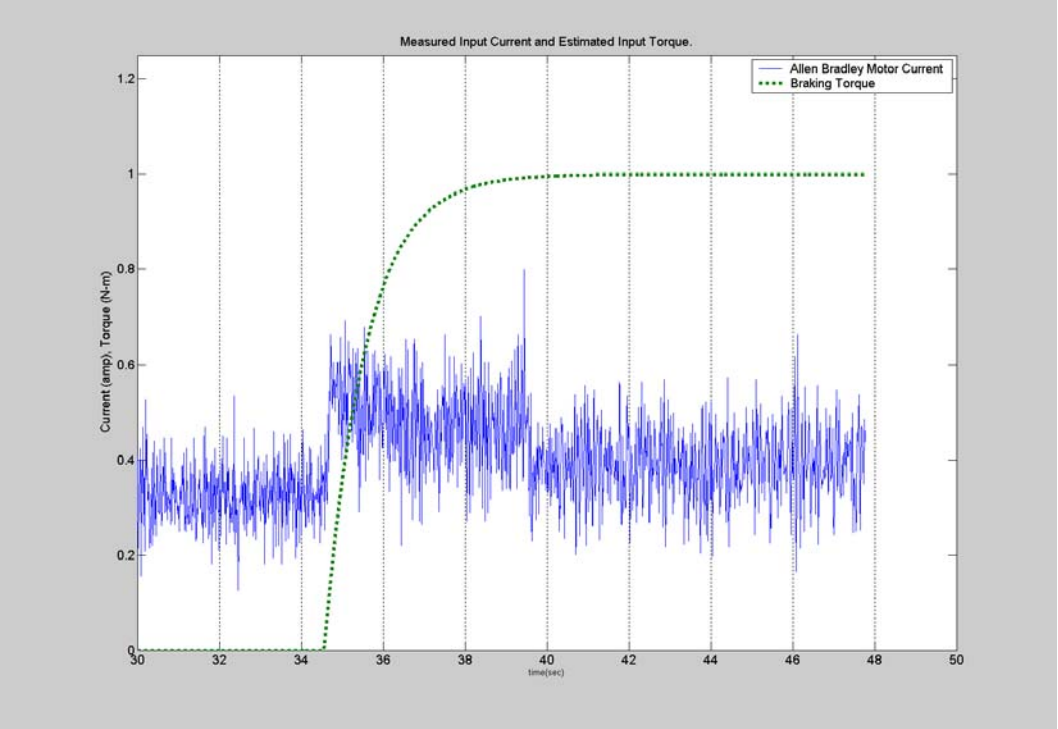


Figure 57 - Close up of modified data.

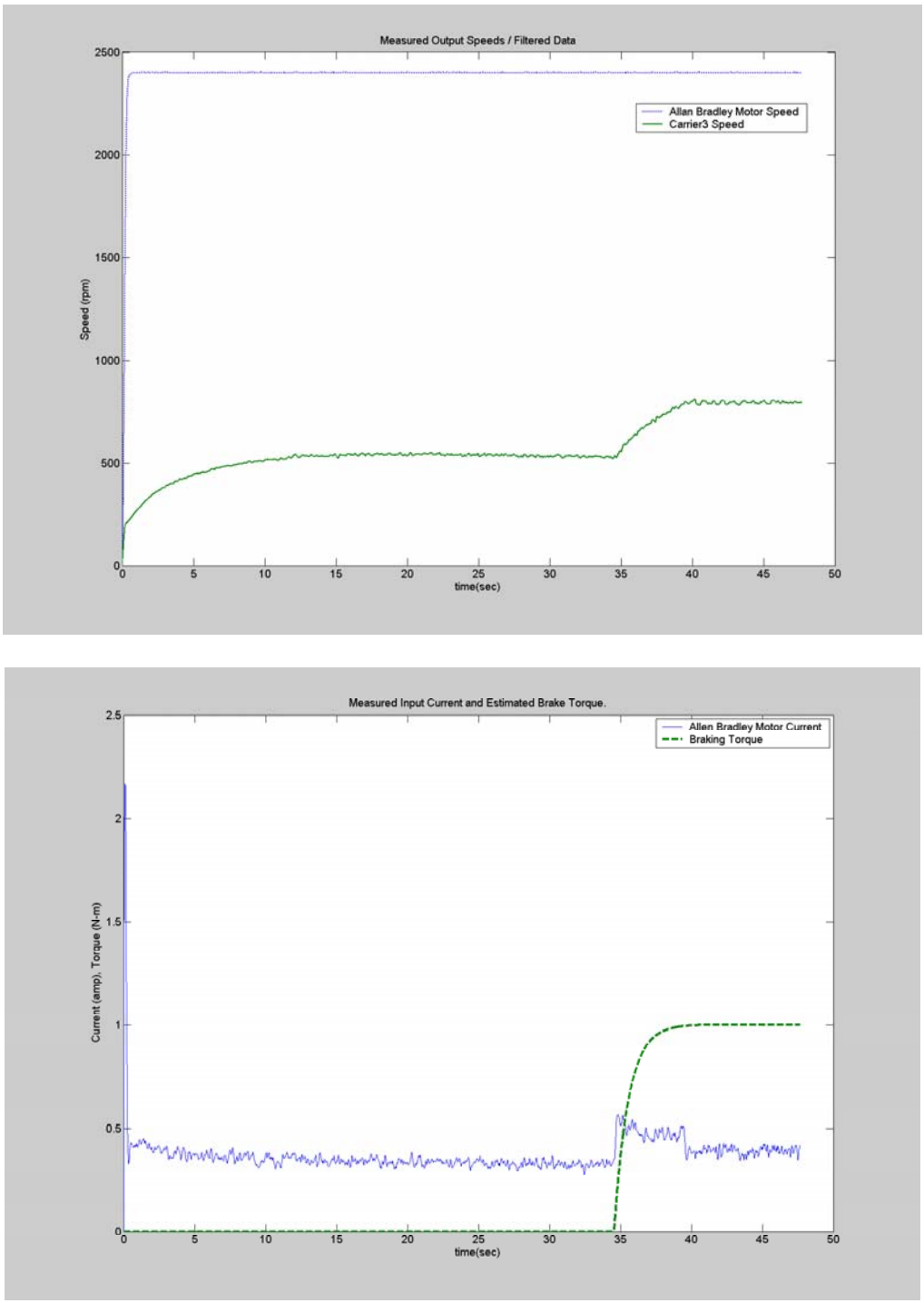


Figure 58 - Filtered data.

The filtered data seemed to retain the important features of the raw data and were less cluttered by disturbances. The following sets of matrices were used as an initial guess in the OEM modeling process on the filtered data.

$$A(\psi) = \begin{bmatrix} -0.9908 & -1.3268 \\ 0.77357 & -0.10205 \end{bmatrix}$$

$$B(\psi) = \begin{bmatrix} 2390 & 1.1443 \\ -674.84 & 343.24 \end{bmatrix}$$

$$C(\psi) = \begin{bmatrix} 1 & 0 \\ 0 & 1 \end{bmatrix}$$

$$K(\psi) = \begin{bmatrix} 0 & 0 \\ 0 & 0 \end{bmatrix}$$

The matrices above were determined by first running a default PEM analysis on the system and finding an initial $A(\psi)$ and $B(\psi)$ to begin with, a starting point. Once a good starting point was found a user-defined model was created. The values above were then run in the user defined OEM, the results of the analysis were,

$$A(\psi) = \begin{bmatrix} -1.4532 & 2.5443 \\ -0.061856 & -0.060044 \end{bmatrix}$$

$$B(\psi) = \begin{bmatrix} 2690.5 & -911.31 \\ 229.32 & -10.956 \end{bmatrix}$$

$$C(\psi) = \begin{bmatrix} 1 & 0 \\ 0 & 1 \end{bmatrix}$$

$$K(\psi) = \begin{bmatrix} 0 & 0 \\ 0 & 0 \end{bmatrix}$$

The model fits were 51.76% for the sun shaft speed output and 94.88% for the carrier speed output; this fit is computed as the percentage of the output variation that is reproduced by the model [13]. The plots of the final results are shown in figure 59. So, a model that has a fit of 0% gives the same mean square error as just setting the model output to be the mean of the measured output [15]. The results are excellent so far but more investigation needs to be done into the robustness of this model. The step responses of both the OEM and the data were compared and are shown in figure 60. The plots show the response of both carrier3 speed and sun shaft speed to step inputs from both AB motor current and braking motor current. The correlation is fairly good except for the brake motor current to carrier3 speed. The examination of the y-axis' sizes shows that the effect is small from brake motor current to both outputs. This poor correlation between model and data could be a result of the low range of excitation used in the data collection procedure. The next step in grading the model will be to compare it using the data from the other runs.

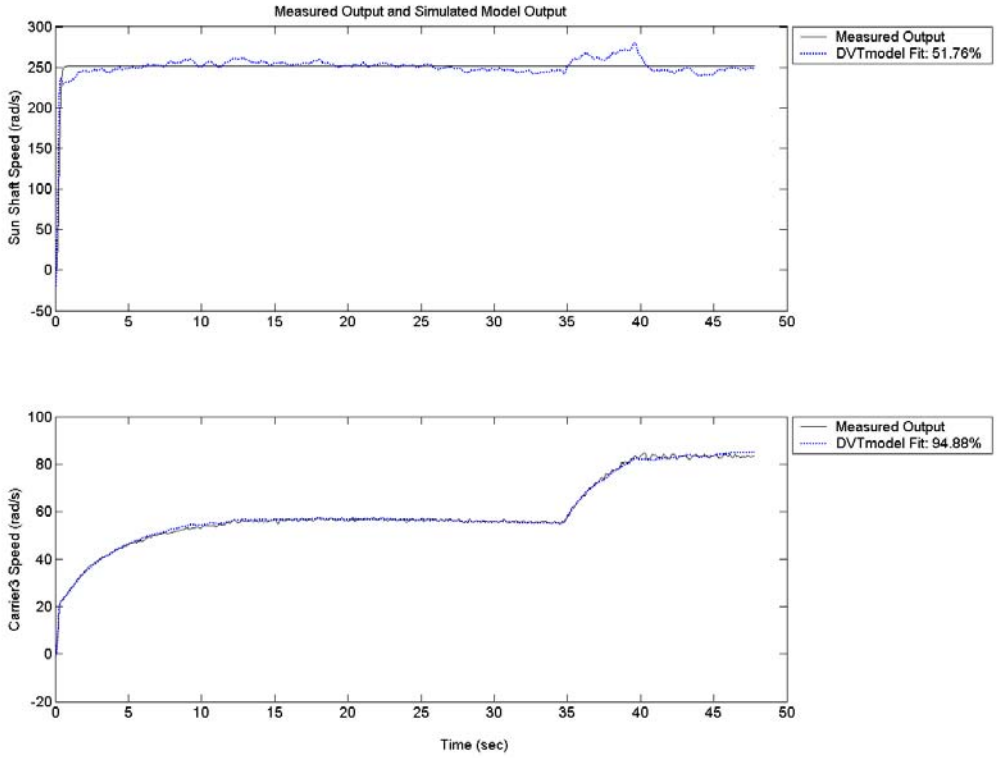


Figure 59 - Results from OEM modeling with filtered data set.

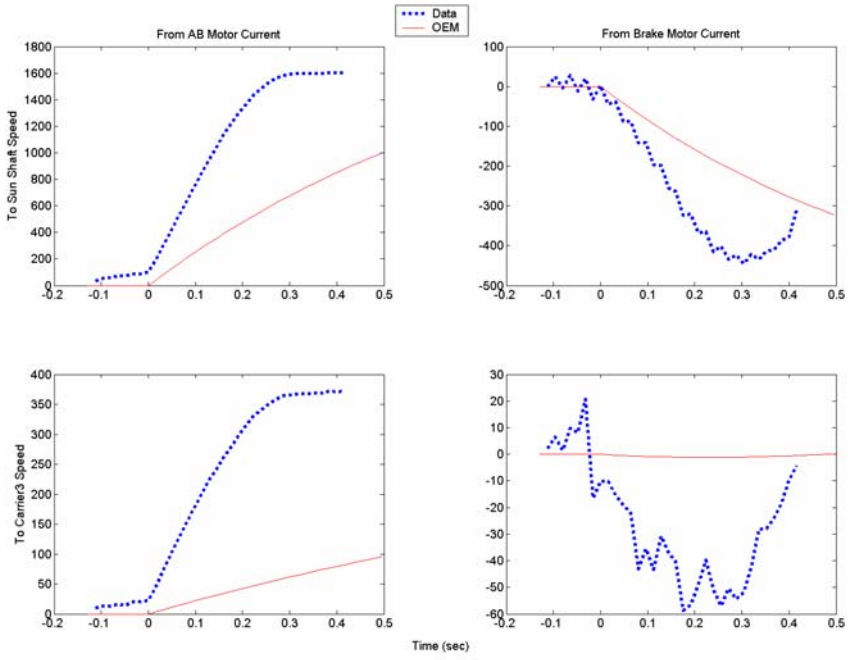


Figure 60 - Step response for data and model.

The ability of the model created at 2400rpm to reproduce results taken at 2000 rpm is poor, as shown in figure 61. This validates that the model is only good for the particular circumstances under which it was created. The correlation to the other data sets was even lower.

To determine the inertia and viscous damping terms given by the software the derived equations of motion were implemented.

$$\begin{bmatrix} .001665 & -.0059856 \\ -.0059856 & .0028709 \end{bmatrix} \begin{bmatrix} \ddot{\theta}_s \\ \ddot{\theta}_{c3} \end{bmatrix} = \begin{bmatrix} -.0265 & .04604 \\ .04604 & -.1180 \end{bmatrix} \begin{bmatrix} \dot{\theta}_s \\ \dot{\theta}_{c3} \end{bmatrix} + \begin{bmatrix} 1 & -.492 \\ 0 & 1.492 \end{bmatrix} \begin{bmatrix} T_m \\ T_{Brake} \end{bmatrix} \tag{4.93}$$

The following can represent the above equation.

$$[J][\dot{\omega}] = [b][\omega] + [q][u] \tag{4.94}$$

When the highest order derivatives were found earlier the following operations took place,

$$[\dot{\omega}] = [J]^{-1}[b][\omega] + [J]^{-1}[q][u] \tag{4.95}$$

and the result was,

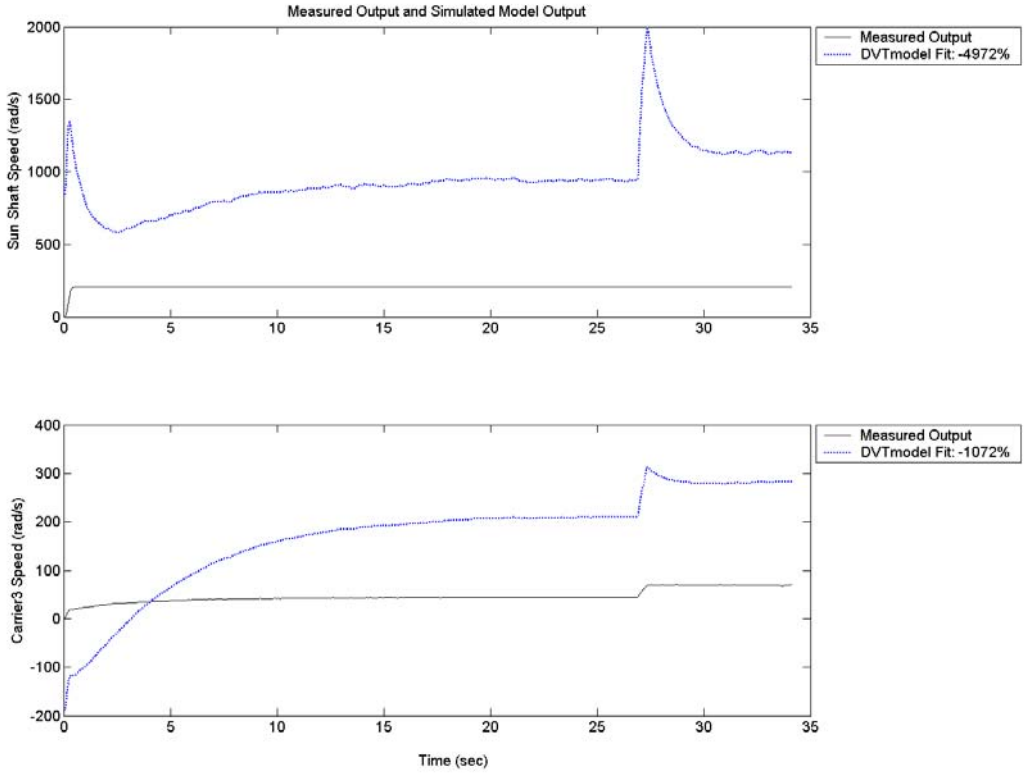


Figure 61 - Comparison of OEM to 2000rpm data set.

$$\begin{bmatrix} \dot{\omega}_s \\ \dot{\omega}_{c3} \end{bmatrix} = \begin{bmatrix} 6.4256 & -27.006 \\ -2.639 & -15.204 \end{bmatrix} \begin{bmatrix} \omega_s \\ \omega_{c3} \end{bmatrix} + \begin{bmatrix} -92.468K_M & -242.147T_{static} \\ -192.789K_M & 14.839T_{static} \end{bmatrix} \begin{bmatrix} i_M(t) \\ (1-e^{\frac{-t}{\tau}}) \end{bmatrix} \tag{4.96}$$

where,

$$K_M = .3732 \frac{N \cdot m}{amp}$$

$$T_{static} = 1 N \cdot m$$

$$[q] = \begin{bmatrix} .3732 & -.492 \\ 0 & 1.492 \end{bmatrix}$$

The software returned a model equation in the form,

$$[\dot{\omega}] = [A][\omega] + [B][u] \tag{4.97}$$

with,

$$A(\psi) = \begin{bmatrix} -1.4532 & 2.5443 \\ -0.061856 & -0.060044 \end{bmatrix}$$

$$B(\psi) = \begin{bmatrix} 2690.5 & -911.31 \\ 229.32 & -10.956 \end{bmatrix}$$

Since $[q]$ was known from the dynamics of the system, independent of damping and inertia, both equations, derived and calculated, could be utilized to find the inertia and damping matrices determined by the software.

$$[J]^{-1}[q] = [B] \tag{4.98}$$

$$[J] = [q][B]^{-1} \tag{4.99}$$

$$[J] = \begin{bmatrix} .0006057 & -.005469 \\ -.001906 & .02236 \end{bmatrix}$$

Now knowing $[J]$, the viscous damping term could be found.

$$[J]^{-1}[b] = A \tag{4.100}$$

$$[b] = [J][A] \tag{4.101}$$

$$[b] = \begin{bmatrix} -.00054134 & .00187 \\ .0013866 & -.00619 \end{bmatrix}$$

The comparison is fair. The form of the equations (negative signs) is what it should be and the relative sizes are close. This is some confirmation that the initial derived mathematical model did at least capture the proper form.

$$J_{software} = \begin{bmatrix} .0006057 & -.005469 \\ -.001906 & .02236 \end{bmatrix} \qquad J_{derived} = \begin{bmatrix} .001665 & -.0059856 \\ -.0059856 & .0028709 \end{bmatrix}$$

$$b_{software} = \begin{bmatrix} -.00054134 & .00187 \\ .0013866 & -.00619 \end{bmatrix} \qquad b_{derived} = \begin{bmatrix} -.0265 & .04604 \\ .04604 & -.1180 \end{bmatrix}$$

Chapter 5

Conclusions and Future Work

5.1 Conclusions

The DVT was in general a success. Dr. Sewoong Kim verified the performance requirements with the use of a dynamometer [20], and is shown if figure 62. Several problems were encountered in the fabrication and assembly of the DVT. The first was in improper tolerance on the motor locator hole. The drawings for the motor called for an opening of 3.74 inches in diameter. The drawings were made to this specification. However this was not correct. The hole should have been made to 3.74+tol to allow for an easy fit. This problem was corrected by taking a small amount of material from the locator hole. A problem was also encountered when the brake bands were placed into the housings. Because of the inability to ensure tolerances on brake bands by the manufacturer a small amount of material had to be removed from inside the housings to allow for proper seating of the eyelets of the brake bands. The locators that connected the housings together were also improperly toleranced. This prevented the housings from fitting together properly and a small amount of material had to be removed from the locator on each housing. This solved the problem of a "tight" fit on the housings. A major problem that arose was not in assembly but in the testing phase of the DVT. It was realized that proper measures were not taken to ensure that the DVT did not leak any transmission fluid during its operation. This was partially solved by the use of RTV sealant on all possible openings or cracks that

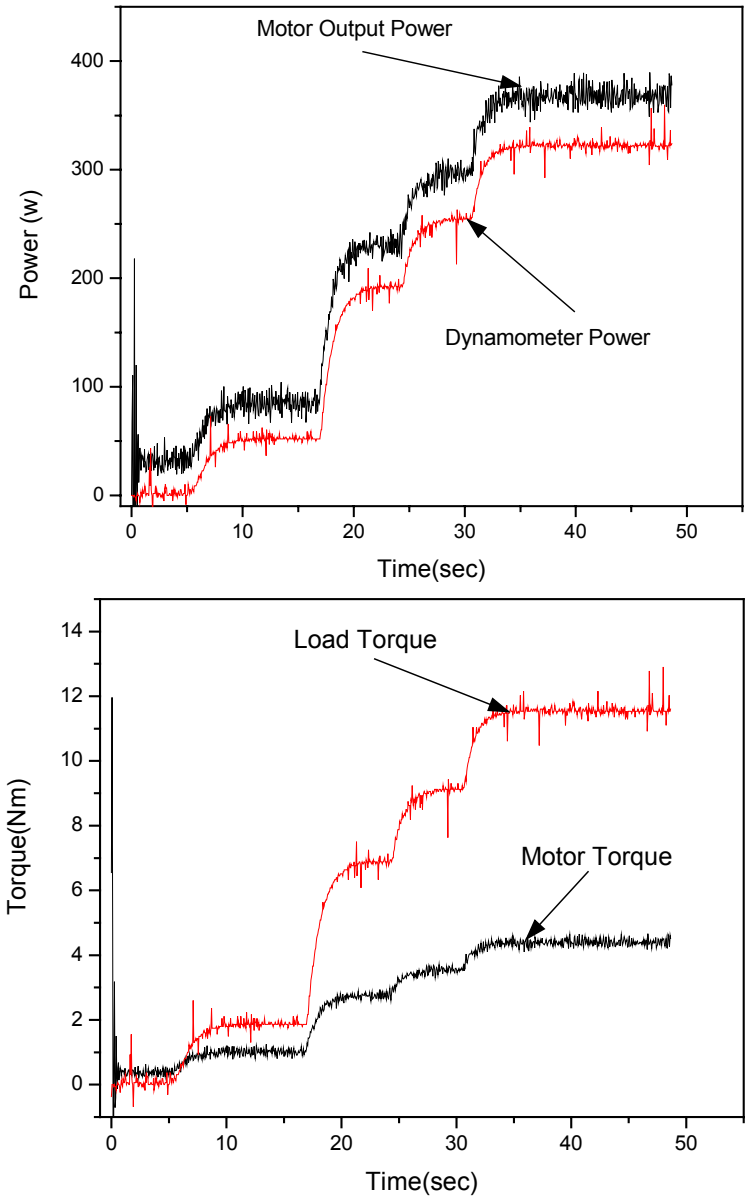


Figure 62 - Results from DVT dynamometer test [20].

could allow leaks and a spring loaded bearing seal on the input shaft. The leakage around the slider portion of the brake mechanism could no be solved with sealant and will require the use of a boot because there can be no restriction of movement between the slider and the housing. The only error made by the fabricator was an error in center distance on one of the planet carriers. When the three planets were placed into the carrier they then would not mesh inside the ring, as shown in figure 63. To correct the problem of fit a "Philadelphia Fit" was implemented which is to mark or dimple the outer edge of the spindle hole thereby holding in the cupped needle-bearing shaft. This would be better solved in a future version of the DVT by using woodruff keys or steel sleeves to protect the planet carriers, if they are to be made of aluminum.

The results of the parameter identification study were not spectacular. The simplicity of the model was its ultimate weakness. Inertia and viscous damping terms were the only parameters included in the derivation when in reality many more factors were at work. Non-linear gear friction, backlash and inaccuracies in modeling the actual braking characteristics, along with improper system excitation all contributed to the poor model quality. The system excitation problems were the frankly the result of a very slow sampling time in the data collection equipment. A fundamental rule of identification is that if gear friction or other nonlinearities exist in the system then the excitation should be very large in comparison. The inputs should be as large as possible as to decrease the relative effect on the system [18]. The opposite was done in the data collection procedure

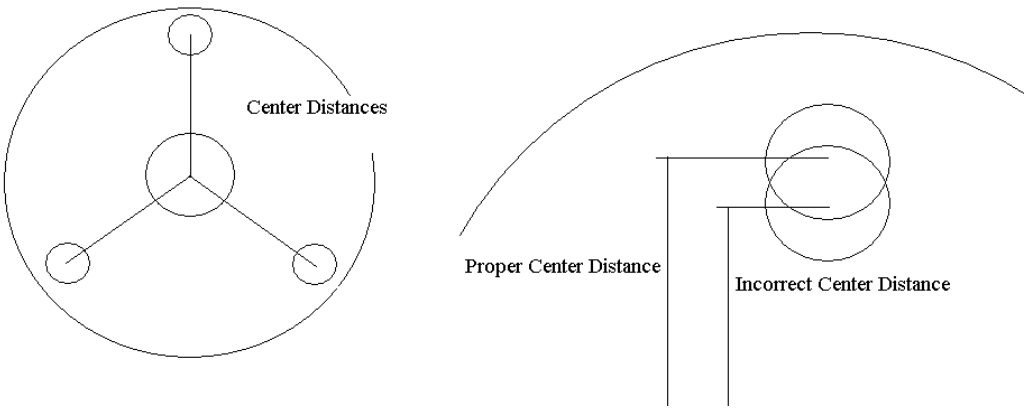


Figure 63 - Improper center distance for planets in carrier.

here. The inputs to the system had to be reduced to as small as possible to extend the braking time long enough to capture enough data points. This in essence made the un-modeled parameters even more critical to achieving a robust model. Gear friction is non-linear with speed, as shown in figure 64, and therefore may have been distributed between both of the coefficients. Windage losses could have also played a role in the poor modeling. Windage losses of a gearbox are very difficult to measure or calculate but can be assumed to be present when large gear faces are present [3]. Aside from the physics of the problem, the SID toolbox can experience problems when dealing with multivariate systems. Generally speaking, the fit gets better when more inputs are included and often gets worse when more outputs are included. To understand the latter fact, it should be realized that a model that has to explain the behavior of several outputs has a tougher job than one that just must account for a single output [13]. All of these may have played a role in the poor results of the model.

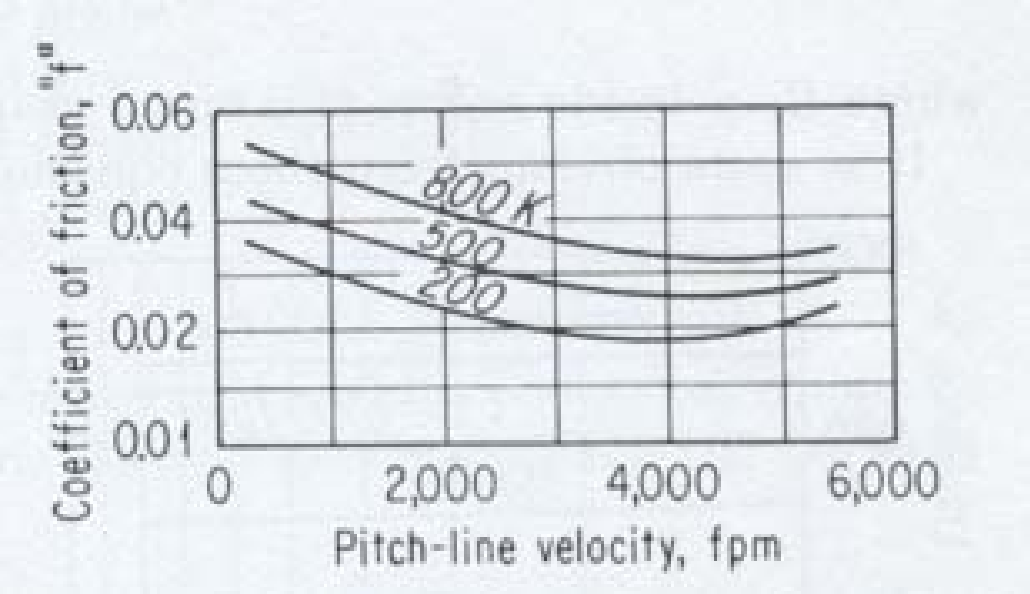


Figure 64 - Non-linear gear friction [3].

5.2 Future Work

Considering the damping and inertial terms separate from the braking could be a better approach in the parameter identification process. Creating a test rig involving a brake band and actuator with a spinning disk driven by a motor could produce reliable numbers for the braking characteristics. This would remove all other influences from the test data. For determining the inertia and damping terms, running the system in each gear without brake engagement while changing directions would provide much more information about the system. The two separate analyses could combined into an overall general model in which there would be no mixing of braking terms with other parameters. The braking torque could also be found without the use of parameter identification in the sense that was discussed earlier. Using the same spinning disk test rig, position and velocity data are all that would be needed. Since the change in kinetic energy is equal to the work done on the system the following equation could be used [19].

$$\Delta t \Delta KE = work\ done \tag{5.1}$$

$$(t_f - t_i)\frac{1}{2}J\dot{\theta}_f^2 - \frac{1}{2}J\dot{\theta}_i^2 = T_{Brake}\theta_{distance} \tag{5.2}$$

Knowing the time, velocity and position of the spinning disk the dynamic braking torque could be found. Once these characteristics were found they could then be used to describe the input to the DVT in a more complex model in SID.

Bibliography

[1] W.R. Hamel and T.C. Widner. “Fundamental Control Concepts for Implementation of Transmission-Based Actuators in Robotics and Automation”. Proceedings of the IEEE International Conference on Robotics and Automation. Leuven, Belgium 1998.

[2] W.R. Hamel, S. Kim, R. Zhou and A. Lumsdaine. “Dynamic Modeling and Analysis of a Transmission-based Robot Servoactuator”. Proceedings of the IEEE International Conference on Robotics and Automation. Taipai, Taiwan 2003.

[3] Darle W. Dudley. “Gear Handbook”. Massachusetts, USA. McGraw-Hill Book Company. 1962.

[4] Kalyana B. Ganti. “Analysis and Design of a Gear Shifting Mechanism for Transmission-Based Actuators” Masters Thesis, MABE Department. University of Tennessee, Knoxville.

[5] Darle W. Dudley. “Handbook of Practical Gear Design”. Florida, USA. CRC Press. 1994.

[6] Allan S. Hall, Alfred R. Holowenko, Herman G. Laughlin. “Schaum’s Outline of Theory and Problems of Machine Design” New York, USA. McGraw-Hill Book Company. 1961.

[7] “Torrington Service Catalog”. Torrington Fafnir Kilian. 2001.

[8] Aaron Deutschman, Walter J. Michels, Charles E. Wilson “Machine Design Theory and Practice”, New York, USA. Macmillan Publishing Co., Inc., 1975.

[9] Society of Automotive Engineers Inc., “Involute Splines and Inspection”. Warrendale, PA. 1970.

[10] Arcon Ring and Specialty Corporation. Retaining rings product catalog.

[11] RulandCorporation. Coupling product catalog.

[12] Lennart Ljung and Torkel Glad. “Modeling of Dynamic Systems”, New Jersey, USA. Prentice-Hall., Inc., 1994.

[13] Lennart Ljung. “System Identification Theory for the User”, China, Tsinghua University Press, 1999.

[14] S. Graham Kelly. “Fundamentals of Mechanical Vibrations”, Boston, USA, McGraw-Hill, 2000.

[15] William T. Thomson and Marie Dillon Bahleh. “Theory of Vibrations with Applications”, New Jersey, USA, Prentice-Hall, 1998.

[16] James B. Hartman and Vladimir L. Maleev. “Machine Design”, Pennsylvania, USA, International Textbook Company, 1954.

[17] Y. Fujii, W.E. Tobler and T.D. Snyder. “Prediction of Wet Band Brake Dynamic Engagement Behavior: Part Mathematical Model Development”. Proceedings of the Institute of Mechanical Engineers. Volume 215, Part D. 2000.

[18] Lennart Andersson, Ulf Jonsson and Karl Johansson. “A Manual for System Identification”.

[19] Rattan S.S., “Theory of Machines”, New Delhi, India. Tata McGraw-Hill Publishing Company Ltd., 1998.

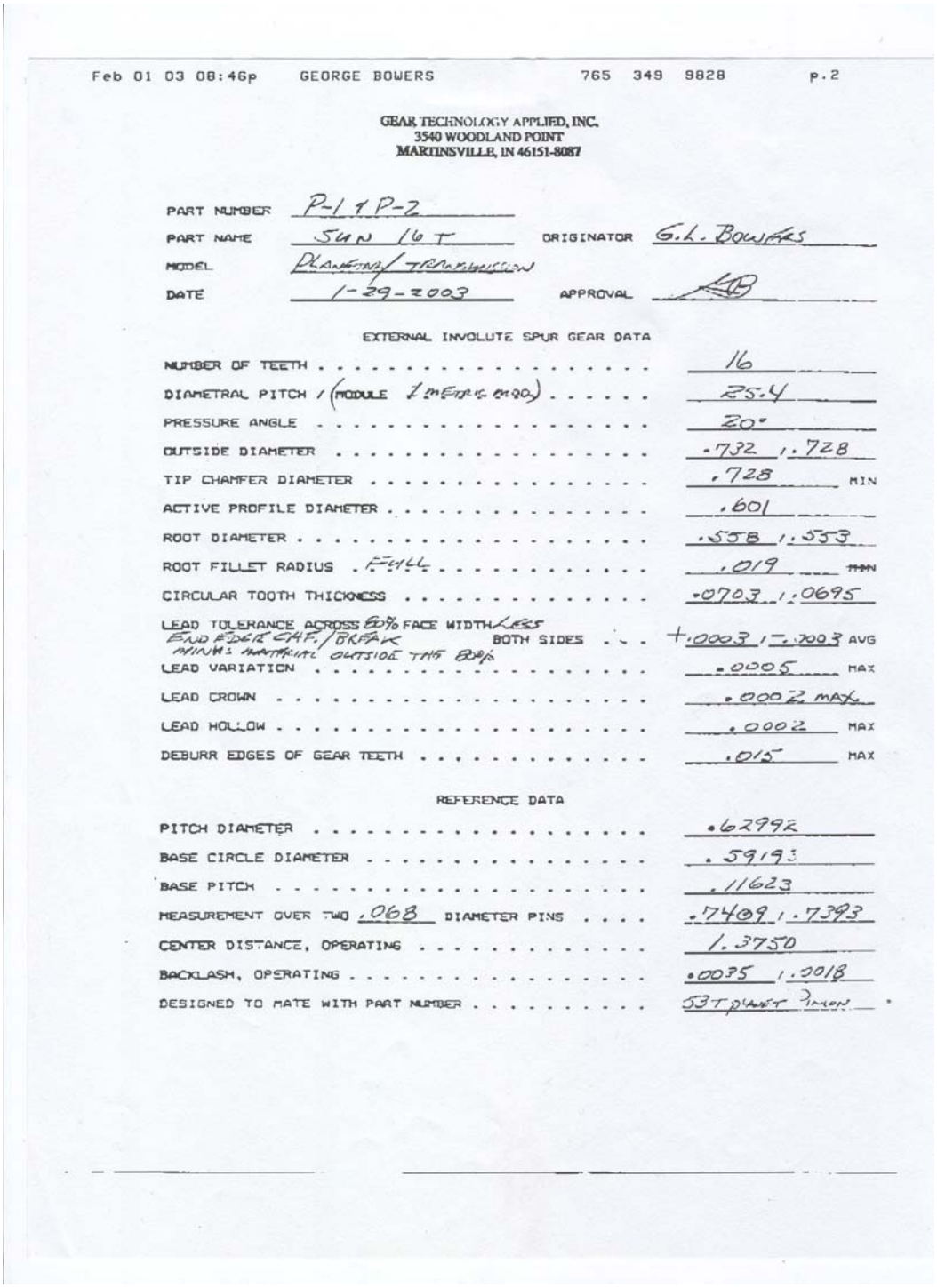
[20] W.R. Hamel. “Transmission-Based Electrical servoactuators: Final Report”. Work Performed Under Contract: DE-AC26-01NT41309, DOE 2003.

[21] Raymond J. Drago. “Fundamentals of Gear Design Design”, Boston, USA, Butterworths, 1988.

Appendix

Gear data for the DVT gears

Sun Gear 1 and 2



Feb 01 03 08:46p GEORGE BOWERS 765 349 9828 p.2

GEAR TECHNOLOGY APPLIED, INC.
3540 WOODLAND POINT
MARTINSVILLE, IN 46151-8087

PART NUMBER P-1 & P-2
PART NAME SUN 16 T ORIGINATOR G.L. BOWERS
MODEL PLANETARY TRANSMISSION
DATE 1-29-2003 APPROVAL

EXTERNAL INVOLUTE SPUR GEAR DATA

NUMBER OF TEETH	16
DIAMETRAL PITCH / (MODULE 1 METRIC ONLY)	25.4
PRESSURE ANGLE	20°
OUTSIDE DIAMETER	.732 / .728
TIP CHAMFER DIAMETER	.728 MIN
ACTIVE PROFILE DIAMETER	.601
ROOT DIAMETER	.558 / .553
ROOT FILLET RADIUS FULL	.019 MIN
CIRCULAR TOOTH THICKNESS	.0703 / .0695
LEAD TOLERANCE ACROSS 80% FACE WIDTH LESS END EDGE CHF./BREAK MINOR MATERIAL OUTSIDE THIS 80% BOTH SIDES	+.0003 / -.0003 AVG
LEAD VARIATION	.0005 MAX
LEAD CROWN	.0002 MAX
LEAD HOLLOW	.0002 MAX
DEBURR EDGES OF GEAR TEETH	.015 MAX

REFERENCE DATA

PITCH DIAMETER	.62992
BASE CIRCLE DIAMETER	.59193
BASE PITCH	.11623
MEASUREMENT OVER TWO .068 DIAMETER PINS	.7409 / .7393
CENTER DISTANCE, OPERATING	1.3750
BACKLASH, OPERATING	.0035 / .0018
DESIGNED TO MATE WITH PART NUMBER	53T PLANET PINION

Planet Gear 1 and 2

Feb 01 03 08:46p GEORGE BOWERS 765 349 9828 p.4

GEAR TECHNOLOGY APPLIED, INC.
3540 WOODLAND POINT
MARTINSVILLE, IN 46151-8087

PART NUMBER P-1 & P-2
PART NAME PLANET PINION 53T ORIGINATOR G.L. BOWERS
MODEL PLANETARY TRANSMISSION
DATE 1-29-2003 APPROVAL

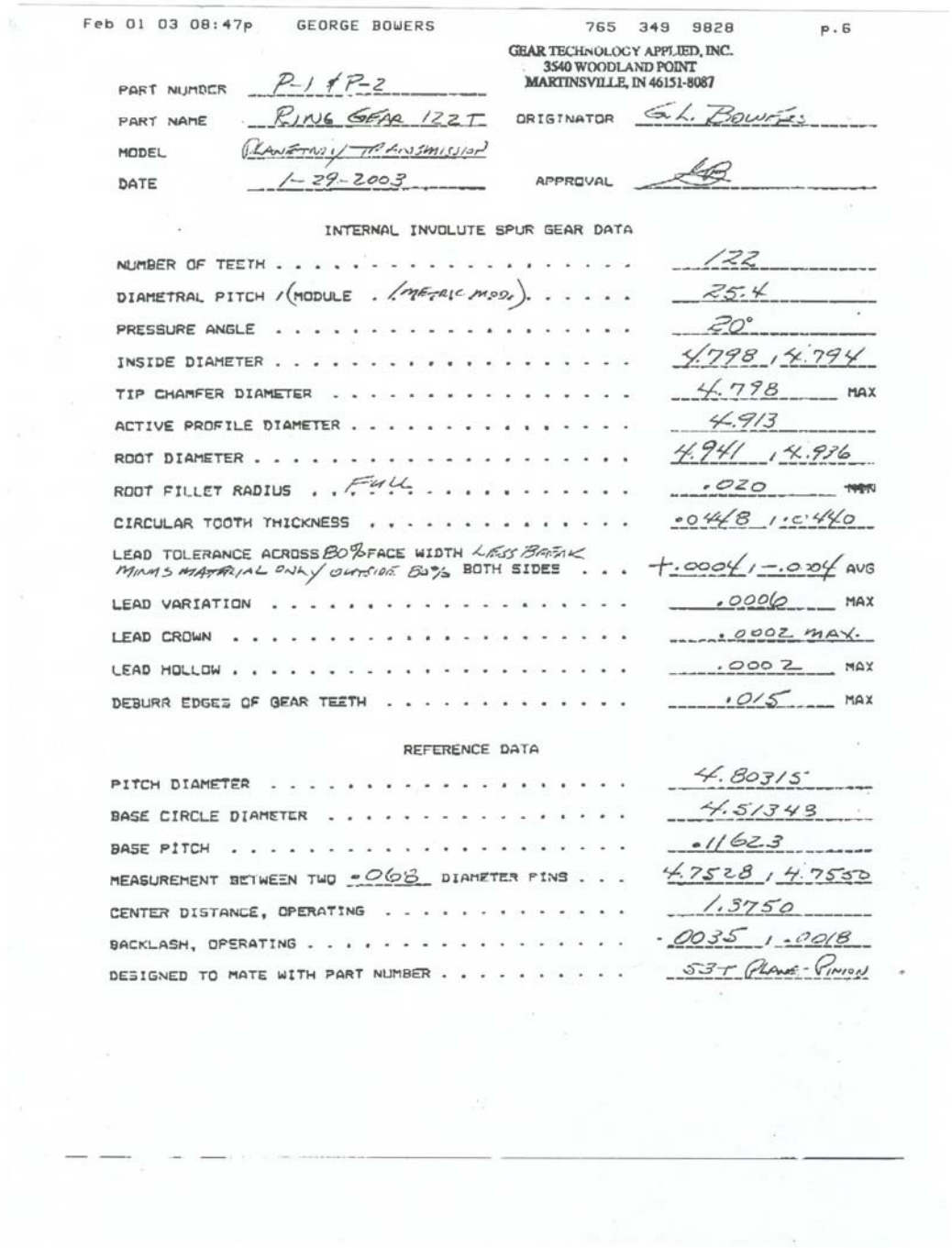
EXTERNAL INVOLUTE SPUR GEAR DATA

NUMBER OF TEETH	53
DIAMETRAL PITCH / (MODULE 1 METRIC MOD)	25.4
PRESSURE ANGLE	20°
OUTSIDE DIAMETER	2.165 / 2.161
TIP CHAMFER DIAMETER	2.161 MIN
ACTIVE PROFILE DIAMETER	2.048
ROOT DIAMETER	1.998 / 1.993
ROOT FILLET RADIUS FULL	.019 MIN
CIRCULAR TOOTH THICKNESS	.0643 / .0635
LEAD TOLERANCE ACROSS 80% FACE WIDTH LESS END EDGE CHAMFER/BREAK MINIMS MATERIAL OUTSIDE 80% BOTH SIDES	+.0003 / -.0003 AVG
LEAD VARIATION	.0005 MAX
LEAD CROWN	.0004 MAX.
LEAD HOLLOW	.0002 MAX
DEBURR EDGES OF GEAR TEETH	.015 MAX

REFERENCE DATA

PITCH DIAMETER	2.0861
BASE CIRCLE DIAMETER	1.96078
BASE PITCH	.11623
MEASUREMENT OVER TWO .068 DIAMETER PINS	2.1874 / 2.1851
CENTER DISTANCE, OPERATING	1.3750
BACKLASH, OPERATING	.0035 / .0018
DESIGNED TO MATE WITH PART NUMBER	16T SUN & 122T RING

Ring Gear 1 and 2



Feb 01 03 08:47p GEORGE BOWERS 765 349 9828 p.6

GEAR TECHNOLOGY APPLIED, INC.
3540 WOODLAND POINT
MARTINSVILLE, IN 46151-8087

PART NUMBER P-1 & P-2
PART NAME RING GEAR 122T
ORIGINATOR G.L. BOWERS
MODEL PLANETARY TRANSMISSION
DATE 1-29-2003
APPROVAL

INTERNAL INVOLUTE SPUR GEAR DATA

NUMBER OF TEETH	122
DIAMETRAL PITCH / (MODULE . / METRIC MOD.)	25.4
PRESSURE ANGLE	20°
INSIDE DIAMETER	4.798 / 4.794
TIP CHAMFER DIAMETER	4.798 MAX
ACTIVE PROFILE DIAMETER	4.913
ROOT DIAMETER	4.941 / 4.936
ROOT FILLET RADIUS . . FULL	.020 MIN
CIRCULAR TOOTH THICKNESS	.0448 / .0440
LEAD TOLERANCE ACROSS 80% FACE WIDTH LESS BEVEL MINUS MATERIAL ONLY / OUTSIDE 80% BOTH SIDES	+.0004 / -.0004 AVG
LEAD VARIATION	.0006 MAX
LEAD CROWN	.0002 MAX.
LEAD HOLLOW	.0002 MAX
DEBURR EDGES OF GEAR TEETH	.015 MAX

REFERENCE DATA

PITCH DIAMETER	4.80315
BASE CIRCLE DIAMETER	4.51343
BASE PITCH	.1162.3
MEASUREMENT BETWEEN TWO .068 DIAMETER PINS	4.7528 / 4.7550
CENTER DISTANCE, OPERATING	1.3750
BACKLASH, OPERATING	.0035 / .0018
DESIGNED TO MATE WITH PART NUMBER	53T PLANET-PINION

Sun Gear 3

Feb 01 03 08:47p GEORGE BOWERS 765 349 9828 p.8

GEAR TECHNOLOGY APPLIED, INC.
3540 WOODLAND POINT
MARTINSVILLE, IN 46151-8087

PART NUMBER P-3
PART NAME SUN 20T ORIGINATOR G.L. BOWERS
MODEL PLANETARY TRANSMISSION
DATE 1-29-2003 APPROVAL

EXTERNAL INVOLUTE SPUR GEAR DATA

NUMBER OF TEETH	20
DIAMETRAL PITCH / MODULE (1 METRIC MOD.)	25.4
PRESSURE ANGLE	20°
OUTSIDE DIAMETER	.875 / .871
TIP CHAMFER DIAMETER	.871 MIN
ACTIVE PROFILE DIAMETER	.753
ROOT DIAMETER	.699 / .694
ROOT FILLET RADIUS . FULL	.019 MIN
CIRCULAR TOOTH THICKNESS	.0644 / .0636
LEAD TOLERANCE ACROSS 80% FACE WIDTH LESS END EDGE CHAMFER/BREAK BOTH SIDES	+.0003 / -.0003 AVG
MINUS MATERIAL ONLY OUTSIDE THE 80% LEAD VARIATION	.0005 MAX
LEAD CROWN	.0002 MAX.
LEAD HOLLOW	.0002 MAX
DEBURR EDGES OF GEAR TEETH	.015 MAX

REFERENCE DATA

PITCH DIAMETER	.78740
BASE CIRCLE DIAMETER	.73992
BASE PITCH	.11623
MEASUREMENT OVER TWO .068 DIAMETER PINS	.8871 / .8853
CENTER DISTANCE, OPERATING	1.375
BACKLASH, OPERATING	.0035 / .0018
DESIGNED TO MATE WITH PART NUMBER	50T PLANET PINION

Planet Gear 3

Feb 01 03 08:47p GEORGE BOWERS 765 349 9828 p.10

GEAR TECHNOLOGY APPLIED, INC.
3540 WOODLAND POINT
MARTINSVILLE, IN 46151-8087

PART NUMBER P-3
PART NAME PLANET PINION 50T ORIGINATOR G.L. BOWERS
MODEL PLANETARY TRANSMISSION
DATE 1-29-2003 APPROVAL

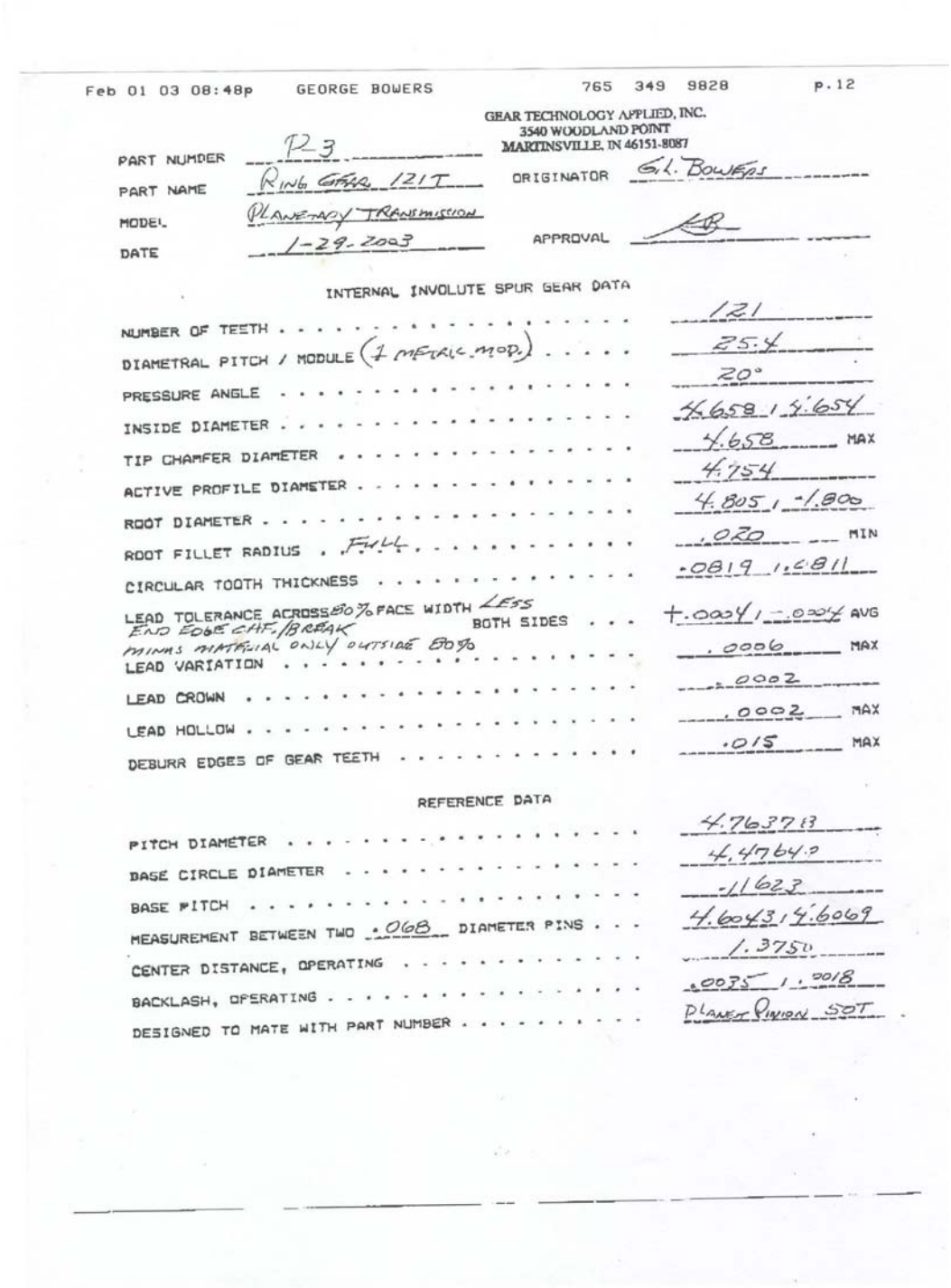
EXTERNAL INVOLUTE SPUR GEAR DATA

NUMBER OF TEETH	50
DIAMETRAL PITCH / (MODULE METRIC MOD.)	25.4
PRESSURE ANGLE	20°
OUTSIDE DIAMETER	2.010 / 2.006
TIP CHAMFER DIAMETER	2.006 MIN
ACTIVE PROFILE DIAMETER	1.906
ROOT DIAMETER	1.855 / 1.950
ROOT FILLET RADIUS . FULL	.019 MIN
CIRCULAR TOOTH THICKNESS	.0553 / .0545
LEAD TOLERANCE ACROSS 80% FACE WIDTH LESS END EDGE CHF/BREAK MINUS MATERIAL ONLY OUTSIDE 80% BOTH SIDES	+.0003 / -.0023 AVG
LEAD VARIATION	.0005 MAX
LEAD CROWN	.0004 MAX.
LEAD HOLLOW	.0002 MAX
DEBURR EDGES OF GEAR TEETH	.015 MAX

REFERENCE DATA

PITCH DIAMETER	1.96850
BASE CIRCLE DIAMETER	1.84979
BASE PITCH	.11623
MEASUREMENT OVER TWO .068 DIAMETER PINS	2.0472 / 2.0451
CENTER DISTANCE, OPERATING	1.3750
BACKLASH, OPERATING	.0035 / .0018
DESIGNED TO MATE WITH PART NUMBER	20T SUN & 72T RING

Ring Gear 3



Feb 01 03 08:48p GEORGE BOWERS 765 349 9828 p.12

GEAR TECHNOLOGY APPLIED, INC.
3540 WOODLAND POINT
MARTINSVILLE, IN 46151-8087

PART NUMBER R3
PART NAME RING GEAR 121T
MODEL PLANETARY TRANSMISSION
DATE 1-29-2003
ORIGINATOR G.L. BOWERS
APPROVAL

INTERNAL INVOLUTE SPUR GEAR DATA

NUMBER OF TEETH	121
DIAMETRAL PITCH / MODULE (1 METRIC MOD.)	25.4
PRESSURE ANGLE	20°
INSIDE DIAMETER	4.658 / 4.654
TIP CHAMFER DIAMETER	4.658 MAX
ACTIVE PROFILE DIAMETER	4.754
ROOT DIAMETER	4.805 / 4.800
ROOT FILLET RADIUS . FULL	.020 MIN
CIRCULAR TOOTH THICKNESS	.0819 / .0811
LEAD TOLERANCE ACROSS 80% FACE WIDTH BOTH SIDES (LESS END EDGE CHAMFER/BREAK MINUS MATERIAL ONLY OUTSIDE 80%)	+.0004 / -.0004 AVG
LEAD VARIATION	.0006 MAX
LEAD CROWN	.0002
LEAD HOLLOW	.0002 MAX
DEBURR EDGES OF GEAR TEETH	.015 MAX

REFERENCE DATA

PITCH DIAMETER	4.763783
BASE CIRCLE DIAMETER	4.47642
BASE PITCH	.11623
MEASUREMENT BETWEEN TWO .068 DIAMETER PINS	4.6043 / 4.6069
CENTER DISTANCE, OPERATING	1.3750
BACKLASH, OPERATING	.0035 / .0018
DESIGNED TO MATE WITH PART NUMBER	PLANET PINION 50T

MATLAB CODE FOR OEM

```
load nrga2400.txt;%LOADING THE DATA INTO THE SOFTWARE

SunShaftSpeed=(2*3.14/60).*nrga2400(:,2);%CREATING DATA STREAMS
Carrier3Speed=(2*3.14/60).*nrga2400(:,4);
ABMotorCurrent=nrga2400(:,6);
BrakeMotorTorque=nrga2400(:,7);

DVT=iddata([SunShaftSpeed,Carrier3Speed],[ABMotorTorque,BrakeMotorTorque],.016);
%CREATING THE IDDATA OBJECT

DVT.InputName={'AB Motor Current'; 'Brake Motor Current'};%DEFINING INPUT
DATA STREAMS
DVT.OutputName={'Sun Shaft Speed';'Carrier3 Speed'};%DEFINING OUTPUT DATA
STREAMS

DVT=IDFILT(DVT,2,.1)%LOW PASS FILTER

pause,plot(DVT),pause%PLOTTING DATA TO SEE RELATIONSHIPS

As = [NaN NaN;NaN NaN]; %CREATING FREE PARAMETER MATRICES/USER
DEFINED MODEL
Bs = [NaN NaN;NaN NaN];
Cs = [1 0;0 1];
Ds = [0 0; 0 0];
Ks = [0 0; 0 0];
```

```
X0s = [0; 0];   %X0 is the initial value of the state vector;


A = [-0.95421      -1.3268;0.77357     -0.10205];%MAKING AN INTIAL GUESS

B = [2390       1.1443;;-674.84       343.24];

C = [1 0;0  1];

D = [0 0; 0 0];

K = [0 0; 0 0];

X0 = [0; 0];


DVTa = idss(A,B,C,D,K,X0);%CREATING THE NOMINAL STATE SPACE MODEL

setstruc(DVTa,As,Bs,Cs,Ds,Ks,X0s);%SETTING THE STRUCTURE

set(DVTa,'Ts',0)%DENOTING A CONTINUOUS TIME MODEL

DVTmodel = pem(DVT,DVTa);

pause, DVTmodel, pause % DISPLAYING MODEL

pause, compare(DVT,DVTmodel); %COMPARING DATA TO OEM


DVTstep=step(DVT);

pause,step(DVTstep),pause%STEP RESPONSE

pause,step(DVT,2,'b',DVTmodel,'r'),pause

DVTsp=spa(DVT);

w = {0,1000}

pause,bode(DVTsp,'b',DVTmodel,'r',w),pause%BODEPLOTS
```

VITA

Kelley P. Brown was born in Kingsport, Tennessee on the 2nd day of February 1974. He went to Dobyns-Bennett High School where he played football for the Indians. He obtained his bachelors degree in mechanical engineering from the University of Tennessee, Knoxville in May 2002 and his masters degree in fall 2004.